LARGE TARGET TISSUE NECROSIS OF RADIOFREQUENCY ABLATION USING MATHEMATICAL MODELLING

A Thesis Submitted to the

College of Graduate Studies and Research

in Partial Fulfilment of the Requirements

for the Degree of Doctor of Philosophy

in the Division of Biomedical Engineering

University of Saskatchewan

Saskatoon

By

Bing Zhang

PERMISSION TO USE

In presenting this thesis in partial fulfilment of the requirements for a Postgraduate degree from the University of Saskatchewan, I agree that the Libraries of this University may make it freely available for inspection. I further agree that permission for copying of this thesis in any manner, in whole or in part, for scholarly purposes may be granted by the professor or professors who supervised my thesis work or, in their absence, by the Head of the Department or the Dean of the College in which my thesis work was done. It is understood that any copying or publication or use of this thesis or parts thereof for financial gain shall not be allowed without my written permission.

It is also understood that due recognition shall be given to me and to the University of Saskatchewan in any scholarly use which may be made of any material in my thesis.

Requests for permission to copy or to make other use of material in this thesis in whole or part should be addressed to:

Head of the Division of Biomedical Engineering

University of Saskatchewan

57 Campus Drive, Saskatoon, SK S7N 5A9, Canada

ABSTRACT

Radiofrequency ablation (RFA) is a clinic tool for the treatment of various target tissues. However, one of the major limitations with RFA is the 'small' size of target tissues that can be effectively ablated. By small it is meant the size of the target tissue is less than 3 cm in diameter of the tissue otherwise 'large' size of tissue in this thesis. A typical problem with RFA for large target tissue is the incompleteness of tumour ablation, which is an important reason for tumour recurring. It is widely agreed that two reasons are responsible for the tumour recurring: (1) the tissue charring and (2) the 'heat-sink' effect of large blood vessels (i.e. $\geq$3 mm in diameter). This thesis study was motivated to more quantitatively understand tissue charring during the RFA procedure and to develop solutions to increase the size of target tissues to be ablated.

The thesis study mainly performed three tasks: (1) evaluation of the existing devices and protocols to give a clear understanding of the state of arts of RFA devices in clinic, (2) development of an accurate mathematical model for the RFA procedure to enable a more quantitative understanding of the small target tissue size problem, and (3) development of a new protocol based on the existing device to increase the size of target tissues to be ablated based on the knowledge acquired from (1) and (2). In (1), a design theory called axiomatic design theory (ADT) was applied in order to make the evaluation more objective. In (2), a two-compartment finite element model was developed and verified with *in vitro* experiments, where liver tissue was taken and a custom-made RFA system was employed; after that, three most commonly used internally cooled RFA systems (constant, pulsed, and temperature-controlled) were employed to demonstrate the maximum size of tumour that can be ablated. In (3) a novel feedback temperature-controlled RFA protocol was proposed to overcome the small target tissue size problem, which includes (a) the judicious selection of control areas and target control temperatures and (b) the use of the tissue temperature instead of electrode tip temperature as a feedback for control.

The conclusions that can be drawn from this thesis are given as follows: (1) the decoupled design in the current RFA systems can be a critical reason for the incomplete target tissue necrosis (TTN), (2) using both the constant RFA and

pulsed RFA, the largest TTN can be achieved at the maximum voltage applied (MVA) without the roll-off occurrence. Furthermore, the largest TTN sizes for both constant RFA and pulsed RFA are all less than 3 cm in diameter, (3) for target tissues of different sizes, the MVA without the roll-off occurrence is different and it decreases with increase of the target tissue size, (4) the largest TTN achieved by using temperature-controlled RFA under the current commercial protocol is still smaller 3 cm in diameter, and (5) the TTN with and over 3 cm in diameter can be obtained by using temperature-controlled RFA under a new protocol developed in this thesis study, in which the temperature of target tissue around the middle part of electrode is controlled at 90 ℃ for a standard ablation time (i.e. 720 s).

There are a couple of contributions with this thesis. First, the underlying reason of the incomplete TTN of the current commercially available RFA systems was found, which is their inadequate design (i.e. decoupled design). This will help to give a guideline in RFA device design or improvement in the future. Second, the thesis has mathematically proved the empirical conclusion in clinic that the limit size of target tissue using the current RFA systems is 3 cm in diameter. This has advanced our understanding of the limit of the RFA technology in general. Third, the novel protocol proposed by the thesis is promising to increase the size of TTN with RFA technology by about 30%. The new protocol also reveals a very complex thermal control problem in the context of human tissues, and solving this problem effectively gives implication to similar problems in other thermal-based tumour ablation processes.

ACKNOWLEDGEMENTS

I would like to extend my earnest appreciation and gratitude to my supervisor Professor Wenjun (Chris) Zhang for his incomparable help throughout my PhD study. The immense knowledge and remarkable enthusiasm for learning he has shown inspired me to overcome each challenge in my study. Besides the study, he helped me get accustomed to the life in Canada when I just came to here in the first couple of months and gave me many useful suggestions on my career development as well. Without these he has done for me, it would be impossible for me to complete this thesis.

I would also like to thank my co-supervisor Professor Michael Moser for giving his guidance and help with respect to the clinical stuff in my research. Appreciation also goes to other members of my advisory committee, Professor Madan M. Gupta, Professor Fangxiang Wu, and Professor Venkatesh Meda for providing me valuable suggestions and ideas which greatly improved my research.

Special thanks go to Mr. Doug Bitner in the Department of Mechanical Engineering for his willingness to help me for the experiments presented in this thesis.

Many thanks to my friends for their mental or physical help and support every single day of my study. They are Dr. Lin Cao and his wife Xue Yong, Zhen Wang and his wife Ying Yan, Dong He, Andy Hu, Gary Huang, Bin Han, and Rain Zhao on the campus of University of Saskatchewan, Rob Arthur and his wife Edith Arthur, Gerry Fork and his wife Shirley Fork in the church community.

Last but definitely not the least, I want to express my deepest gratitude to my family in China. My parents Yuchun Zhang and Hua Zhou and my sister Wenjuan Zhang have been so supportive and understanding for every decision I have made over the years.

This thesis is dedicated to

my parents, my niece Ziru Xu, and Lei.

CONTENTS

PERMISSION TO USE i

ABSTRACT ii

ACKNOWLEDGEMENTS iv

CONTENTS vi

LIST OF TABLES x

LIST OF FIGURES xi

LIST OF ABBREVIATIONS xiv

1 INTRODUCTION 1

1.1 Background 1

1.2 Motivations and objectives 3

1.3 Organization of the thesis 4

1.4 Contributions of the primary investigator 5

REFERENCES 6

2 LARGE TARGET TISSUE NECROSIS OF RADIOFREQUENCY ABLATION: A REVIEW OF CLINICAL RESULTS AND MATHEMATICAL MODELLING 8

2.1 Introduction 8

2.2 Large target tissue necrosis of RFA with clinical results 10

2.2.1 Limitations of current RFA systems 10

2.2.2 Target tissue charring 11

2.2.3 Current methods to achieve a large size of TTN 13

2.3 Mathematical Modelling of RFA 18

2.3.1 Modelling of heat transfer in biological tissue 19

2.3.2 Mechanism and mathematical modelling of RFA-induced biological tissue death 21

2.3.3 Validation of the mathematical models of RFA 24

2.4 Temperature-controlled RFA 25
2.5 Conclusions and future issues 26
REFERENCES 29
3 EVALUATION OF THE CURRENT RADIOFREQUENCY ABLATION SYSTEMS USING AXIOMATIC DESIGN THEORY 38
3.1 Introduction 38
3.2 Analysis of incomplete TTN 40
3.3 Brief introduction of ADT 42
3.4 Engineering evaluation 44
3.4.1 Current RFA systems 44
3.4.2 ADT evaluation 47
3.5 Case study 51
3.5.1 Case setup 51
3.5.2 FE modelling for the system 52
3.5.3 Initial and boundary conditions in the model 53
3.5.4 Simulation results and discussion 53
3.6 Conclusions 55
REFERENCES 57
4 STUDY OF THE RELATIONSHIP BETWEEN THE TARGET TISSUE NECROSIS VOLUME AND THE TARGET TISSUE SIZE IN LIVER TUMOURS USING TWO-COMPARTMENT FINITE ELEMENT RFA MODELLING 61
4.1 Introduction 62
4.2 Materials and methods 64
4.2.1 Electric-thermal model of two-compartment RFA 64
4.2.2 Finite element analysis of the two-compartment RFA model 66
4.3 Results and discussion 70
4.4 Conclusions 78
REFERENCES 80

5 NUMERICAL ANALYSIS OF THE RELATIONSHIP BETWEEN THE AREA OF TARGET TISSUE NECROSIS AND THE SIZE OF TARGET TISSUE IN LIVER TUMOURS WITH PULSED RADIOFREQUENCY ABLATION 85
5.1 Introduction 86
5.2 Materials and methods 87
5.2.1 Finite element modelling of PRFA 87
5.2.2 TTN area evaluation 92
5.2.3 The *in vitro* experiment for validation of the FEM 93
5.3 Results and discussion 94
5.3.1 Experimental results for validation of the FEM 94
5.3.2 Computational results for analysis of the pulsed RFA 95
5.3.3 Limitations 102
5.4 Conclusions 103
REFERENCES 105
6 JUDICIOUS SELECTION OF TARGET CONTROL AREAS AND TARGET TEMPERATURES TO INCREASE THE SIZE OF TARGET TISSUE NECROSIS BY RADIOFREQUENCY ABLATION 109
6.1 Introduction 110
6.2 Materials and methods 111
6.2.1 Finite element model of RFA 111
6.2.2 Temperature-controlled RFA and judicious selection of the control target in the target tissue area 116
6.2.3 Validation of target control areas using *in vitro* experiments 119
6.3 Results and discussion 120
6.3.1 TTN sizes of control areas from the FEM 120
6.3.2 *In vitro* experimental results 128
6.4 Conclusions 130
REFERENCES 132
7 CONCLUSIONS AND FUTURE WORK 136
7.1 Conclusions 136

7.2 Future work 137
APPENDIX A A RADIOFREQUENCY ABLATION DEVICE FOR SMALL ANIMALS 139
APPENDIX B LIST OF PUBLICATIONS 143
APPENDIX C COPYRIGHT PERMISSIONS 144

LIST OF TABLES

2.1. Clinical results of tumours with various sizes using RFA in recent years. 11

3.1. Design matrix of the current RFA systems. 50

3.2. Thermal and electrical properties of the materials in the case study. 53

4.1. Thermal and electrical properties of the modelling elements used in the present study. 67

4.2. Computational results for four target tissue sizes during different RFA protocols. 71

4.3. Volumetric percentage of thermal damage to the healthy liver tissue during different RFA protocols. 73

5.1. Thermal and electrical properties of the modelling elements used in the present study. 89

5.2. Comparisons of TTN areas from the FEM and *in vitro* experiments. 95

5.3. The computational results of TTN area for all PRFA protocols in the present study. 98

6.1. Properties of the elements in the model in the present study. 113

6.2. Results of the TTN areas from the *in vitro* experiments. 129

LIST OF FIGURES

2.1. Schematic diagram of the current RFA system and its mechanism of heat generation. 9

2.2. Three factors causing the failure of RFA in the treatment of tumours ≥3 cm in diameter. 12

2.3. Schematic diagrams of the growth of charred tissue (A) and impedance (B) in RFA. 13

2.4. Schematic diagrams for (A) the cluster electrode, (B) the multitined expandable electrode, (C) the internally cooled electrode, and (D) the perfusion electrode. 15

2.5. Zones of biological tissue in the treatment of RFA (adapted from [35]). 22

2.6. Typical RF applicators with a thermal sensor embedded at of the tip of RF electrode with the target tissue. 26

3.1. Overview of the typical current used RFA procedure. 40

3.2. Monopolar RF applicator. (A typical RF applicator contains an insulated shaft and RF electrode. 41

3.3. Design domains in the ADT 43

3.4. Schematic diagrams of current RF electrode designs.. 44

3.5. Application of RF energy. 46

3.6. CAs, FRs, and DPs in the current RFA systems. 48

3.7. FE modelling of the case study.. 52

3.8. Temperature gradient after a single RFA treatment session. (the third needle is not shown in the plot) 54

3.9. The 50℃ isothermal contour. 55

4.1. Dimensions (out of scale and in mm) and boundary conditions of the two-compartment RFA model used in the present study. 65

4.2. Placements of the five measured points (out of scale, dimension in mm). 70

4.3. TTN volume for each target tissue size at different voltages applied. 72

4.4. MVA without the roll-off occurrence for each target tissue size. 74

4.5. Computer simulation results for the TTN of target tissues of different sizes at the MVA. 75

4.6. Temperature change during the 12-min ablation procedure for each target tissue at its own MVA.....76

4.7. Temperature distributions (in ℃) obtained with the two-compartment RFA model (A) and the homogenous RFA model (B).....77

5.1. 2D axis symmetric RFA model and its boundary conditions used in the present study. 88

5.2. Thermal and electrical conductivities of healthy liver tissue and liver tumour used in the present study 89

5.3. Two pulsed RF power supply methods: (A) half-square waveform and (B) half-sine waveform. 90

5.4. FEMs and their mesh modes used in the present study for three sizes of target tissues. 91

5.5. *In vitro* experimental set up for the validation of the FEM.....93

5.6. Computational and experimental results for two ablation operations.....94

5.7. 100 ℃ isotherm and temperature distribution of the scenario of 47.2 V-720 s at 50 s (A), 442 s (B), and 720 s (C) and the change of the impedance (D).....96

5.8. 100 ℃ isotherm and temperature distribution of the scenario of 48 V-145 s at 25 s (A), 118 s (B), and 145 s (C) and the change of the impedance (D).....97

5.9. Computational results of TTN areas for target tissues with different sizes 100

5.10. Target tissue death rate (%) (D63) at its own MVA: (A) d_x= 25 mm, (B) d_x= 30 mm, and (C) d_x= 35 mm and the changes of the TTN areas (D). 101

5.11. MVA without the roll-off occurrence for each size of target tissue in the present study.....102

6.1. The geometric model of RFA with an elliptical liver tumor (out of scale).....112

6.2. A PID closed loop control system used in the present study. 116

6.3. Growth of the charred tissue (A) and three control areas with 14 control points selected in the present study (B). 118

6.4. *In vitro* experimental set up for the validation.....120

6.5. Temperatures (T_r) measured at points 1-4 selected in Area I. 121

6.6. Temperatures (T_r) measured at points 5-10 selected in Area II.....122

6.7. Temperatures (T_r) measured at points 10-14 selected in Area III.....123

6.8. Target tissue death rate and TTN areas generated using points 1-4 selected in Area I.....124

6.9. Target tissue death rate and TTN areas generated using points 5-10 selected in Area II. 125

6.10. Target tissue death rate and TTN areas generated using points 11-14 selected in Area III. 126

6.11. Temperature distributions (in ℃) of point 5 and point 11 at 720 s for the objective control temperatures of (A) 80 and (B) 90 ℃. 127

6.12. TTN areas generated using the three control areas at 80 and 90 ℃. 127

6.13. TTN areas generated using the three selected points at the control temperatures of (A) 80 ℃ and (B) 90 ℃ from the *in vitro* experiments. 129

LIST OF ABBREVIATIONS

ADT	axiomatic design theory
CAs	customer attributes
CLM	colorectal liver metastases
CLgM	colorectal lung metastases
CRFA	constant radiofrequency ablation
CT	computed tomography
DPs	design parameters
FEM	finite element model
FRs	functional requirements
GBC	gallbladder carcinoma
HCC	hepatocellular carcinoma
HIFU	high intensity focused ultrasound
HPA	hepatic adenoma
MVA	maximum voltage applied
MWA	microwave ablation
NA	not available
PID	proportional-integral-derivative
PRFA	pulsed radiofrequency ablation
PVs	process variables
RCC	renal cell carcinoma
RFA	radiofrequency ablation
TTC	triphenyl tetrazolium chloride
TTN	target tissue necrosis

1 INTRODUCTION

1.1 Background

Despite significant progress in understanding, diagnosing, treating, and preventing the disease in the past decades, tumour still remains the major threat to human beings [1]. Nowadays, open surgery is still recognized as the most used curative medical method for patients with various tumours. However, there is only 60% of diagnosed tumours that can be treated in this manner (or resected) [2]. Thermal ablation, acting as an alternate method to open surgery, has been used in the treatment of various target tissues (tumour tissues or dysfunctional tissues) for a long time [3]. Thermal ablation tries to destroy the target tissue by using a fatal high (≥ 43 ℃) or low (≤ -20 ℃) temperature to induce the irreversible cellular death of biological tissues. Although thermal ablation is a relative new terminology, using heat to treat illness for medical purpose can be traced back to thousands of years ago. For instance, the steam baths used by the ancient Greeks, the Chinese herbal baths used in ancient China, and the use of cautery for treatment of the breast tumours in ancient Egypt [4]. The following famous statement by Hippocrates (460-370 BC) who was considered as one of the most outstanding figures in the history of medicine [4,5] is cited herein regarding the history of thermal therapy to signal the importance of thermal therapy:

> *'Those diseases which medicines do not cure, iron cures; those which iron cannot cure, fire cures; and those which fire cannot cure, are to be reckoned wholly incurable.'*

The fundamental principle behind any thermal therapy is that when the biological tissue is undergone with a fatal high or low temperature for a certain period of time, destroy to tissue cells will be induced at the membrane and subcellular levels [3]. For a fatal high temperature, the destroy takes place in the form of cell membrane collapse and protein denaturation [6]. For a fatal low temperature, the destroy is due to the cellular dehydration and high extracellular solute concentration, which is further attributed to ice crystal formation within the cells and further destroy of the integrity of organelles and the cell membrane [6,7]. Details of tissue death due to the fatal temperatures (low and high) will be discussed further in Chapter 2.

Thermal ablation can be classified into several methods in terms of how heat is generated, e.g.:

Radiofrequency ablation (RFA): it uses an alternating current with high frequency (around 500 kHz) to generate heat to kill the target tissue. The heat (frictional or joule heat) is due to the interaction between the ions within the biological tissue and electrons that form the alternating current.

Microwave ablation (MWA): similarly with RFA, it also uses an alternating current with higher frequency (900-2500 MHz) to generate heat to ablate the target tissue. The heat (dielectric heat) is created by forcing the polar molecules with intrinsic dipoles (usually water) within the biological tissue to continuously realign with the oscillating electric current [8], which is known as rotating dipoles. The rotation of the molecules increase their kinetic energy, which leads to the increase in the temperature of the biological tissue [6].

Laser ablation: it induces electromagnetic heating to elevate the temperature of the target tissue to a cytotoxic level [3]. The heat is generated due to the collisions of particles, like atoms within the biological tissue and infrared electrons that make up the absorbed light.

Ultrasound or high intensity focused ultrasound (HIFU) ablation: it is to deliver the sound energy to the target tissue primarily due to frictional effects, which can elevate the temperature of the target tissue to a fatal level [9].

Magnetic nanoparticles hyperthermia: it uses the embedded nanoparticles within the target tissue to generate heat to kill the target tissue when the nanoparticles are exposed to an alternating magnetic field [10]. The heating using magnetic nanoparticles is due to the magnetic effect (magnetic hysteresis losses) in an external alternating magnetic field [11].

Cryoablation: in contrast to the methods mentioned above, it uses cold temperature to kill the target tissue. In the current commercial cryoablation system, particularly liquid gas (e.g. argon or nitrogen) is used to reduce the temperature of the target tissue when the gas is expanded in a small chamber at the distal part of cryoprobe [3,6].

Among these thermal ablation methods, RFA has undoubtedly been the most investigated and clinically relevant one [3]. This thesis study was mainly focused on the method of RFA. RFA has been used in the treatment of various

target tissues in different organ sites, such as liver [12], lung [13], breast [14], and kidney [15] with many favourite clinical results and no serious complications. Its efficacy (usually evaluated on the 5-year survival rate) can be competitive with the open surgery when the treated target tissue is in small size (i.e. $<$ 3 cm in diameter) and at its early stage [3]. Further, it has several advantages over open surgery, such as *minimal invasiveness*, which reduces significantly the time of hospital stay and the rate of complications, *reservation of healthy tissue*, which benefits the patients with weak organs function, and *no need to have the general anaesthesia*. However, many clinical results have also shown that RFA does not have acceptable effective rates for large target tissues $\geq$3 cm in diameter [16-20]. This phenomenon could be caused by various reasons for different patients, but the most important one can be the incomplete TTN in the treatment of large target tissues, which leads to the high local recurrence. Details of the inefficacy of RFA in the treatment of large target tissues will be discussed in Chapter 2.

1.2 Motivations and objectives

To overcome the deficiency of RFA for large target tissues, many works have been done, which include design of RF electrode, combination RFA with other adjunct methods, optimization of RF power delivery, and optimal displacement of RF electrode [21-25]. However, the clinical results are still not good for large target tissues (see the conclusions in Chapter 2). This has motivated this thesis study. Particularly, this thesis study has taken two questions: why is RFA not suitable to large target tissues especially $\geq$3 cm in diameter? Any method can be further developed to overcome this limitation?

Based on the discussion above, the research objectives of this study were defined as follows:

Objective 1: To evaluate the efficacy of the current RFA systems in the treatment of target tissues $\geq$3 cm in diameter using engineering design methods.

Objective 2: To investigate the relationship between the size of the target tissue and the size of TTN and further theoretically to prove that only target tissues $<$3 cm in diameter can be ablated completely using the current RFA systems.

Objective 3: To design a novel RFA protocol to overcome the deficiency of the current RFA systems with the help of mathematical modelling and feedback control techniques.

Objective 4: To design and make a RFA system especially for small animals to be useful to verify the theoretical development in the aforementioned objectives especially Objectives 2 and 3.

1.3 Organization of the thesis

This thesis is organized in a manuscript-based style. It is presented in the form of published or prepared manuscripts. At the beginning of each chapter, a brief introduction is included to describe the relation between the manuscript and the context of the thesis. The status of each manuscript is also given at the beginning of each chapter. To produce a coherent and defendable thesis, all published or prepared manuscripts have been formatted on the consistency of format and style.

The remainder of the thesis is organized as follows: Chapter 2 is a comprehensive review of large TTN of radiofrequency ablation in clinical results and mathematical modelling techniques. Chapter 3 discusses the evaluation of the current radiofrequency ablation systems on the achievement of large TTN using axiomatic design theory. By using mathematical modelling techniques, Chapter 4 and 5 verify the existing clinical finding that the current constant and pulsed RFA systems are only effective for the target tissues <3 cm in diameter. Chapter 6 proposes a new protocol potentially to overcome the 3-cm problem of RFA systems. Conclusions and several future studies in the context of this thesis are given in Chapter 7. Appendix A introduces a radiofrequency ablation device for small animals. The list of published and prepared manuscripts is given in Appendix B, and the copyright permissions of all published manuscripts used in this thesis are in Appendix C.

1.4 Contributions of the primary investigator

It is noted that all published or prepared manuscripts are co-authored. However, it is mutual understanding of all authors that Bing Zhang, as the first author, is the primary investigator. The contributions of other authors are limited to the advisory and editorial capacity.

REFERENCES

1. Tamarov KP, Osminkina LA, Zinovyev SV et al. Radio frequency radiation-induced hyperthermia using Si nanoparticle-based sensitizers for mild cancer therapy. Sci Rep 2014;4:7034.
2. Custodio A, Puente J, Sastre J, Díaz-Rubio E. Second-line therapy for advanced pancreatic cancer: a review of the literature and future directions. Cancer Treat Rev 2009;35:676-84.
3. Ahmed M, Brace CL, Lee FT, Goldberg SN. Principles of and advances in percutaneous ablation. Radiology 2011;258:351-69.
4. Berjano E, Romero-Méndez R, Franco W. Radiofrequency based hyperthermia therapy: A centennial technique serving modern surgery. Rev Mex Ing Biomedica 2010;23:42-153.
5. He X. Thermostability of biological systems: fundamentals, challenges, and quantification. Open Biomed Eng J 2011;5:47-73.
6. Chu KF, Dupuy DE. Thermal ablation of tumours: biological mechanisms and advances in therapy. Nat Rev Cancer 2014;14:199-208.
7. Sabel MS. Cryo-immunology: a review of the literature and proposed mechanisms for stimulatory versus suppressive immune responses. Cryobiology 2009;58:1-11.
8. Lubner MG, Brace CL, Hinshaw JL, Lee FT. Microwave tumor ablation: mechanism of action, clinical results, and devices. J Vasc Interv Radiol 2010;21:S192-203.
9. ter Haar G, Coussios C. High intensity focused ultrasound: physical principles and devices. Int J Hyperthermia 2007;23:89-104.
10. Hilger I. In vivo applications of magnetic nanoparticle hyperthermia. Int J Hyperthermia 2013;29:828-34.
11. Dutz S, Hergt R. Magnetic particle hyperthermia—a promising tumour therapy? Nanotechnology 2014;25:452001.
12. Solbiati L, Livraghi T, Goldberg SN et al. Percutaneous Radio-frequency ablation of hepatic metastases from colorectal Cancer: Long-term results in 117 Patients. Radiology 2001;221:159-66.
13. Gillams A, Khan Z, Osborn P, Lees W. Survival after radiofrequency ablation in 122 patients with inoperable colorectal lung metastases. Cardiovasc Intervent Radiol 2013;36:724-30.
14. Kinoshita T, Iwamoto E, Tsuda H, Seki K. Radiofrequency ablation as local therapy for early breast carcinomas. Breast Cancer 2011;18:10-7.

15. Zagoria RJ, Pettus JA, Rogers M et al. Long-term outcomes after percutaneous radiofrequency ablation for renal cell carcinoma. Urology 2011;77:1393-7.

16. Gillams A, Lees W. Radiofrequency ablation of colorectal liver metastases. Abdom Imaging 2005;30:419-26.

17. Jakobs TF, Hoffmann R-T, Trumm C et al. Radiofrequency ablation of colorectal liver metastases: mid-term results in 68 patients. Anticancer Res 2006;26:671-80.

18. Abitabile P, Hartl U, Lange J, Maurer C. Radiofrequency ablation permits an effective treatment for colorectal liver metastasis. Eur J Surg Oncol 2007;33:67-71.

19. Sørensen SM, Mortensen FV, Nielsen DT. Radiofrequency ablation of colorectal liver metastases: long-term survival. Acta Radiol 2007;48:253-8.

20. Gillams A, Lees W. Five-year survival in 309 patients with colorectal liver metastases treated with radiofrequency ablation. Eur Radiol 2009;19:1206-13.

21. Lencioni R, Goletti O, Armillotta N et al. Radio-frequency thermal ablation of liver metastases with a cooled-tip electrode needle: Results of a pilot clinical trial. Eur Radiol 1998;8:1205-11.

22. Gazelle GS, Goldberg SN, Solbiati L, Livraghi T. Tumor ablation with radio-frequency energy. Radiology 2000;217:633-46.

23. Lee J, Lee JM, Yoon J-H et al. Percutaneous radiofrequency ablation with multiple electrodes for medium-sized hepatocellular carcinomas. Korean J Radiol 2012;13:34-43.

24. Lorentzen T. A cooled needle electrode for radiofrequency tissue ablation: Thermodynamic aspects of improved performance compared with conventional needle design. Acad Radiol 1996;3:556-63.

25. Goldberg SN, Stein MC, Gazelle GS et al. Percutaneous radiofrequency tissue ablation: optimization of pulsed-radiofrequency technique to increase coagulation necrosis. J Vasc Interv Radiol 1999;10:907-16.

2 LARGE TARGET TISSUE NECROSIS OF RADIOFREQUENCY ABLATION: A REVIEW OF CLINICAL RESULTS AND MATHEMATICAL MODELLING

*This chapter is submitted as **Bing Zhang** et al. "Large target tissue necrosis of radiofrequency ablation: A review of clinical results and mathematical modelling" to **Physica Medica** in 2015 (**under review**).*

Abstract

Radiofrequency ablation (RFA) is an effective clinical method for tumour ablation with minimum intrusiveness. However, the use of RFA is mostly restricted to small tumours, especially those <3 cm in diameter. This paper discusses the state-of-the-art of RFA, drawn from clinical results, for large tumours (i.e. ≥ 3 cm in diameter). In particular, the paper investigates clinical results related to target tissue necrosis (TTN) and mathematical modelling of the RFA procedure to understand the mechanism behind the small TTN phenomenon with RFA. This paper also discusses the control of the temperature of target tissue in the RFA procedure, which has the potential to increase the size of TTN. This paper ends with a discussion regarding how to address the so-called 3-cm phenomenon or problem with RFA.

2.1 Introduction

Radiofrequency ablation (RFA) is a medical procedure that uses heat to eradicate tumours in various locations, including the liver [1], lungs [2], kidneys [3], bones [4], and breasts [5]. Figure 2.1 shows a general procedure of an RFA system used in current clinical settings. RFA systems usually comprise three parts: (1) an RF power generator that generates alternating currents with high frequency, (2) an RF applicator that consists of an RF electrode and insulated shaft, and (3) ground pads that are usually placed on the patient's back or thigh. In an RFA procedure, the RF applicator is usually inserted percutaneously into the target tissue with the help of an image-guided device (computed tomography, ultrasound imaging or magnetic resonance imaging) [6]. With the developments of the last several decades, RFA has become an alternative medical modality in the treatment of various tumours for patients,

especially those with early and small tumours or those who are not candidates for open surgery. Compared with other medical modalities, RFA has two primary advantages: minimal damage to peripheral normal tissue and no need for general anaesthetic [7]. In RFA, the target tissue (the tumour or dysfunctional tissue) is ablated by the heat generated from a high-frequency alternating current (approximately 500 kHz).

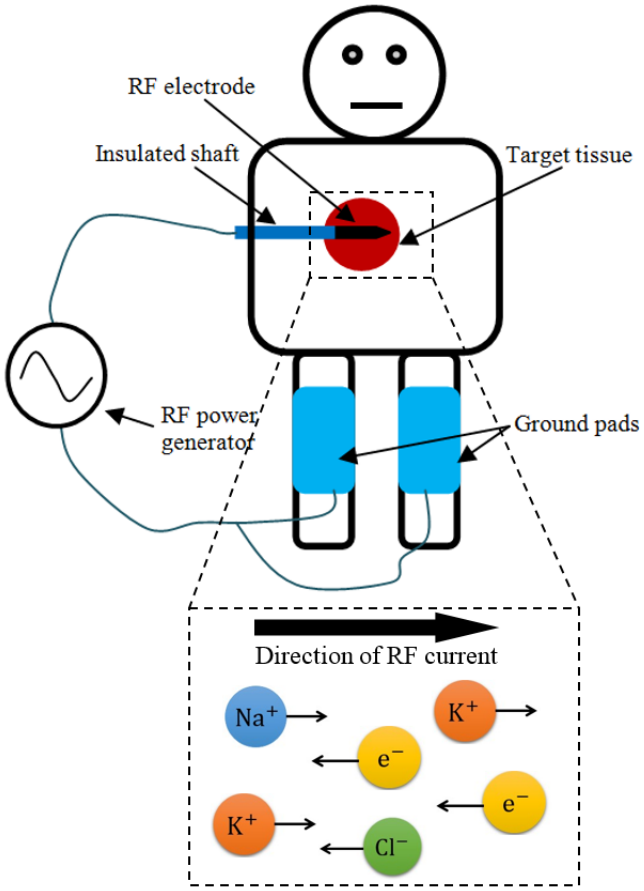

Figure 2.1. Schematic diagram of the current RFA system and its mechanism of heat generation.

The heat in RFA is known as the Joule heat or resistive heat, and it is generated via the interaction between the electrons (e^-) that form the alternating current and the ions that make up the resistor (e.g. Na^+, K^+, and Cl^- in biological tissue). As shown in Figure 2.1, a closed electric circuit can be formed if there is an electric path inside the body. It is noted that there are usually two heating areas in the situ of RFA treatment: the direct heating area and the indirect heating area [7]. The direct heating area is close to the RF electrode and has high current density. Heat generated in this area is due to the interaction between the electrons and ions. The indirect heating area is the effect

of heat transfer from the direct heating area. Due to the space limitation, this paper is not intended to be a review of all aspects of the current RFA system but rather a review with a focus on the deficiency of treating target tissues ≥3 cm in diameter with the current RFA system, as well as principles and methods in the current RFA system to tackle the small tumour size problem. In particular, this paper will discuss three issues related to RFA: large target tissue necrosis (TTN) of RFA from the clinical results, mathematical modelling of RFA, and temperature control of RFA.

2.2 Large target tissue necrosis of RFA with clinical results

2.2.1 Limitations of current RFA systems

One of the deficiencies is the poor efficacy of the treatment of large tumours (i.e. ≥3 cm in diameter). Xu et al. [8] concluded that there was a significant difference in terms of complete ablation between a tumour <3 cm in diameter and a tumour ≥3 cm in diameter. These researchers treated 137 patients of hepatocellular carcinoma (HCC) with RFA in a non-interruptive manner. The rates of complete ablation for tumours ≤3 cm, 3.1 to 5 cm, and >5 cm are 95.4%, 82.5%, and 50%, respectively. Llovet et al. [9] also reported in a literature review that more than 80% of HCCs (<3 cm in diameter) can be ablated completely, but the rate is only 50% for tumours that are 3-5 cm in diameter. Gory et al. [10] compared the clinical results from 146 patients who received treatment with RFA ($n = 96$) or hepatic resection (HR) ($n = 52$) for HCCs from 2000 to 2010. They found that, among the patients with HCCs (<3 cm in diameter), there was no significant difference in the overall survival rates of 3 and 5 years between RFA and HR (hepatic resection) (66% and 39% vs. 69% and 59%, respectively; $P = 0.41$). However, for the patients with HCCs in the range of 3-5 cm in diameter, the overall survival rates of 3 and 5 years between RFA and HR were 62% and 37% vs. 66% and 62%, respectively, concluding that the RFA has a poor survival rate for tumours ≥3 cm in diameter. The same conclusions can also be found in [11,12]. These studies showed that there is no significant difference in overall and disease-free survival rates between RFA and HR for HCCs <3 cm in diameter. However, HR is significantly superior to RFA in the treatment of large HCCs ≥3 cm in diameter [13]. Table 2.1 shows the clinical results of tumours with various sizes using RFA treatment in recent years. From Table 2.1, it can be concluded that the efficacy of RFA is far from satisfactory in terms of complete ablation, local recurrence, and

overall survival rate in the treatment of different tumours ≥3 cm in diameter. Consequently, there seems to be a doctrine in effect, that is, no tumour ≥3 in diameter should be treated with RFA.

2.2.2 Target tissue charring

From an engineering point of view, there could be three factors responsible for the failure of RFA for tumours ≥3 cm in diameter: (1) the small size of (TTN) (Figure 2.2A), (2) inaccurate placement of the RF electrode (Figure 2.2B), and (3) inaccuracy of the current imaging system (Figure 2.2C). This paper is limited to the first factor.

Table 2.1. Clinical results of tumours with various sizes using RFA in recent years.

Year	First author	No. of patients-tumours	Tumour type	Complete ablation	Local recurrence	Overall survival
2009	Gillams and Less [16]	309-617*	CLM	NA	NA	5y: 24%& ($D_t < 5$ cm) 5y: 33%& ($D_t < 3.5$ cm)
2009	N'Kontchou et al. [17]	235-307	HCC	94.7%	100%& ($D_t = 3.2 \mp 1.0$ cm) 0%& ($D_t = 2.8 \mp 1.0$ cm) median: 23 months	5y: 32% ($D_t = 2.9 \mp 1.0$ cm)
2011	Shiina et al. [18]	1170-2982*	HCC¥	99.4%	NA	5y: 65.1%& ($D_t \leq 3$ cm) 5y: 46.5%& ($D_t > 3$ cm)
2011	Zagoria et al. [3]	41-48	RCC	NA	12%& median: $D_t = 5.2$ cm 0%& median: $D_t = 2.2$ cm,	5y: 66% median: $D_t = 2.6$ cm (range: 0.7-8.2 cm)
2011	Hung et al. [19]	190#	HCC	NA	NA	5y: 67.4% ($D_t = 2.4 \mp 0.9$ cm)
2012	Baldwin et al. [20]	22-33*	CLM, HCC, GBC, HPA	100%	4.5% median: 24 months	2y: 100% ($D_t = 3.6 \mp 1.3$ cm)
2012	Solbiati et al. [21]	99-202	CLM	NA	11.9% median: 72 months	5y: 47.8% ($D_t = 2.2 \mp 1.1$ cm)

Table 2.1. Continued

Year	First author	No. of patients-tumours	Tumour type	Complete ablation	Local recurrence	Overall survival
2013	Gillams et al. [2]	122-398	CLgM	NA	NA	51 months ($D_t = 0-2$ cm) 31 months ($D_t = 2.1-4$ cm)
2013	Psutka et al. [22]	185[#]	RCC	87%	6.5% median: 30 months	5y: 73.3% median: $D_t = 3$ cm (range: 1-6.5 cm)
2011	Van Tilborg et al. [23]	100-126[*]	CLM	NA	5.6%[&] ($D_t < 3$ cm) 19.5%[&] ($D_t = 3-5$ cm) 41.2%[&] ($D_t > 5$ cm) median: 29 months	5y: 36% median: $D_t = 2.4$ cm (range: 0.2-8.3 cm)

[*]the number of RFA sessions, rather than the number of tumours, was available, [#]both the number of RFA sessions and the number of tumours were unavailable, [¥]transarterial chemoembolization was combined with RFA in patients with tumours larger than 3.0 cm in diameter, [&]statistically significant, CLM: Colorectal liver metastases, HCC: Hepatocellular carcinoma, RCC: Renal cell carcinoma, GBC: Gallbladder carcinoma, HPA: Hepatic adenoma, CLgM: Colorectal lung metastases, NA: Not available, 5 y: 5 years and D_t: Diameter of tumour.

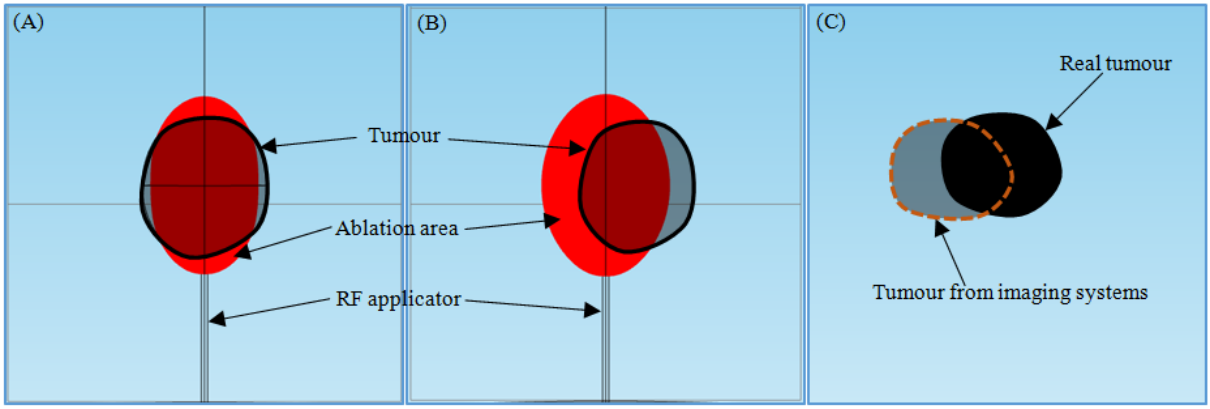

Figure 2.2. Three factors causing the failure of RFA in the treatment of tumours ≥3 cm in diameter.

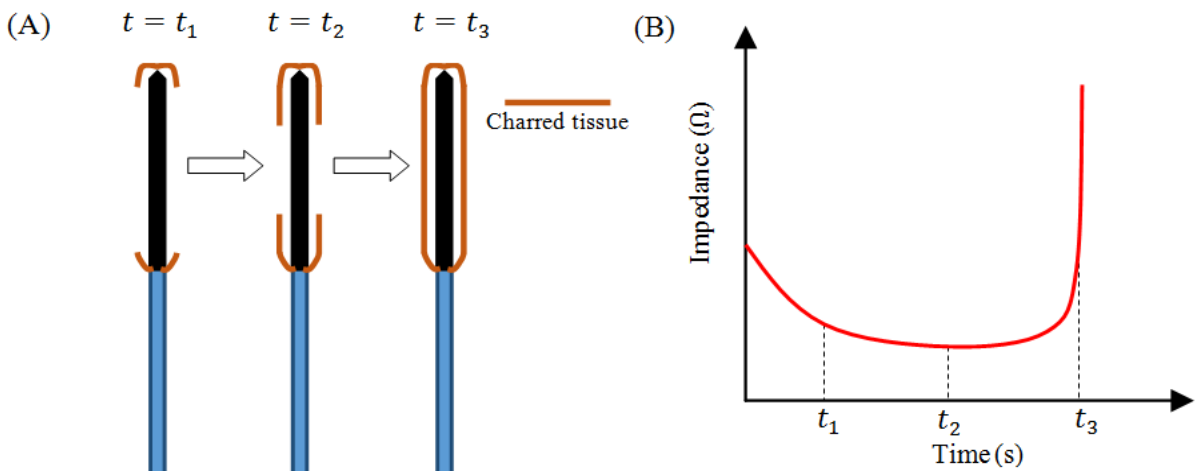

Figure 2.3. Schematic diagrams of the growth of charred tissue (A) and impedance (B) in RFA.

RFA falls into the category of thermal therapeutic methods for tumours, and its small size of TTN is mainly due to the tissue charring and the 'heat-sink' effect of large blood vessels ≥3 mm in diameter [14]. It is known from physics that when the temperature of biological tissue is higher than 100 ℃, the water essentially boils and begins to evaporate and the tissue becomes charred. The charred tissue further leads to a noticeable decrease in its electrical conductivity [7]. For RFA, the charred tissue usually grows from the areas around the proximal and distal parts of the RF electrode to the areas around the middle part of the RF electrode, as shown in Figure 2.3A. Figure 2.3B shows the change of impedance between the RF electrode and the ground pads. When the RF electrode is encircled completely by the charred tissue, such as at the time of t_3, the impedance will have a marked growth [15]. As we mentioned before regarding the mechanism of heating, RFA needs an electrical path to deliver the energy. After t_3, the path is closed. In consequence, the actual output of the RF energy drops. In clinical settings, we call this phenomenon 'roll-off'. Thus, the tissue charring is one of the major reasons behind the small size of TTN in RFA, especially when the charred tissue completely encircles the RF electrode.

2.2.3 Current methods to achieve a large size of TTN

There are a considerable number of methods that have been proposed in an attempt to achieve a large size of TTN with RFA in clinical and animal experiments and simulation. These methods are mainly focused on three aspects,

namely (1) design of the RF electrode, (2) design of the RF power supply, and (3) combining RFA with adjuvant therapies.

2.2.3.1 Design of the RF electrode

The most widely used designs of the RF electrode in current clinical settings are the cluster electrode, multitined expandable electrode, internally cooled electrode, and perfusion electrode, as shown in Figure 2.4.

For the cluster electrode, there are usually three parallel monopolar electrodes spaced closely together that are inserted into the target tissue. These electrodes are usually connected to a monopolar RF power generator. The spaces between these electrodes are determined by the size of the target tissue and the ablation area generated by each electrode. A relatively large overlapping TTN area is expected to be achieved by aggregating all small TTN areas generated by each electrode in the cluster. Furthermore, two operational strategies to activate the electrodes to achieve a large size TTN are proposed in the literature, namely, (1) the sequential strategy and (2) the switching strategy [24]. The sequential strategy implies that in a session of ablation (i.e. 12 min), only one electrode is at work. After the session for the first electrode, the second electrode is activated to work for another session, and then the third one follows. In the switching strategy, the pattern is that for instance, the first electrode is energised for a short period of time (i.e. 1 second), and the second one is energised for 1 second [24]. Only one electrode is at work in the short time interval, but the frequency of switching is notably high. The cluster electrode method is able to achieve a relatively large size of TTN. Its shortcomings include: (1) difficulty in placing the electrodes for an overlapped and aggregated TTN area, (2) difficulty in ablating tumours that are located in critical positions inaccessible to the multi-electrode, (3) more normal tissues are ablated to ensure the overlap of TTN areas, and (4) the increase of occurrences of RFA-related complications and of patient's pain due to an increased number of electrode insertions.

The multitined expandable electrode usually has several tines that act as the electrodes stored in a single needle lumina, as shown in Figure 2.4B. After the RF applicator is inserted into the targeted area, these tines are deployed or spanned according to the size of the tumour. Occasionally, a protocol using a stepped deployment with the incremental extension of the tines is used in clinical settings [25]. However, this method has fallen out of fashion in recent years for the following two reasons. First is that tissues around the tines are easily overheated because there is

no internal cooling effect in tines. Thus, the charred tissues tend to stick onto the tines, which makes the retrieval of tines difficult and increases the possibility of tumour cell seeding as well. Second is the mismatch between the TTN shape forced by the multitined expandable electrode (e.g. an umbrella or Christmas tree shape) and the TTN shape in its natural state, which is similar in shape to a sphere or ellipsoid. The mismatch is a reason why incomplete ablation or the ablation of more healthy tissues may occur.

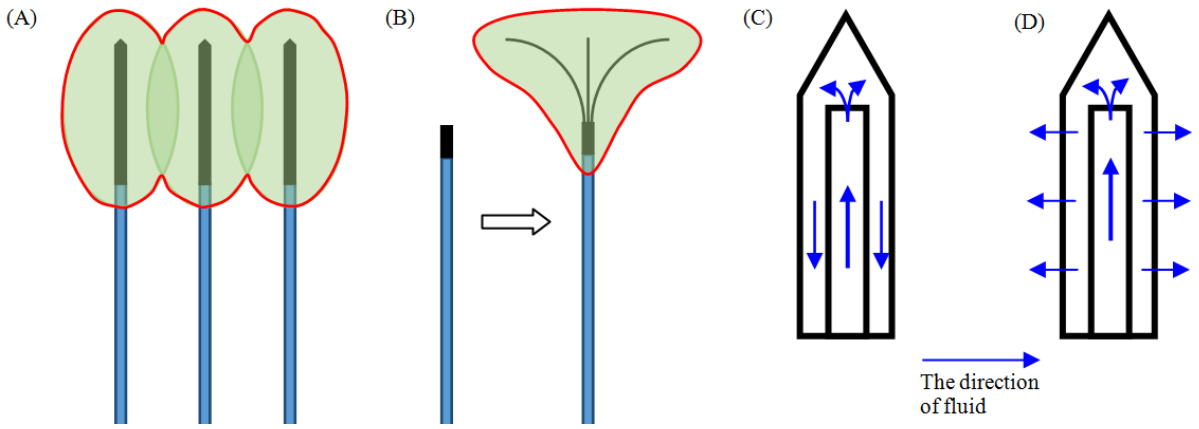

Figure 2.4. Schematic diagrams for (A) the cluster electrode, (B) the multitined expandable electrode, (C) the internally cooled electrode and (D) the perfusion electrode.

The internally cooled electrode has chilly fluids (e.g. water or gas) to cool down the RF electrode to delay the overheating and tissue charring. The chilly fluids are usually pumped into the RF electrode through an inner lumina, and the fluids subsequently flow into the outer lumina, as shown in Figure 2.4C. This capability makes it possible to delivery more RF energy to the target tissue. However, this method cannot avoid tissue charring and just shifts the charred tissue 1-2 mm away from the electrode surface according to [26]. Thus, the TTN generated by the monopolar internally cooled electrode still cannot meet the requirements of treatment of tumours ≥3 cm in diameter with RFA.

The perfusion electrode uses fluids (i.e. hypertonic saline) to cool down the RF electrode. However, the fluids are also irrigated into the target tissue, as shown in Figure 2.4D. In such a case, the fluids can cool down the target tissue to avoid tissue charring. Furthermore, the thermal and electrical conductivities of a target tissue immersed in

hypertonic saline change to more preferable conditions for the large size of TTN. However, a significant issue with this method is that the saline solution can flow everywhere, even to healthy tissue and vital organs. Thus, the size and shape of the ablation area become unpredictable with this RFA method.

2.2.3.2 Design of the RF power supply

The initial method of the power supply for RFA is a continuous and constant high power input (i.e. constant voltage or current). This can easily lead to tissue overheating or charring, and the charred tissue ultimately interferes with the power supply due to the roll-off [27]. There are various ways to improve the design of the RF power supply. One of them is the pulsed power supply method, which applies high levels of voltage or current in a pulsed manner for a large size of TTN [28]. The principle of achieving the large size of TTN is the application of low levels of voltage or current, which separate the high levels of voltage or current. With an appropriate optimization of high and low levels of voltage or current, the tissues around the electrode can be cooled down (within the periods of low levels of voltage or current). Thus, more RF energy can be delivered to the target tissue, and a relatively large size of TTN may be achieved. However, this method is still unable to avoid tissue charring and roll-off, which makes this method inadequate as well in the treatment of tumours $\geq$3 cm in diameter.

Another method that is now used in clinical settings is the temperature-controlled RFA [29,30]. For this method to work, the temperature at a specific location is controlled by a control algorithm embedded in the RF power generator to avoid tissue overheating. However, in these systems, the temperature at the tip of the electrode, rather than that of the target tissue, is what is measured and controlled. Therefore, there is room to improve this method and push it further in the direction of the technological development of sensors to measure the temperature of the target tissue directly.

The impedance-controlled RFA is another method of the delivery of RF energy for large TTN [31, 32]. As mentioned before, the charred tissue usually has high impedance. Therefore, controlling the impedance between the RF electrode and ground pad may be able to control the occurrence of charred tissue. The most commonly used control scheme is that in which, when the impedance is higher than a pre-set value, the delivery of RF power stops for a given period of time (e.g. 60 s), during which the charred tissue is cooled. After the impedance becomes lower

than a pre-set value, the RF power generator resumes delivering the RF power again. In one RF operation, this procedure may be performed several times to obtain a large size of TTN.

2.2.3.3 Combining RFA with adjuvant therapies

Combining RFA with conventional treatment (e.g. chemotherapy or radiotherapy) is also used in current clinical settings for tumours ≥3 cm in diameter [33-35]. Combining RFA with adjuvant therapies has the potential to generate the large size of TTN and to achieve complete ablation as well, by filling in untreated gaps within the ablation areas [27]. By combining RFA with chemotherapy, a large size of TTN may be achieved because of the following three reasons [27]: (1) the 'two-hit' effect on the susceptible tumour cells (initial reversible cell injury caused by RFA in the more peripheral ablation zone) followed by irreversible injury by chemicals, (2) increased cell stress leading to necrosis, and (3) temporary occlusion of the blood supply of the tumour, avoiding the 'heat-sink' effect. By combining RFA with radiotherapy, two possible reasons can be taken as the principle of generating a large size of TTN. The first one is "*the sensitization of the tumour to subsequent radiation due to the increased oxygenation resulting from hyperthermia-induced increased blood flow to the tumour*" [36]. The second one is "*an inhibition of radiation-induced repair and recovery and increased free radical formation*" [37]. However, the disadvantages of using chemotherapy and radiotherapy are also obvious. Both of them have a range of side effects (e.g. depression of the immune system, gastrointestinal distress, damage to epithelia surfaces, etc.).

2.2.3.4 Experimental and clinical results

Although the methods discussed above solely have the ability to generate a relatively large size of TTN, it is worth mentioning that a combined method, rather than a sole method, is usually used in the treatment of large tumours (i.e. ≥3 cm in diameter) in animal experiments or clinical settings. For instance, an RFA treatment can be use the cluster electrode method with the internally cooled electrode or the perfusion electrode under the impedance-controlled power delivery method followed by an adjuvant therapy of chemotherapy.

Lee et al. [38] used the sequential cluster electrode (three internally cooled electrodes with 2.5 cm exposure length each and an inter-electrode distance of 4 cm) with a 200 W and 480 kHz RF generator in *in vivo* experiments using a

porcine liver model (n=11). With a 36-min session of ablation (12 min for each electrode), the minimum and maximum diameters of the central TTN they obtained were 4.03±0.40 (mean±standard deviation) and 4.91±0.26 cm, respectively. Similar results were also found in the work of Yoon et al. [39]. They used the switching cluster electrode (same monopolar electrode but 2.0- or 2.5-cm inter-electrode distance) with a 200 W and 480 kHz RF generator in a 12-min session of ablation. They switched the three electrodes to active based on the occurrence of roll-off. The minimum and maximum diameters of the central TTN were 4.1±0.8 and 4.8±0.9 cm, respectively. Solbiati et al. [21] reported that a favourable clinical result (93.1% primary technical success, 11.9% local tumour progression and 47.8% five-year survival rate) was achieved by using a combination of RFA and chemotherapy for CLMs >1.5 cm in diameter. They used a cluster electrode with three internally cooled and 17-gauge electrodes (2.5-4.0 cm length) and an RF generator that is capable of producing 150-200 W output power. All patients also received systemic chemotherapy using the Douillard chemotherapy regimen (irinotecan, leucovorin, and 5-fluorouracil) or the FOLFOX regimen (folinic acid, fluorouracil, oxaliplation). Morimoto et al. [40] achieved a large size of TTN (5.8±1.3 and 5.0±1.1 cm for the maximum and minimum diameter, respectively) using RFA plus transcatheter arterial chemoembolization (TACE) in the treatment of HCCs. Compared with RFA alone, RFA plus TACE achieved a significant low local tumour progression rate (6%) at the end of the third year ($P = 0.012$). A mildly significant 3-year survival rate (93%) was also reached in the group of RFA and TACE ($P = 0.369$). Lu et al. [41] also concluded that RFA plus TACE significantly improved the 1-, 3- and 5-year survival rates compared with RFA alone in patients with HCCs ≥3 cm in diameter (P <0.0004, 0.0002 and 0.0001, respectively). Two types of electrode were used in their study, namely, a multitined, 15-gauge and 15-cm long expandable electrode with maximum dimensions of 3.5 cm or 4 cm and a 17-gauge internally cooled electrode 3-cm in length. The RF energy was applied by a RF generator (RF3000 Generator; Boston Scientific or Series CC-1; Valleylab).

2.3 Mathematical Modelling of RFA

Mathematical modelling has been used in the study of RFA for many years, especially in the design of new RFA protocols [42-44], optimization and improvement of existing RFA protocols [45-47], and investigation of electrical and thermal effects of biological tissue during various RFA procedures [15,26,48,49]. Due to its low cost and low time consumption, mathematical modelling can be used to assess the therapeutic feasibility of RFA protocols with

devices in different target tissues [50]. Further, mathematical modelling may play a critical role in the development of patient-specific RFA protocol plans [51,52].

2.3.1 Modelling of heat transfer in biological tissue

The most widely used model for describing the heat transfer in biological tissue during the procedure of RFA is the Pennes bioheat transfer equation, which is as follows [53]:

$$\rho c \frac{\partial T(\mathbf{x},t)}{\partial t} = \nabla \cdot \left(k \nabla T(\mathbf{x},t)\right) - \rho_b c_b \omega_b (T(\mathbf{x},t) - T_b) + Q_m(\mathbf{x},t) + Q_{hs}(\mathbf{x},t) \qquad x \in \mathbf{\Lambda} \tag{2.1}$$

where ρ (kg m^{-3}) is the density, c (J $\mathrm{kg}^{-1}\mathrm{K}^{-1}$) is the specific heat, $T(\mathbf{x}, \mathrm{t})$ (℃) is the temperature, $\mathbf{x} = \{x, y, z\}$ in the Cartesian coordinate system, $\mathbf{\Lambda}$ denotes the analysed spatial domains, k (W $\mathrm{m}^{-1}\mathrm{K}^{-1}$) is the thermal conductivity, ρ_b (kg m^{-3}) is the blood density, c_b (J $\mathrm{kg}^{-1}\mathrm{K}^{-1}$) is the blood specific heat, ω_b (s^{-1}) is the blood perfusion rate, T_b is the temperature of the blood entering the tissue, $Q_m(\mathbf{x}, t)$ (W m^{-3}) is the volumetric heat generated by metabolism, which is negligible due to the following two reasons: (1) within the ablated area, the biological tissue has lost its metabolic ability (due to cell death) and (2) in the non-ablated areas (where the tissues are healthy liver tissues in this study), the heat generated by metabolism is small compared with the other terms in Eq. (2.1) (note that according to [97], the maximum percentage of the metabolic heat is only 0.2% under 10 volts of the applied voltage with 1 MHz), and $Q_{hs}(\mathbf{x}, t)$ (W m^{-3}) is the spatial heat generated by the RF electrical current, which is given as follows:

$$Q_{hs}(\mathbf{x},t) = \boldsymbol{J} \cdot \boldsymbol{E} = \left(\sigma + \epsilon_0 \epsilon_r \frac{\partial}{\partial t}\right)(-\nabla V) \cdot (-\nabla V) \tag{2.2}$$

where $\boldsymbol{J}$ (A m^{-2}) is the current density, $\boldsymbol{E}$ (V m^{-1}) is the electric file intensity, σ (S m^{-1}) is the electrical conductivity, $\epsilon_0 = 8.8541 \times 10^{-12}$ ($\frac{\mathrm{F}}{\mathrm{m}}$) is the vacuum permittivity, ϵ_r is the relative permittivity of the material and relevant to the applied frequency (for example, at the frequency of RFA, $\epsilon_r = 2770$ for liver tissue. Thus, Eq. (2.2) is usually approximated by $\sigma|\nabla V|^2$), and V (V) is the applied voltage, which can be evaluated using Laplace's equation as follows:

$$\nabla \cdot \sigma \nabla V = 0 \tag{2.3}$$

The Pennes bioheat transfer equation approximates the heat transfer between small blood vessels and heated tissue, with the term $\rho_b c_b \omega_b (T(\mathbf{x}, t) - T_b)$ acting as a heat sink [53]. The Pennes model assumes that blood enters heated tissue at the arterial temperature, T_b, and leaves at an equilibrated temperature, $T(\mathbf{x}, t)$, which is the same as the heated tissue temperature (namely, thermal equilibration presumably occurs in the capillary bed), regardless of the size of blood vessels and the counter-current flow in the target tissue. Although these assumptions have been questioned for many years, and various improved models have been proposed [54-56], besides RFA, the Pennes model is also used in the computational modelling of other thermal therapies, such as microwave ablation (MWA) [57], high-intensity focused ultrasound (HIFU) [51], and laser ablation [58]. The reasons can be given as [59]: (1) the improved models accounting for the effects of vessel size and counter-current flow require knowledge of the complex anatomy of the vasculature in a specific tissue, which is often unknown beforehand and (2) many *in vivo* and *in vitro* experimental studies have verified the applicability of the Pennes model in tissues where small blood vessels $<$0.3 mm in diameter dominate. However, attention should be paid to the large blood vessels $\geq$0.3 mm in diameter in computational modelling because these blood vessels have a significant cooling effect on heated tissue, which is, however, not considered in the Pennes model. The method to solve this problem is to model the structure of the blood vessels in the target tissue as realistically as possible.

One of the factors that can significantly affect the accuracy of a computational model using the Pennes model is the blood perfusion rate, ω_b. Thus, many studies have focused on the modelling of ω_b by using more realistic vasculature data. There are two cases in the modelling of ω_b, *in vitro* and *in vivo*. For an *in vitro* situation, the blood perfusion is not taken into consideration by setting $\omega_b = 0$ because the blood source is cut off in this situation. For an *in vivo* situation, several models have been used in prior studies to describe the change of blood perfusion rate. In the early stages of the computational modelling of RFA, ω_b was usually considered as a constant [60-62]. However, further studies have shown that ω_b is strongly dependent on both the heating temperature and the ablation time [59,63]. Thus, given the characteristics of the temperature and time dependence, various dynamic models have been used in the literature to describe ω_b, such as the piecewise function model [63,64] and the models that consider injury to the vasculature [65,66].

The accuracy of the computational model of RFA is also dependent on the modelling of physical properties of biological tissue (σ, k, ρ, and c). Usually, the values of these properties can be found in previous *in vivo* or *in vitro* experimental literature [67-71]. Many researchers assume that these properties are taken as constants in the computational modelling of RFA. However, more and more studies [72-74] are considering the temperature-dependence of these properties in a more realistic way, especially thermal and electrical conductivities (k and σ). For k and σ, the most used models can be given as follows: below 100 ℃, σ increases exponentially [72,75] or linearly [76,77] with the increase of temperature and then drops to a value close to zero when the temperature is above 100 ℃ due to water evaporation. It is noted that σ is also found to be affected by the frequency of applied RF power in a previous study [47]. Below 100 ℃, k is also modelled as experiencing linear growth with the increase of temperature and then remaining constant when the temperature is above 100 ℃ [72]. By considering the phase change of biological tissue, especially at temperatures above 100 ℃, several researchers have also considered the temperature dependence of density and specific heat of biological tissues [66,78]. In this situation, ρ and c are also modelled as functions of the temperature. However, this situation is mainly considered in the procedure of MWA, which usually uses a higher temperature than RFA to ablate the target tissue. MWA is able to heat target tissue well above 100 ℃ and maintain this temperature for several minutes [57].

Another issue that should be addressed is the inhomogeneity of biological tissues during the RFA treatment. It is worth mentioning that computational modelling with realistic human anatomy [50] or a two-compartment model [79] is of vital importance for predicting the size of TTN.

2.3.2 Mechanism and mathematical modelling of RFA-induced biological tissue death

The process of biological tissue destruction occurs in at least two phases in the procedure of RFA, through direct and indirect mechanisms [80]. As shown in Figure 2.5, three zones can be found in the biological tissue under the treatment of RFA, such as the coagulation necrosis zone, the sub-lethal damage zone, and the normal tissue zone [7].

For the coagulation necrosis zone, it exists immediately around the RF electrode, and it undergoes ablation-induced coagulation necrosis. Direct destruction occurs in this zone at several levels, from the sub-cellular level to the tissue

level. In this zone, cell membrane collapse is considered a major cause of RFA-induced cell death due to the change of cell membrane fluidity and permeability. Protein denaturation is also taken as another major cause of tissue death. Major protein denaturation starts from 40 to 45 ℃, dependent on the heating rate, and continues to occur at more than 100 ℃ [59]. Above 60 ℃, protein denaturation occurs immediately, which leads to coagulation necrosis [80]. The inactivation of vital enzymes is an initial feature of injury [35]. Mitochondrial dysfunction has also been assumed to be relevant to the heat-induced injury due to the leakage of protons through the inner mitochondrial membrane [81].

For the sub-lethal damage zone, it is either undergoing apoptosis or recovering from reversible injury. Indirect destruction of biological tissue usually occurs in this zone. There are various phenomena relating to this area, such as metabolite accumulation and the inhibition of DNA replication due to heat-mediated reproductive cell death [82]. For tumour ablation, cytokine release and further stimulation of an immune response can be found in this zone [80,83]. Various preclinical and clinical studies have shown that the induction of apoptosis, ischaemia due to vascular damage and the release of lysosomal contents can occur because of indirect damage, even after cessation of RFA [80,83].

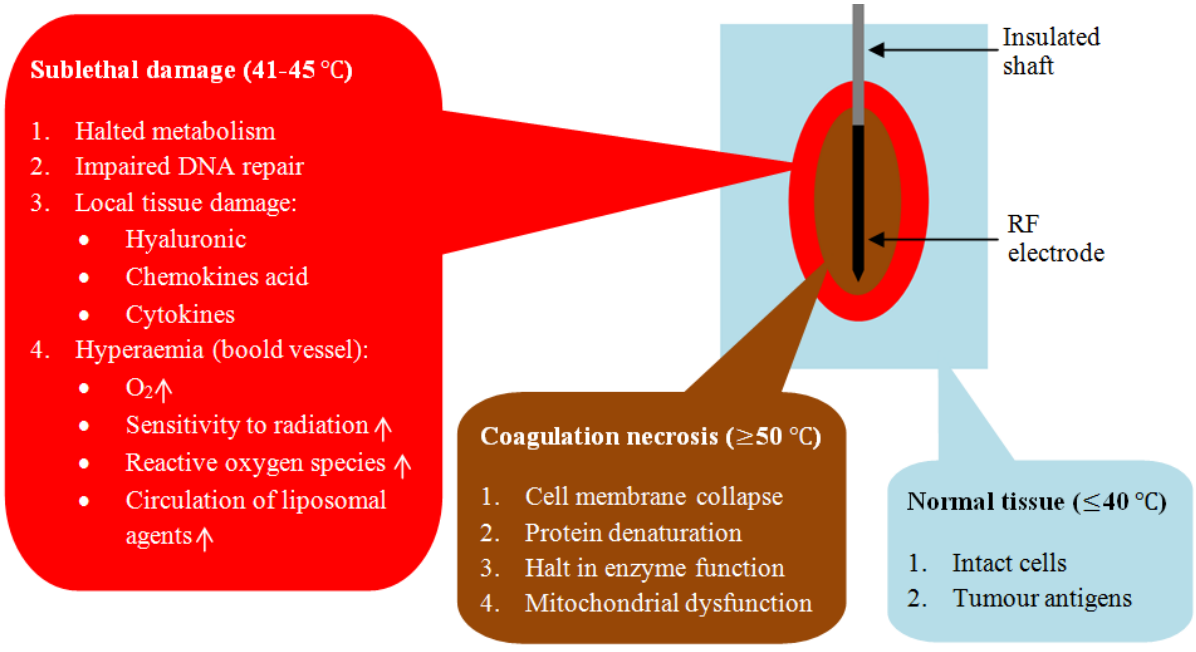

Figure 2.5. Zones of biological tissue in the treatment of RFA (adapted from [35]).

The normal tissue zone is unaffected by ablation and maintains its natural state with the release of tumour antigens from nearby lymph nodes.

To evaluate and compare the tissue death in various RFA protocols, several theoretical models have been used in the computational modelling of RFA, such as isotherm contour, thermal isoeffective dose (TID) and Arrhenius models. For the method of isotherm contour, 50 ℃ was the most frequently used temperature to evaluate the tissue death in the computational modelling of RFA [78,84] because Panescu et al. [85] concluded that the *in vivo* TTN volume after RFA can be defined by the volume enclosed by the 50 ℃ isotherm contour in their study. However, other researchers have claimed that using the 50 ℃ isotherm contour may overestimate the size of TTN. Thus, 55 [86] and 59 ℃ [87] isotherm contours have also been used. As discussed before, the death of biological tissue in RFA is dependent not only on the local temperature but also the target tissue type and ablation time. Thus, TID [50,88,89] and Arrhenius [26,43,50,84] models have been used in the computational modelling of RFA.

The TID model derives an equivalent ablation time (thermal dose) at a reference temperature (usually 43 ℃) from the actual temperature history [90]. Thus, the TID model is usually measured in cumulative equivalent minutes at 43 ℃ (CEM_{43}), which can be calculated as follows:

$$\mathrm{CEM}_{43} = \sum_{i=1}^{N} [R_{CEM}]^{(43-T_i)} t_i \tag{2.4}$$

where R_{CEM} is a dimensionless factor, and T_i ℃ is the constant temperature, which is applied for the time t_i (min). In a previous study [88], the value of R_{CEM} was set as 0.25 and 0.5 for temperatures below and above 43 ℃, respectively. The tissue can be considered dead when the value of CEM_{43} equals 120 or 240 min [59]. However, the TID model is only able to predict the tissue death caused by lower temperatures, such as 43-50 ℃. For temperatures ≥50 ℃, it is considered inapplicable [90].

The Arrhenius model is the most used method for predicting tissue death in the computational modelling of RFA by using a first-order irreversible kinetic equation, which is given as follows:

$$\Omega(t) = \int_0^t A e^{\frac{-\Delta E}{RT(\tau)}} d\tau \tag{2.5}$$

where $\Omega(t)$ is the degree of tissue death, A (s^{-1}) is the frequency factor, ΔE (J mol^{-1}) is the activation energy for the irreversible damage reaction, R (J mol^{-1} K^{-1}) is the universal gas constant, and $T(\tau)$ (K) is the absolute temperature, which is a function of the ablation time. It is noted that A and ΔE account for the morphological changes in tissue related to the thermal degradation of proteins [91] and dependent on the tissue type [92]. There are two primary values of Arrhenius damage that are used in the literature, $\Omega(t) = 1$ and $\Omega(t) = 4.3$, corresponding to 63% and 99% tissue cell death, respectively. It is noted that the TID model is based on the Arrhenius model, but assumes that temperature varies only within a small range [90]. However, when the information of A and ΔE in the Arrhenius model is unknown, TID model can be used to find A and ΔE with the experiment and model fit procedure [90].

2.3.3 Validation of the mathematical models of RFA

Although a computer model using realistic values exists in previous academic literature, validation using *in vivo* or *in vitro* experimental results is still necessary and important. The primary experimental measurements of interest of RFA are the temperature gradient or profile and the TTN size to validate the accuracies of the used computer models or the conclusions of new RFA protocols in computational modelling. Several studies have compared numerically evaluated TTN size using an isotherm profile with an experimentally measured TTN size using visual examination or imaging analysis. For example, Lim et al. [46] compared the temperature profile from a 3D FE model with a greyscale image from *in vitro* experiments after 10 and 15 min treatments of RFA using liver tissues. They demonstrated that the TTN sizes of a 3D FE model using an isotherm contour of 47 ℃ have good agreement with those determined experimentally, regardless of ablation time. Furthermore, Gonzalez-Suarez et al. [44,93] measured the experimentally determined TTN size assessed by the central ‘pale zone’, which corresponds to protein denaturation (coagulation necrosis zone) as shown in Figure 2.5. They compared the size of the pale zone in the experiments with the size of $\Omega(t) = 1$ in the computer model. Similarly, in a study of Arenas et al. [84], the size of the pale zone was measured and compared with the size of an isotherm contour of 60 ℃ obtained from a computer model to validate the accuracy of the utilized computer model. However, measuring the central pale zone most likely underestimates the size of the dead zone. As shown in Figure 2.5, a narrow zone (sub-lethal damage zone)

around the central pale zone, where the tissue cells are dead but the proteins are not denatured completely to become whitish, can be revealed by the triphenyl tetrazolium chloride (TTC) staining technique.

Temperature measurement is another method that can be used in the validation of computational modelling. To verify the findings obtained from the computer model, Trujillo et al. [15] measured the temperatures of three points close to the electrode surface in an experimental study on *in vitro* bovine liver tissue using three ultra-fine thermocouples. The technique of thermo-sensitive MRI contrast agents also has the potential for use in the measurement of temperature during the procedure of RFA. The state of the contrast agent will change when the temperature increases from the physiological temperature to the phase transition temperature [94].

2.4 Temperature-controlled RFA

Temperature is the most important factor in the RFA procedure and directly determines the death of the target tissue cells and the efficacy of various RFA protocols. Therefore, a feedback control strategy for the temperature of the target tissue should be a promising method to overcome the deficiency of RFA (failure in the treatment of tumours ≥ 3 cm in diameter). A straightforward means to control the charring of the target tissue is to measure the temperature of the target tissue in real-time or via the RFA procedure.

There are only a small number of studies [45,95,96] concerning the issue of temperature-controlled RFA in the literature. Further, these studies only obtain information of the temperature around the area of the tip of the RF electrode for feedback control. This is because it is much easier to have a sensor installed in the RF applicator (Figure 2.6) than to have a sensor on the target tissue. For the convenience of subsequent discussions, the feedback control strategy based on the temperature information of the electrode is called electrode-based temperature control. Alba-Martinez et al. [45] took the electrode-based feedback control strategy and devised a PI controller in an RFA system for cardiac tissue using two different RF applicators, as shown in Figure 2.6. They found no significant variations in the size of TTN among the tissues with various thermal and electrical properties and different control parameters K_p and K_i. In a more recent work, Jamil et al. [49] proposed a feedback strategy to control the temperature in the entire region of the target tissue such that it is less than a prescribed value (e.g. 100 ℃). No

detailed information is given in their work, and moreover, there was seemingly no experiment conducted to demonstrate that the approach may increase the size of TTN.

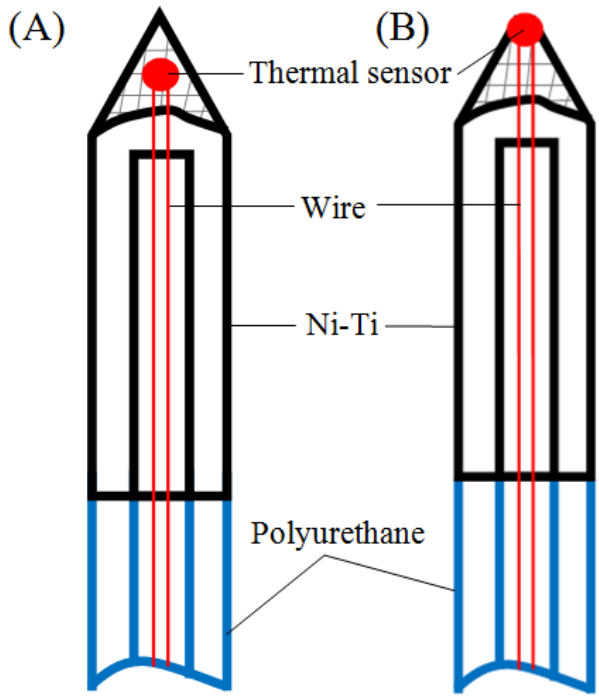

Figure 2.6. Typical RF applicators with a thermal sensor embedded at of the tip of RF electrode: no-contact (A) and contact (B) with the target tissue.

In contrast to the popular idea that the effective temperature control should be out of the target tissue, especially the areas around the middle part of the RF electrode, Trujillo et al. [15] showed that the roll-off usually occurs at the point where the charred tissue completely encircles the RF electrode, as shown in Figure 2.3. They have also verified that this closure usually completes in the tissue around the middle part of the RF electrode. Thus, the temperature of this area is quite critical to the occurrence of roll-off and further, to the size of TTN.

2.5 Conclusions and future issues

RFA has been applied in the treatment of different tumours due to its effectiveness, lower invasiveness, and lesser damage to normal tissue. RFA has a comparative overall survival rate with open surgery when it is used to treat

early and small tumours. Several recent studies also show that RFA can induce an immune response in non-ablated areas of the patient's body. The characteristic of immunotherapy makes RFA have a promising future with regard to expanding its application for different phases of tumours in different locations. However, the most critical factor that hinders RFA from developing or improving is its failure in the treatment of large tumours (i.e. ≥3 cm in diameter).

To address the 3-cm problem, great efforts should be made in all aspects of the RFA technique, especially in the following areas:

First, comprehensive understanding and evaluation of the current commercially available RFA systems is still needed. As mentioned above, there are many solutions that have been proposed to attempt to overcome the deficiency of current RFA systems. However, there is a lack of knowledge regarding the systematic evaluation of these solutions. Analysis and evaluation of current RFA systems from an engineering point of view are worthwhile, especially in regard to the failure of RFA in the treatment of large tumours ≥3 cm in diameter. Analysis and evaluation using engineering methods are able to touch the solution principles of current RFA systems and help researchers understand the deficiency from a conceptual design level. Further, the 3-cm problem of current RFA systems is most likely addressable in a comprehensive manner.

Second, understanding of the underlying mechanism behind the 3-cm problem with RFA is needed. All results regarding the size limit of 3-cm in diameter of current RFA systems come from clinical settings. There is not any understanding of the mechanism of this conclusion in current RFA systems using a theoretical modelling method. We are inclined to believe that a proof of the size limit can consolidate the results from clinical settings and assist clinicians in strategically planning the protocols of RFA. Several interesting findings regarding the changes of temperature and charred tissue when the current RFA systems reach their limit in treating tumours is also worth investigating.

Third, improved RFA protocols that are able to overcome the 3-cm restriction are needed. One of the methods that is able to overcome the 3-cm restriction of current RFA systems may be the temperature controlled RFA, especially when the temperature of the target tissue is going to be controlled and optimised. To measure and control the target

tissue temperature, improvements must be made to the RF electrode of current RFA systems for minimal invasiveness.

Acknowledgments

This article was supported by the Saskatchewan Health Research Foundation (SHRF) through the 'BioNEMS Phase I' grant and the National Natural Science Foundation of China (grant no. 51175179). The first author (Bing Zhang) also received financial support from the China Scholarship Council (CSC) for this research.

REFERENCES

1. Solbiati L, Livraghi T, Goldberg SN, Ierace T, Meloni F, Dellanoce M, et al. Percutaneous radio-frequency ablation of hepatic metastases from colorectal cancer: Long-term results in 117 Patients. Radiology 2001;221:159-66.
2. Gillams A, Khan Z, Osborn P, Lees W. Survival after radiofrequency ablation in 122 patients with inoperable colorectal lung metastases. Cardiovasc Intervent Radiol 2013;36:724-30.
3. Zagoria RJ, Pettus JA, Rogers M, Werle DM, Childs D, Leyendecker JR. Long-term outcomes after percutaneous radiofrequency ablation for renal cell carcinoma. Urology 2011;77:1393-7.
4. Ogura K, Miyake R, Shiina S, Shinoda Y, Okuma T, Kobayashi H, et al. Bone radiofrequency ablation combined with prophylactic internal fixation for metastatic bone tumor of the femur from hepatocellular carcinoma. Int J Clin Oncol 2012;17:417-21.
5. Kinoshita T, Iwamoto E, Tsuda H, Seki K. Radiofrequency ablation as local therapy for early breast carcinomas. Breast Cancer 2011;18:10-7.
6. Zhang B, Moser M, Zhang E, Zhang W. Radiofrequency ablation technique in the treatment of liver tumours: Review and future issues. J Med Eng Technol 2013;37:150-9.
7. Ahmed M, Brace CL, Lee Jr FT, Goldberg SN. Principles of and advances in percutaneous ablation. Radiology 2011;258:351-69.
8. Xu H-X, Lu M-D, Xie X-Y, Yin X-Y, Kuang M, Chen J-W, et al. Prognostic factors for long-term outcome after percutaneous thermal ablation for hepatocellular carcinoma: A survival analysis of 137 consecutive patients. Clin Radiol 2005;60:1018-25.
9. Llovet JM, Bruix J. Novel advancements in the management of hepatocellular carcinoma in 2008. J Hepatol 2008;48:S20-37.
10. Gory I, Fink M, Bell S, Gow P, Nicoll A, Knight V, et al. Radiofrequency ablation versus resection for the treatment of early stage hepatocellular carcinoma: A multicenter Australian study. Scand J Gastroenterol 2015;50:567-76.
11. Guglielmi A, Ruzzenente A, Valdegamberi A, Pachera S, Campagnaro T, D'Onofrio M, et al. Radiofrequency ablation versus surgical resection for the treatment of hepatocellular carcinoma in cirrhosis. J Gastroint Surg 2008;12:192-8.

12. Hiraoka A, Horiike N, Yamashita Y, Koizumi Y, Yamamoto Y, Hasebe A, et al. Efficacy of radiofrequency ablation therapy compared to surgical resection in 164 patients in Japan with single hepatocellular carcinoma smaller than 3 cm, along with report of complications. Hepatogastroenterology 2008;55:2171-4.
13. Zhou Y, Zhao Y, Li B, Xu D, Yin Z, Xie F, et al. Meta-analysis of radiofrequency ablation versus hepatic resection for small hepatocellular carcinoma. BMC Gastroenterol 2010;10:78.
14. Brace CL. Radiofrequency and microwave ablation of the liver, lung, kidney, and bone: What are the differences? Curr Probl Diagn Radiol. 2009;38:135-43.
15. Trujillo M, Alba J, Berjano E. Relationship between roll-off occurrence and spatial distribution of dehydrated tissue during RF ablation with cooled electrodes. Int J Hyperthermia 2012;28:62-8.
16. Gillams A, Lees W. Five-year survival in 309 patients with colorectal liver metastases treated with radiofrequency ablation. Eur Radiol 2009;19:1206-13.
17. N'Kontchou G, Mahamoudi A, Aout M, Ganne- Carrié N, Grando V, Coderc E, et al. Radiofrequency ablation of hepatocellular carcinoma: Long- term results and prognostic factors in 235 Western patients with cirrhosis. Hepatology 2009;50:1475-83.
18. Shiina S, Tateishi R, Arano T, Uchino K, Enooku K, Nakagawa H, et al. Radiofrequency ablation for hepatocellular carcinoma: 10-year outcome and prognostic factors. Ame J Gastroenterol 2011;107:569-77.
19. Hung HH, Chiou YY, Hsia CY, Su CW, Chou YH, Chiang JH, et al. Survival rates are comparable after radiofrequency ablation or surgery in patients with small hepatocellular carcinomas. Clin Gastroenterol Hepatol 2011;9:79-86.
20. Baldwin K, Katz SC, Rubin A, Somasundar P. Bipolar radiofrequency ablation of liver tumors: Technical experience and interval follow- up in 22 patients with 33 ablations. J Surg Oncol 2012;106:905-10.
21. Solbiati L, Ahmed M, Cova L, Ierace T, Brioschi M, Goldberg SN. Small liver colorectal metastases treated with percutaneous radiofrequency ablation: Local response rate and long-term survival with up to 10-year follow-up. Radiology 2012;265:958-68.
22. Psutka SP, Feldman AS, McDougal WS, McGovern FJ, Mueller P, Gervais DA. Long-term oncologic outcomes after radiofrequency ablation for T1 renal cell carcinoma. Eur Urol 2013;63:486-92.

23. Van Tilborg A, Meijerink M, Sietses C, Van Waesberghe J, Mackintosh M, Meijer S, et al. Long-term results of radiofrequency ablation for unresectable colorectal liver metastases: A potentially curative intervention. Br J Radiol 2011;84:556-65.

24. Haemmerich D, Lee FT, Schutt DJ, Sampson LA, Webster JG, Fine JP, et al. Large-volume radiofrequency ablation of ex vivo bovine liver with multiple cooled cluster electrodes. Radiology 2005;234:563-8.

25. Ahmed M, Solbiati L, Brace CL, Breen DJ, Callstrom MR, Charboneau JW, et al. Image-guided tumor ablation: standardization of terminology and reporting criteria—a 10-year update. Radiology 2014;273:241-60.

26. Trujillo M, Berjano E. Review of the mathematical functions used to model the temperature dependence of electrical and thermal conductivities of biological tissue in radiofrequency ablation. Inte J Hyperthermia 2013;29:590-7.

27. Ahmed M, Tasawwar B, Goldberg SN. Tumor ablation: An evolving technology. Image-Guided Cancer Therapy: A Multidisciplinary Approach 2013:1-19.

28. Goldberg S, Solbiati L, Hahn P, Cosman E, Conrad J, Fogle R, et al. Large-volume tissue ablation with radio frequency by using a clustered, internally cooled electrode technique: Laboratory and clinical experience in liver metastases. Radiology 1998;209:371-9.

29. Deneke T, Schade A, Mueller P, Schmitt R, Christopoulos G, Krug J, et al. Acute safety and efficacy of a novel multipolar irrigated radiofrequency ablation catheter for pulmonary vein isolation. J Cardiovasc Electrophysiol 2014;25:339-45.

30. Yuyun MF, Stafford PJ, Sandilands AJ, Samani NJ, Andre Ng G. The impact of power output during percutaneous catheter radiofrequency ablation for atrial fibrillation on efficacy and safety outcomes: A systematic review. J Cardiovasc Electrophysiol 2013;24:1216-23.

31. Rempp H, Voigtländer M, Schenk M, Enderle MD, Scharpf M, Greiner TO, et al. Internally gas-cooled radiofrequency applicators as an alternative to conventional radiofrequency and microwave ablation devices: An in vivo comparison. Eur J Radiol 2013;82:e350-5.

32. Tsuchiya K, Asahina Y, Tamaki N, Yasui Y, Hosokawa T, Ueda K, et al. Risk factors for exceeding the Milan criteria after successful radiofrequency ablation in patients with early-stage hepatocellular carcinoma. Liver Transpl 2014;20:291-7.

33. Moussa M, Goldberg SN, Kumar G, Sawant RR, Levchenko T, Torchilin V, et al. Radiofrequency ablation–induced upregulation of hypoxia-inducible factor-1α can be suppressed with adjuvant bortezomib or liposomal chemotherapy. J Vasc Interv Radiol 2014;25:1972-82.

34. Peng Z-W, Zhang Y-J, Chen M-S, Xu L, Liang H-H, Lin X-J, et al. Radiofrequency ablation with or without transcatheter arterial chemoembolization in the treatment of hepatocellular carcinoma: A prospective randomized trial. J Clin Oncol 2013;31:426-32.

35. Chu KF, Dupuy DE. Thermal ablation of tumours: biological mechanisms and advances in therapy. Nat Rev Cancer 2014;14:199-208.

36. Mayer R, Hamilton-Farrell MR, van der Kleij AJ, Schmutz J, Granström G, Sicko Z, et al. Hyperbaric oxygen and radiotherapy. Strahlenther Onkol 2005;181:113-23.

37. Solazzo SA, Ahmed M, Schor-Bardach R, Yang W, Girnun GD, Rahmanuddin S, et al. Liposomal doxorubicin increases radiofrequency ablation-induced tumor destruction by increasing cellular oxidative and nitrative stress and accelerating apoptotic pathways. Radiology 2010;255:62-74.

38. Lee ES, Lee JM, Kim WS, Choi SH, Joo I, Kim M, et al. Multiple-electrode radiofrequency ablations using Octopus® electrodes in an in vivo porcine liver model. Br J Radiol 2012;85:e609-15.

39. Yoon JH, Lee JM, Hwang EJ, Hwang IP, Baek J, Han JK, et al. Monopolar radiofrequency ablation using a dual-switching system and a separable clustered electrode: Evaluation of the In vivo efficiency. Korean J Radiol 2014;15:235-44.

40. Morimoto M, Numata K, Kondou M, Nozaki A, Morita S, Tanaka K. Midterm outcomes in patients with intermediate-sized hepatocellular carcinoma. Cancer 2010;116:5452-60.

41. Lu Z, Wen F, Guo Q, Liang H, Mao X, Sun H. Radiofrequency ablation plus chemoembolization versus radiofrequency ablation alone for hepatocellular carcinoma: a meta-analysis of randomized-controlled trials. Eur J Gastroenterol Hepatol 2013;25:187-94.

42. Romero-Méndez R, Tobajas P, Burdío F, Gonzalez A, Navarro A, Grande L, et al. Electrical-thermal performance of a cooled RF applicator for hepatic ablation with additional distant infusion of hypertonic saline: In vivo study and preliminary computer modeling. Int J Hyperthermia 2012;28:653-62.

43. Trujillo M, Ribera V, Quesada R, Berjano E. Applicator for RF thermokeratoplasty: feasibility study using theoretical modeling and ex vivo experiments. Ann Biomed Eng 2012;40:1182-91.

44. González-Suárez A, Trujillo M, Burdío F, Andaluz A, Berjano E. Feasibility study of an internally cooled bipolar applicator for RF coagulation of hepatic tissue: Experimental and computational study. Int J Hyperthermia 2012;28:663-73.

45. Alba-Martínez J, Trujillo M, Blasco-Giménez R, Berjano E. Could it be advantageous to tune the temperature controller during radiofrequency ablation? A feasibility study using theoretical models. Int J Hyperthermia 2011;27:539-48.

46. Lim D, Namgung B, Woo DG, Choi JS, Kim HS, Tack GR. Effect of input waveform pattern and large blood vessel existence on destruction of liver tumor using radiofrequency ablation: Finite element analysis. J Biomech Eng. 2010;132:061003.

47. Haemmerich D, Schutt DJ. RF ablation at low frequencies for targeted tumor heating: In vitro and computational modeling results. IEEE Trans Biomed Eng 2011;58:404-10.

48. Pérez JJ, d'Avila A, Aryana A, Berjano E. Electrical and Thermal effects of esophageal temperature probes on radiofrequency catheter ablation of atrial fibrillation: Results from a computational modeling study. J Cardiovasc Electrophysiol 2015;26:556-64.

49. Jamil MaN, EYK. Quantification of the effect of electrical and thermal parameters on radiofrequency ablation for concentric tumour model of different sizes. J Therm Biol 2015;51:23-32.

50. Zorbas G, Samaras T. Simulation of radiofrequency ablation in real human anatomy. Int J Hyperthermia 2014;30:570-8.

51. Prakash P, Salgaonkar VA, Diederich CJ. Modelling of endoluminal and interstitial ultrasound hyperthermia and thermal ablation: Applications for device design, feedback control and treatment planning. Int J Hyperthermia 2013;29:296-307.

52. Scott SJ, Salgaonkar V, Prakash P, Burdette EC, Diederich CJ. Interstitial ultrasound ablation of vertebral and paraspinal tumours: Parametric and patient-specific simulations. Int J Hyperthermia 2014;30:228-44.

53. Pennes HH. Analysis of tissue and arterial blood temperatures in the resting human forearm. J Appl Physiol 1948;1:93-122.

54. Diller KR, Valvano JW, Pearce JA. Bioheat transfer. CRC Handbook of Thermal Engineering. 2000;4:114-215.

55. Arkin H, Xu L, Holmes K. Recent developments in modeling heat transfer in blood perfused tissues. IEEE Trans Biomed Eng 1994;41:97-107.

56. Charny CK. Mathematical models of bioheat transfer. Advances in Heat Transfer 1992;22:19-155.

57. Chiang J, Birla S, Bedoya M, Jones D, Subbiah J, Brace CL. Modeling and validation of microwave ablations with internal vaporization. IEEE Trans Biomed Eng 2014;62:657-63.

58. Manuchehrabadi N, Zhu L. Development of a computational simulation tool to design a protocol for treating prostate tumours using transurethral laser photothermal therapy. Int J Hyperthermia 2014;30:349-61.

59. He X. Thermostability of biological systems: fundamentals, challenges, and quantification. Open Biomed Eng J 2011;5:47-73.

60. Haemmerich D, Tungjitkusolmun S, Staelin ST, Lee Jr FT, Mahvi DM, Webster JG. Finite-element analysis of hepatic multiple probe radio-frequency ablation. IEEE Trans Biomed Eng 2002;49:836-42.

61. Tungjitkusolmun S, Staelin ST, Haemmerich D, Tsai J-Z, Cao H, Webster JG, et al. Three-dimensional finite-element analyses for radio-frequency hepatic tumor ablation. IEEE Trans Biomed Eng 2002;49:3-9.

62. Tungjitkusolmun S, Woo E, Cao H, Tsai J, Vorperian V, Webster J. Thermal—electrical finite element modelling for radio frequency cardiac ablation: effects of changes in myocardial properties. Med Biol Eng Comput 2000;38:562-8.

63. Liu Z, Ahmed M, Sabir A, Humphries S, Goldberg S. Computer modeling of the effect of perfusion on heating patterns in radiofrequency tumor ablation. Int J Hyperthermia 2007;23:49-58.

64. Zhu Q, Shen Y, Zhang A, Xu LX. Numerical study of the influence of water evaporation on radiofrequency ablation. Biomed Eng Online. 2013;12:127.

65. He X, McGee S, Coad J, Schmidlin F, Iaizzo P, Swanlund D, et al. Investigation of the thermal and tissue injury behaviour in microwave thermal therapy using a porcine kidney model. Int J Hyperthermia 2004;20:567-93.

66. Bourantas GC, Ghommem M, Kagadis GC, Katsanos K, Loukopoulos VC, Burganos VN, et al. Real-time tumor ablation simulation based on the dynamic mode decomposition method. Medi Phys 2014;41:053301.

67. Gabriel C, Gabriel S, Corthout E. The dielectric properties of biological tissues: I. Literature survey. Phy Med Biol 1996;41:2231-49.

68. Duck FA. Physical properties of tissues: A comprehensive reference book: Academic Press; 2013.

69. Haemmerich D, Schutt DJ, Wright AS, Webster JG, Mahvi DM. Electrical conductivity measurement of excised human metastatic liver tumours before and after thermal ablation. Physiol Meas 2009;30:459-66.

70. Haemmerich D, Staelin S, Tsai J, Tungjitkusolmun S, Mahvi D, Webster J. In vivo electrical conductivity of hepatic tumours. Physiol Meas 2003;24(2):251-60.

71. Prakash S, Karnes M, Sequin E, West J, Hitchcock C, Nichols S, et al. Ex vivo electrical impedance measurements on excised hepatic tissue from human patients with metastatic colorectal cancer. Physiol Meas 2015;36(2):315-28.

72. Jo B, Aksan A. Prediction of the extent of thermal damage in the cornea during conductive keratoplasty. J Therm Biol 2010;35:167-74.

73. Haemmerich D, Chachati L, Wright AS, Mahvi DM, Lee Jr FT, Webster JG. Hepatic radiofrequency ablation with internally cooled probes: effect of coolant temperature on lesion size. IEEE Trans Biomed Eng 2003;50:493-500.

74. Jarrard J, Wizeman B, Brown RH, Mitzner W. A theoretical model of the application of RF energy to the airway wall and its experimental validation. Biomed Eng Online. 2010;9:81.

75. Berjano EJ, Alió JL, Saiz J. Modeling for radio-frequency conductive keratoplasty: Implications for the maximum temperature reached in the cornea. Physiol Meas 2005;26(3):157-72.

76. Miller SF, Geiger JD, Shih AJ. Thermal-electric finite element analysis and experimental validation of bipolar electrosurgical cautery. J Manuf Sci Eng 2008;130:021015.

77. Lau M, Hu B, Werneth R, Sherman M, Oral H, Morady F, et al. A theoretical and experimental analysis of radiofrequency ablation with a multielectrode, phased, duty- cycled system. Pacing Clin Electrophysiol 2010;33:1089-100.

78. Pérez JJ, Pérez-Cajaraville JJ, Muñoz V, Berjano E. Computer modeling of electrical and thermal performance during bipolar pulsed radiofrequency for pain relief. Med Phys 2014;41:071708.

79. Zorbas G, Samaras T. Parametric study of radiofrequency ablation in the clinical practice with the use of two-compartment numerical models. Electromagn Biol Med 2013;32:236-43.

80. Nikfarjam M, Muralidharan V, Christophi C. Mechanisms of focal heat destruction of liver tumors. J Surg Res 2005;127:208-23.

81. Willis W, Jackman M, Bizeau M, Pagliassotti M, Hazel J. Hyperthermia impairs liver mitochondrial function in vitro. Am J Physiol Regul Integr Comp Physiol 2000;278:R1240-6.

82. Warters RL, Roti JLR. Hyperthermia and the cell nucleus. Radiat Res 1982;92:458-62.

83. Fajardo LF, Egbert B, Marmor J, Hahn GM. Effects of hyperthermia in a malignant tumor. Cancer 1980;45:613-23.

84. Arenas J, Perez JJ, Trujillo M, Berjano E. Computer modeling and ex vivo experiments with a (saline-linked) irrigated electrode for RF-assisted heating. Biomed Eng Online 2014;13:164.

85. Panescu D, Whayne JG, Fleischman SD, Mirotznik MS, Swanson DK, Webster JG. Three-dimensional finite element analysis of current density and temperature distributions during radio-frequency ablation. IEEE Trans Biomed Eng 1995;42:879-90.

86. Huang H-W. Influence of blood vessel on the thermal lesion formation during radiofrequency ablation for liver tumors. Med phys 2013;40:073303.

87. Jain MK, Wolf PD. A three-dimensional finite element model of radiofrequency ablation with blood flow and its experimental validation. Ann Biomed Eng 2000;28:1075-84.

88. Prakash P, Diederich CJ. Considerations for theoretical modelling of thermal ablation with catheter-based ultrasonic sources: Implications for treatment planning, monitoring and control. Int J Hyperthermia 2012;28:69-86.

89. Pearce JA. Comparative analysis of mathematical models of cell death and thermal damage processes. Int J Hyperthermia 2013;29:262-80.

90. Reddy G, Dreher MR, Rossmann C, Wood BJ, Haemmerich D. Cytotoxicity of hepatocellular carcinoma cells to hyperthermic and ablative temperature exposures: In vitro studies and mathematical modelling. Int J Hyperthermia 2013;29:318-23.

91. Baldwin SA, Pelman A, Bert JL. A heat transfer model of thermal balloon endometrial ablation. Ann Biomed Eng 2001;29:1009-18.

92. Chang IA, Nguyen UD. Thermal modeling of lesion growth with radiofrequency ablation devices. Biomed Eng Online 2004;3:27.

93. González-Suárez A, Trujillo M, Burdío F, Andaluz A, Berjano E. Could the heat sink effect of blood flow inside large vessels protect the vessel wall from thermal damage during RF-assisted surgical resection? Med Phys 2014;41:083301.

94. Berjano EJ. Theoretical modeling for radiofrequency ablation: state-of-the-art and challenges for the future. Biomed Eng Online 2006;5:24.

95. Haemmerich D, Webster JG. Automatic control of finite element models for temperature-controlled radiofrequency ablation. Biomed Eng Online 2005;4:42.

96. Jain MK, Wolf PD. Temperature-controlled and constant-power radio-frequency ablation: what affects lesion growth? IEEE Trans Biomed Eng 1999;46:1405-12.

97. Lv YG, Deng ZS, Liu J. 3-D numerical study on the induced heating effects of embedded micro/nanoparticles on human body subject to external medical electromagnetic field. IEEE Trans NanoBiosci 2005;4:284-94.

3 EVALUATION OF THE CURRENT RADIOFREQUENCY ABLATION SYSTEMS USING AXIOMATIC DESIGN THEORY

This chapter is derived from an article published by SAGE Publications in ***Proceedings of the Institute of Mechanical Engineers, Part H: Journal of Engineering in Medicine*** *on April 1, 2014. Available online: http://www.sagepub.com/ doi:10.1177/0954411914530104.*

Abstract

This paper evaluates current Radiofrequency ablation (RFA) systems using axiomatic design theory (ADT). Due to its minimally invasive procedure, short-time hospital stay, low cost, and tumour metastasis treatment, the RFA technique has been playing an important role in tumour treatment in recent decades. Although the RFA technique has many advantages, some issues still need to be addressed. Among these issues, the two most important are (1) the size of tumours to be ablated (has to be larger than 3 cm in diameter) and (2) completeness of the ablation. Many device solutions have been proposed to address the two issues. However, there is a lack of knowledge regarding the systematic evaluation of these solutions. This paper evaluates these systems in terms of their solution principles (or simply called conceptual design in general product design theory) using a design theory called ADT. In addition, with the ADT, a better conceptual design in terms of its feasibility to cope with incomplete target tissue necrosis (TTN) from the large size of tumours has been found. The detailed analysis and simulation of the new conceptual design is conducted using finite element approach. The results in this paper are proved by the information of animal experiments and clinical practices obtained from the literature. This study thus contributes to the current knowledge to further developments in RFA systems and procedure guidelines for physicians to perform the RFA operation more effectively.

3.1 Introduction

Radiofrequency ablation (RFA) technique has been an alternative method for excision of many different tumours, such as liver, kidney, lung, bone, and so on [1,2]. This technique is usually used for patients who are not eligible for

resection due to various reasons, such as too many tumours, tumours in unresectable locations, insufficient tissue reserve to tolerate resection and other medical conditions that make patients poor surgical candidates [1]. The principle of the RFA technique is to use electromagnetic-generated heat to ablate target tissue (usually tumour tissue together with tissues surrounding the tumour tissue). Figure. 3.1 shows a generic RFA system currently available in literature and medical institutes, which consists of RF generator, RF applicator (RF electrode and insulated shaft), ground pads, and electrical wires. These components constitute a close electric circuit with the inclusion of the patient's body as a part of the circuitry element. Physicians could insert the RF electrode into the tumour tissue through a tiny incision on the skin under image guidance (e.g. CT scan or ultrasound) or through open surgery where the RF electrode is inserted just through the organ's capsule. The ground pads are placed on the thighs or back of the patient, where there is a relatively large contact area with the patient's skin. Ions (sodium, potassium, and chloride) inside the target tissue around the RF electrode are attracted to moving back and forth rapidly along the direction of the alternating current with high frequency (100 kHz - 3 MHz).

The frequency selected for the alternating current is in a safe range for the patient in which human nerve and muscle stimulation is avoided [3]. Frictional heat will be generated due to the motion of the ions. The immediate surrounding tissue around the RF electrode is rapidly heated due to the maximum current density around the RF electrode and the peripheral tissue is heated by thermal conduction at a relatively slower rate. When the tissue is heated to a temperature of approximately 45-50℃, protein denaturation results in irreversible tissue necrosis; when the temperature reaches above 100℃, tissue charring occurs [4] (Charring tissue could increase suddenly the impedance between RF electrode and ground pads, accompanying with a consequent drop of output RF power. We call this phenomenon 'roll-off'.).

The mechanism of the foregoing process is related to the conversion of electromagnetic energy into heat energy exhibited on the RF electrode. Specifically, when electromagnetic energy flows through a conductor, heat is generated from the conductor, which is seen as the conversion of electromagnetic energy into thermal energy. The heat transfer inside the target tissue during the RFA procedure is governed by the so-called Pennes bioheat transfer equation [5,6] with an outside energy source as shown in Appendix 3.1.

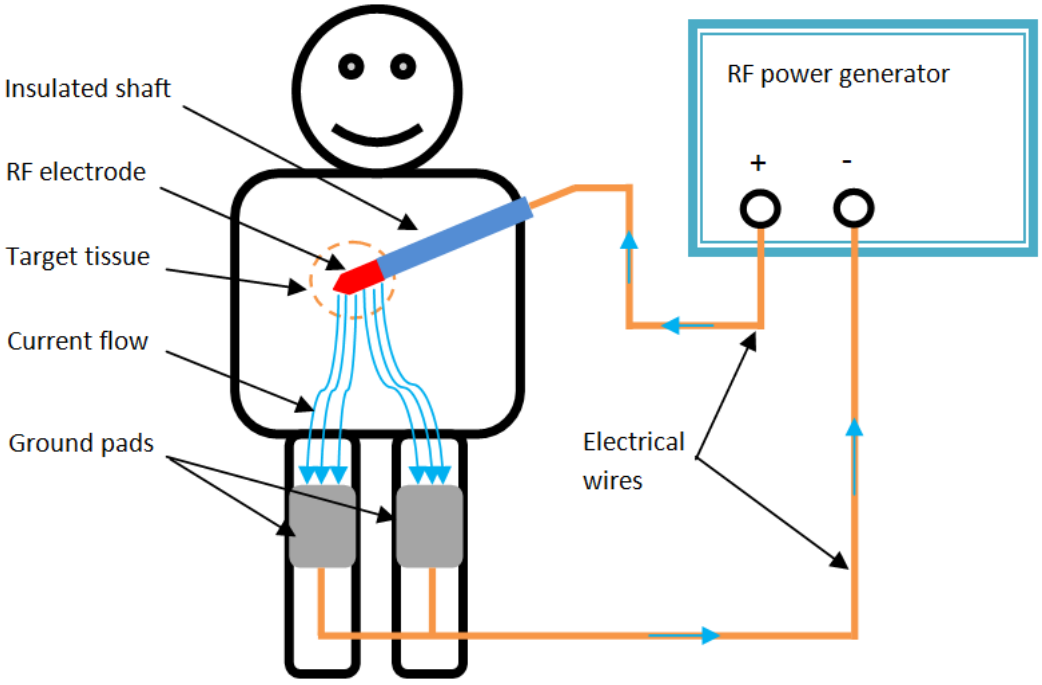

Figure 3.1. Overview of the typical current used RFA procedure.

3.2 Analysis of incomplete TTN

Although the RFA technique could initiate necrosis in the target tissue, the target tissue cannot be ablated completely in a single treatment session, especially for large target tissues (>3 cm in diameter). This incomplete ablation of target tissue increases the possibilities of local recurrences. It is well known that local recurrence is the main reason of failure with the RFA technique in the treatment of large tumours.

In summary, there are three main causes leading to this deficiency with the RFA technique (i.e. TTN).

The first cause is that the size of TTN in a single treatment session with the current RFA technique is small. In a previous study [7], a monopolar applicator (as shown in Figure 3.2) with a low RF power generator was proposed. The size of TTN is approximately 1.5 cm in diameter and 2 cm in length.

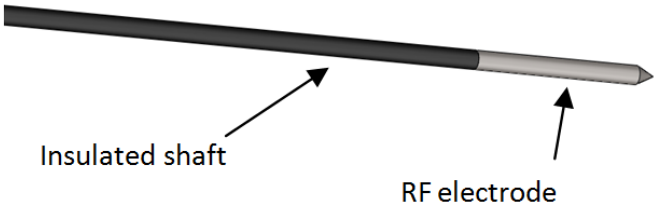

Figure 3.2. Monopolar RF applicator. (A typical RF applicator contains an insulated shaft and RF electrode. The proximal part of the applicator is connected to the RF power generator using electrical wires. The electrode is inserted into the target tissue through the percutaneous method, laparotomy, or open surgery.)

Many clinical studies have shown that the effectiveness of the RFA technique is quite low due to the small TTN [4,8-12]. Generally, the goal of the RFA technique is to destroy both the tumour and the normal tissue that surrounds the tumour tissue with a 0.5-1 cm margin [13]. After accounting for the marginal part of the tumour tissue, the largest tumour tissue RFA could ablate is only 1 cm in diameter according to another study [7]. Thus, the initial RFA systems cannot completely ablate tumour tissues larger than 1 cm.

The second cause is that the current diagnostic imaging system is not very accurate in measuring the profile of the target tissue. The current image-guided methods are Ultrasound Imaging (UI), Computer Tomography (CT), and Magnetic Resonance Imaging (MRI), and all of them have their own problems. The interested reader is referred to the literature [8] for further details.

The inaccurate placement of RF electrode is the third cause of the incomplete TTN. The image-guided methods are used not only to help detect tumour tissues and monitor the effect of the procedure but also to guide the electrode placement [14]. Due to inaccuracy with the image-guided methods, the electrode may be placed in the wrong position. Moreover, the physician's experience is important for the accurate placement of the electrode. Closely related to the placement of the electrode, the literature suggests open surgery [15,16] for the relatively complete ablation of the large target tissues by means of multiple electrode punctures at different angles with the RFA technique. However, open surgery is usually followed by drawbacks such as high complication rates and long hospital stays.

The result of incomplete TTN is that a great number of patients have lost their lives or had to accept more RFA treatment sessions due to the local recurrence of the tumour [9-12]. Many device solutions have been proposed to solve the incomplete TTN problem. Despite some clinic-based evaluations of these solutions, there is a lack of an engineering-oriented evaluation. An engineering-oriented evaluation is indeed important because it provides the root of the problem and thus is helpful in the development of a rational design of new devices. This paper reports a study conducted by our team to evaluate the existing device solutions using a design theory called Axiomatic Design Theory (ADT).

3.3 Brief introduction of ADT

ADT is a design theory and methodology that helps evaluate a design [17], and it has been applied to both design and management (selection) problems [18-22]. Further development of ADT can be found in the literature [23]. There are three salient points in ADT, which are design domain, design axiom, and hierarchy. According to the ADT, the design process takes place in four domains, as shown in Figure 3.3. In the four domains, there are Customer Attributes or Needs (CAs), Functional Requirements (FRs), Design Parameters (DPs), and Process Variables (PVs). The "{}" in Figure 3.3 are the characteristic vectors of each domain. The leftmost domain represents, "what we want to achieve," whereas the rightmost domain represents the design solution of "how we propose to satisfy the requirements in the left domain" [24]. There are two axioms in ADT, which are known as the independence and the information axiom. These two axioms could be expressed in detail as follows [17]:

Axiom 1: maintain the independence of the functional requirements.

Axiom 2: minimize the information content of the design.

Axiom 1 is discussed briefly in the following, as it is actually applied by the study described in the present paper.

CAs could be converted into FRs and Constraints (Cs) by the design process through a series of iterations, and in turn, FRs and Cs could be embodied into DPs [22]. FRs can be defined as "a minimum set of independent requirements that completely characterizes the functional needs of the system in the functional domain"; DPs are the "the key physical variables in the physical domain that characterizes the design that specifies the FRs" [17]. According to the ADT, the first step in evaluating a system is to determine the customer attributes or needs in the

customer domain that the system could satisfy; afterwards, the FRs and Cs in the functional domain are determined. The next step is to map these FRs into the physical domain to identify the DPs. DPs must be chosen such that first, there is no conflict with the Cs, and second, they fulfil the FRs [25].

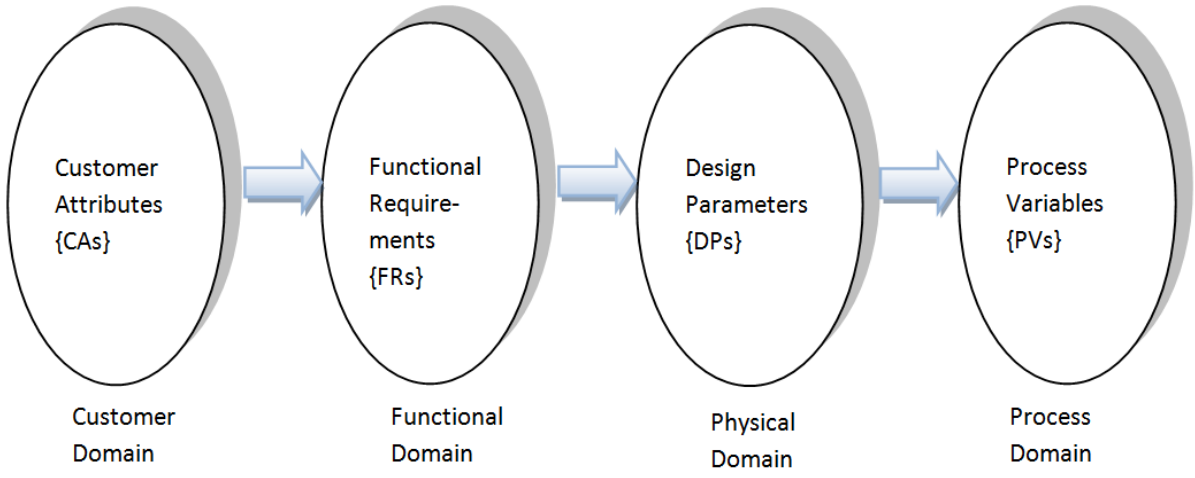

Figure 3.3. Design domains in the ADT

The relationship between the FRs and the DPs can be represented by the following equation:

$$\mathbf{FR} = [A]\mathbf{DP} \tag{3.1}$$

where $[A]$ is the design matrix. If matrix $[A]$ is a diagonal matrix, each FR could be satisfied by a particular DP, and such a design is called the uncoupled design. If matrix $[A]$ is a triangular matrix, the design should follow a sequence. If and only if the DPs are determined in this sequence, the independent axiom (i.e. Axiom 1) is satisfied, and this design is called the decoupled design. If the matrix $[A]$ is neither a diagonal matrix nor a triangular matrix (we do not consider all the elements in matrix $[A]$ are zeros), FRs cannot be determined by FRs independently, and this design is called the coupled design. Eqs. (3.2) through (3.4) show the three scenarios discussed above, assuming *n* FRs and *n* DPs. A coupled design can be decoupled by adding more DPs and this always comes at a cost.

$$\begin{bmatrix} \mathrm{FR}1 \\ \mathrm{FR}2 \\ \vdots \\ \mathrm{FR}n \end{bmatrix} = \begin{bmatrix} A_{11} & & & \\ & A_{22} & & \\ & & \ddots & \\ & & & A_{nn} \end{bmatrix} \begin{bmatrix} \mathrm{DP}1 \\ \mathrm{DP}2 \\ \vdots \\ \mathrm{DP}n \end{bmatrix} \tag{3.2}$$

$$\begin{bmatrix} \mathrm{FR1} \\ \mathrm{FR2} \\ \vdots \\ \mathrm{FR}n \end{bmatrix} = \begin{bmatrix} A_{11} & & & \\ A_{21} & A_{22} & \ddots & \\ \vdots & \vdots & & \\ A_{n1} & A_{n2} & \cdots & A_{nn} \end{bmatrix} \begin{bmatrix} \mathrm{DP1} \\ \mathrm{DP2} \\ \vdots \\ \mathrm{DP}n \end{bmatrix} \tag{3.3}$$

$$\begin{bmatrix} \mathrm{FR1} \\ \mathrm{FR2} \\ \vdots \\ \mathrm{FR}n \end{bmatrix} = \begin{bmatrix} A_{11} & A_{12} & \cdots & A_{1n} \\ A_{21} & A_{22} & \cdots & A_{2n} \\ \vdots & \vdots & \ddots & \vdots \\ A_{n1} & A_{n2} & \cdots & A_{nn} \end{bmatrix} \begin{bmatrix} \mathrm{DP1} \\ \mathrm{DP2} \\ \vdots \\ \mathrm{DP}n \end{bmatrix} \tag{3.4}$$

3.4 Engineering evaluation

3.4.1 Current RFA systems

To overcome the first cause of incomplete TTN in RFA systems (small TTN size), there are several design solutions for the RF electrode and RF power supply algorithm in the current RFA systems.

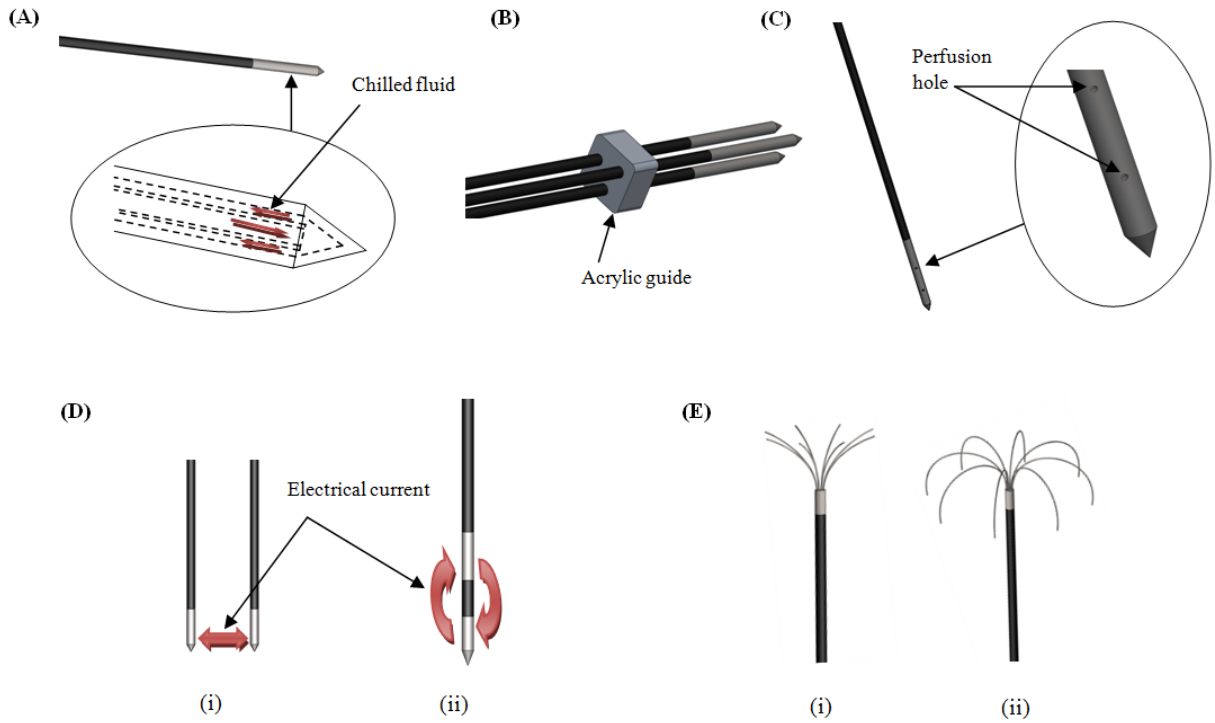

Figure 3.4. Schematic diagrams of current RF electrode designs: (A) internally cooled electrode, (B) cluster electrode, (C) perfusion electrode, (D) bipolar electrode, and (E) extendable electrode.

Figure 3.4 illustrates all of the typical RF electrode designs with the goal of generating large TTN. The designs are the internally cooled (Figure 3.4A), cluster (Figure 3.4B), perfusion (Figure 3.4C), bipolar (Figure 3.4D), and extendable electrode (Figure 3.4E), respectively.

The internally cooled electrode design usually has an internal lumen through which chilled fluid is circulated during RFA treatment. By cooling the electrode during the application of RF energy, it is possible to prevent tissue from charring and cavitation immediately adjacent to the electrode so as to increase RF energy output.

In the cluster electrode design, an acrylic guide usually maintains inter-needles distance, and the distance is a key parameter for RFA operation in the cluster electrode design.

The perfusion electrode design consists of a hollow electrode with one or more perfusion holes at the electrode through which an hypertonic saline solution is injected into the tissue that surrounds the electrode before and during the ablation procedure. As the saline solution (with relative lower temperature) could cool the tissue to prevent tissue from charring. The saline solution also can change the electrical and thermal properties of target tissue, which will make the tissues have better dielectric performance such that more RF energy can be delivered into target tissue.

In the bipolar electrode design, one of the two electrodes used as a ground pad is also inserted into the target tissue with a certain inter-needle distance with the active electrode. There are further two types of devices: (i) two electrodes and (ii) one electrode with two electrodes. In the case of (i), a larger necrosis area could be generated in the plane perpendicular to the electrode axis, and in the case of (ii), a larger necrosis area could be generated in the plane parallel to the electrode axis.

There are two main expandable electrode designs, namely Christmas tree-like fashion (i) and Umbrella-like fashion (ii). Other electrode designs that are not included in this paper are more or less similar to the foregoing designs.

For the RF power supply systems, there are also four typical designs: continuous, pulsed [26], consecutive, and switching supply [27], as shown in Figure 3.5.

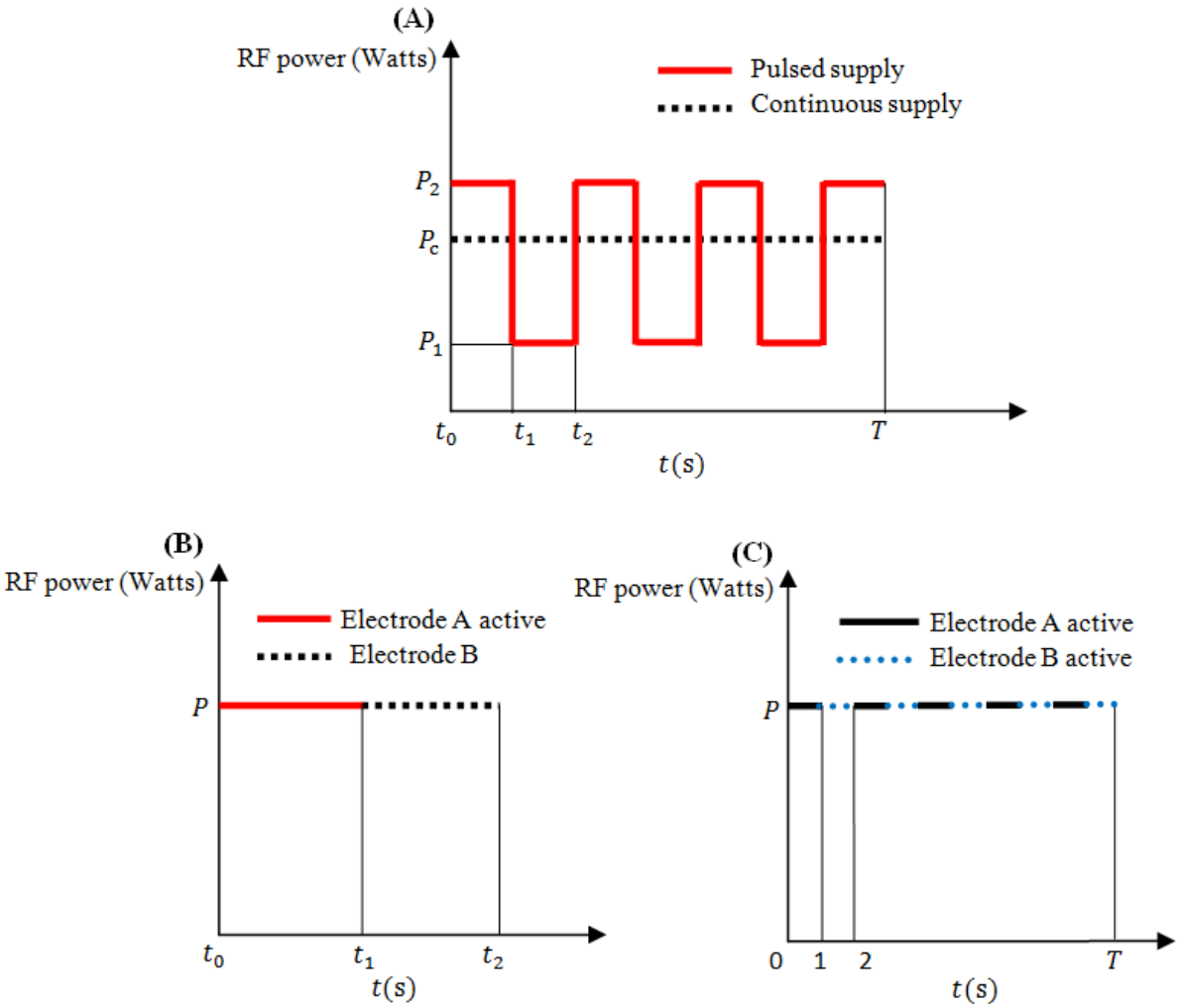

Figure 3.5. Application of RF energy. ((A) pulsed supply: RF energy is applied with peak power P_2 that is maintained for $t_1 - t_0$ and then the power is reduced to P_1 and maintained for $t_2 - t_1$. This procedure repeats continuously until a single RFA treatment duration (T) is finished. For continuous application, RF energy is applied with P_c in a whole single ablation duration. Pulsed application could be applied using any electrode design mentioned above, (B) consecutive supply: RF energy is applied with power P to electrode A until the target tissue around this electrode is killed completely and then the power turns to electrode B and kills the target tissue around electrode B, (C) switching supply: RF energy is applied with power p to electrode A for a small time period (1 sec) and then electrode B is activated for the same time period. This procedure repeats continuously until a single RFA

treatment duration (T) is finished. Consecutive application and switching application could be applied in any electrode design having more than one needle.)

For the second cause for incomplete TTN, diagnostic imaging, advanced imaging techniques and the improvement of RFA equipment are necessary. Using contrast-enhanced UI could be a relatively good way to acquire high quality images and detect minor non-ablated tissue. If the drawbacks of MRI could be solved, MRI would also be an alternative way to detect tumour tissue and non-ablated tissue.

For the third reason for incomplete TTN, the placement of the RF electrode, the success rate of placing the electrode is almost dependent on the knowing the position of target tissue and the experience of the physicians.

3.4.2 ADT evaluation

There are three main issues causing small size of TTN (< 3 cm in diameter) in the current RFA systems that are well known, as given below:

Issue 1: target tissue around the RF electrode is getting charred. After the tissue gets charred, its electrical impedance increases rapidly, such that the charred tissue will prevent more RF energy from being delivering to deep tissue. It is well known that the more electromagnetic heat energy delivered to the target tissue, the larger the size of TTN could be generated [14].

Issue 2: the contact area between the RF electrode and the target tissue is too small. If the contact area is small, the density of electric current is so small that little RF energy could be delivered to the target tissue in a single RFA treatment session.

Issue 3: target tissue is close to large blood vessels. Large blood vessels (i.e. vessel >3 mm in diameter) have a significant cooling effect to RFA because the vessels could absorb the heat energy as ‘heat sinks’.

To make use of the ADT, the device designs need to be stated as a design problem in the context of ADT. To achieve complete TTN is considered as a customer requirement (CA). Then, three functional requirements (FRs) could be derived from the current RFA devices:

FR1: *to achieve large size of TTN;*

FR2: *to discover the target tissue precisely;*

FR3: *to place the RF electrode in the correct position.*

For the FR1, it could be decomposed further into three sub-level functional requirements, which are independent of each other:

FR11: *to keep the temperature of the target tissue below the threshold temperature during a single treatment* (usually the threshold temperature for tissue charring is 100℃ [4]);

FR12: *to increase the contact area between the RF electrode and the target tissue;*

FR13: *to eliminate the heat sink effect of blood vessels;*

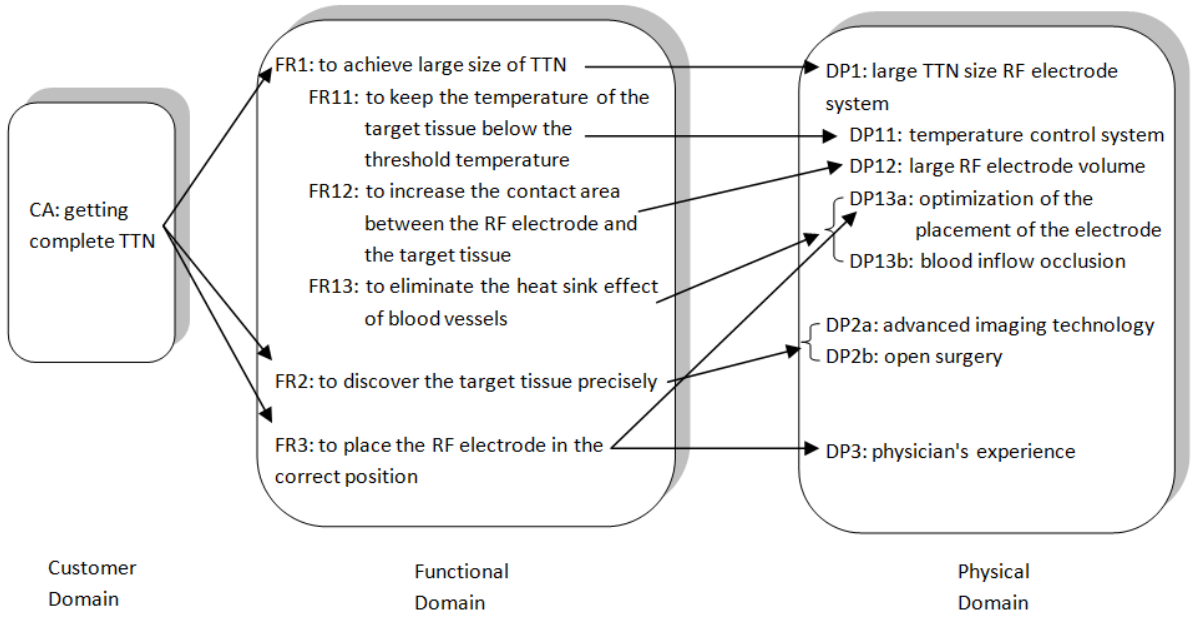

Figure 3.6. CAs, FRs, and DPs in the current RFA systems.

The DPs in the physical domain concluded from the current RFA systems are given as follows:

DP1: *large TTN size RF electrode system;*

DP2a: *advanced imaging technology;*

DP2b: *open surgery;*

DP3: *physician's experience.*

For the sub-level FR1, three sub-level DPs could be derived from the current RFA systems as follows:

DP11: *RFA temperature control system;*

DP12: *large RF electrode volume;*

DP13a: *optimization of the placement of the electrode* [28,29]*;*

DP13b: *blood inflow occlusion* [30,31]*;*

Figure 3.6 shows the FRs and its corresponding DPs in the current RFA systems. DP13a, DP13b, DP2a, and DP2b mean that DP13 and DP2 have two alternatives in the current RFA systems, respectively.

Figure 3.6 illustrates the relationship between FRs and DPs in the current RFA systems according to preceding discussion. However, in the real clinical practices, there are some different processes performed. Within these processes, some relationships between FRs and DPs are decoupled as shown in Table 3.1. For instance, FR3 (*to place the RF electrode in the correct position*) is not only affected by DP3 (*physician's experience*), but also influenced by DP13a (*optimization of the placement of* the *electrode*) as this optimization is aimed to get rid of the influence of heat sink effect of large blood. So there is an interaction between FR3 and DP13a. The same situation occurs at the relationship between FR3 and DP2a (*advanced imaging technology*).

All the possible situations occurred in the real clinical practices are summarised in Table 3.1. From Table 3.1, we could find that some current RF systems (System 1, 2, and 3) are actually decoupled designs, which means that if these systems are not performed in a particular sequence, the independence axiom will not be satisfied. *Therefore, this decoupled design in the current RFA systems is the key reason for incomplete TTN*.

Table 3.1. Design matrix of the current RFA systems.

System	Design parameter	Design matrix
1	DP11, DP12, DP13a, DP2a, DP3	$\begin{bmatrix} X & & & & \\ & X & & & \\ & & X & & \\ & & & X & \\ & & X & X & X \end{bmatrix}$
2	DP11, DP12, DP13b, DP2a, DP3	$\begin{bmatrix} X & & & & \\ & X & & & \\ & & X & & \\ & & & X & \\ & & & X & X \end{bmatrix}$
3	DP11, DP12, DP13a, DP2b, DP3	$\begin{bmatrix} X & & & & \\ & X & & & \\ & & X & & \\ & & & X & \\ & & X & & X \end{bmatrix}$
4	DP11, DP12, DP13b, DP2b, DP3	$\begin{bmatrix} X & & & & \\ & X & & & \\ & & X & & \\ & & & X & \\ & & & & X \end{bmatrix}$

System 4 is an uncoupled design, which is the best design according to ADT. In System 4, five functional requirements can be satisfied by DP11, DP12, DP13b, DP2b, and DP3. There is no interaction between them as it is an uncoupled relationship. Any change from one design parameter just influences its corresponding functional requirement. In this system, blood inflow occlusion and open surgery are chosen to be DP13 and DP2, respectively. If one RFA treatment could be performed under this design process, the potential to obtain complete TTN will increase rapidly. Actually, the results concluded here are consistent with the animal experiments and clinical practice reported in the literature [31-33].

Although System 4 is a relatively good design process for RFA treatment, many issues need to be taken into account carefully before performing RFA treatment. The restrictions associated with this design must be examined before because both the open surgery and the physician's experience are involved. For instance, with open surgery the physician must evaluate the effect of complications of open surgery and local recurrence of incomplete TTN on threatening the patient's life. For the physician's experience, the variety is obvious.

Another way to have complete TTN is with the System 1 and 2 designs in which open surgery is avoided when they are performed in a certain sequence.

3.5 Case study

All discussions discussed above are based on the conceptual level of design of the current RFA systems. To verify the conclusion from the conceptual level of design, a more detailed investigation of System 4 will be discussed through simulation. A detailed case study is given to verify the conclusion that System 4 could generate complete TTN, namely to satisfy the design of CAs.

3.5.1 Case setup

We assume that a large regular ellipsoid-shaped target tissue (40mm×40mm×30mm) investigated in liver tissue, and its geometrical centre is located at (0, -5.77, 50) in the XYZ coordinate, as shown in Figure 3.7A. The function describing the profile of the target tissue could be expressed as:

$$\frac{X^2}{400}+\frac{(Y+5.77)^2}{400}+\frac{(Z-50)^2}{225}=1 \tag{3.5}$$

The treatment objective is to ablate the target tissue completely with System 4. In this case study, the uncertainty in different physicians' experience and anisotropy of the target tissue are ignored. Notably, in many RFA simulations, the liver tissue properties are taken as that of the target tissue because there is a lack of data on tumour tissue. This acceptable approximation is also adopted in this case study. The five DPs in System 4 are *temperature control system, large RF electrode volume, blood inflow occlusion, open surgery, and physician's experience*. These DPs are embodied in the simulation environment, which are given as:

temperature control system: internally cooled electrode;

large electrode volume: cluster electrode;

blood inflow occlusion: omitting large blood vessels in the simulation model;

open surgery: knowing the precise profile and position of the target tissue;

and *physician's experience*: knowing the best position in which the electrode should be placed.

Based on the preceding discussion, a simple protocol could be developed in the following. Cluster-internally cooled electrode with 3 needles was put into the target tissue. These needles are deployed equidistantly at a 20 mm distance. The centre of the cluster-internally cooled electrode is coincident with that of the target tissue in the X-Y plane, as shown in Fig. 3.7A. The locations of these three needles in the X-Y plane are (-10, 0), (10, 0), and (0, -17.32), respectively. The three needles, with a RF electrode 20 mm in length and 3 mm in diameter for each needle, are inserted into the liver tissue 60 mm deep. Large blood vessels are omitted due to blood vessel occlusion.

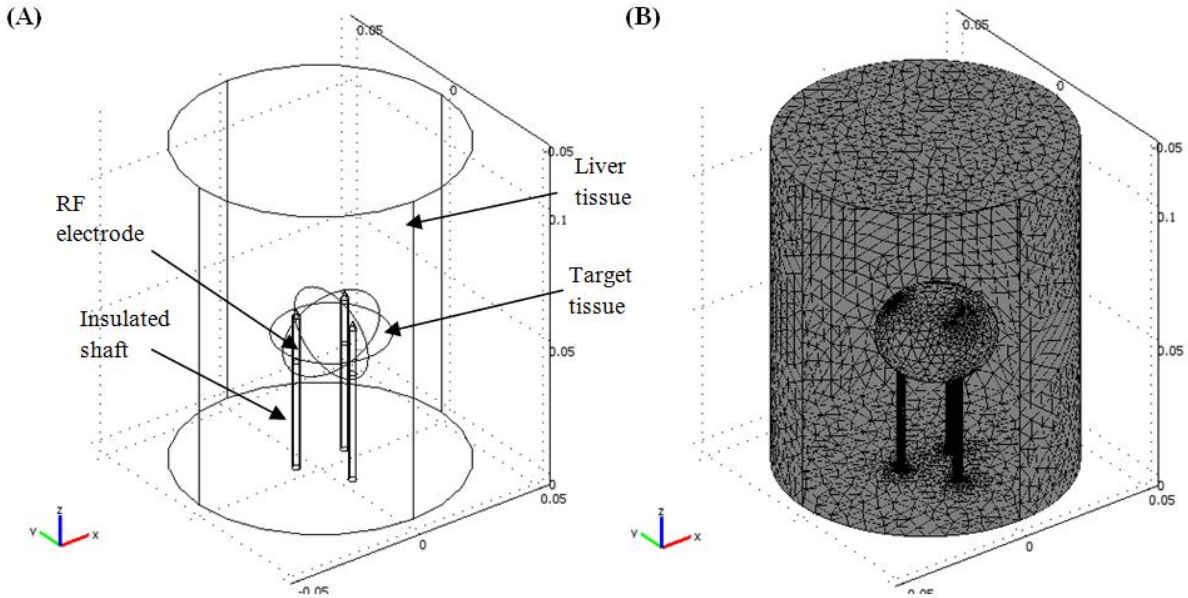

Figure 3.7. FE modelling of the case study. (A) The cylindrical part is modelled as liver tissue with a diameter of 100 mm and 120 mm in length and (B) this 3D model has 305578 tetrahedral elements and 52513 nodes by performing the convergence tests. The spatial meshing size was continuing to be refined until the maximum temperature was within 1% of the maximum temperature obtained from the last step size.

3.5.2 FE modelling for the system

A finite element model (FEM) of System 4 is established in a finite element analysis software - COMSOL Multiphysics (COMSOL, Burlington MA, USA), as shown in Figure 3.7. The material properties used are adopted from the literature [34], as shown in Table 3.2, and the blood perfusion in hepatic tissue, ω_b, is 6.43×10^{-3} s^{-1} [35]. Using the quasi-static approach, the value of 'Direct-Current' (DC) voltage could be calculated from the model

corresponding with the root mean squared (RMS) value of the RF voltage actually employed. In COMSOL software, the analysis uses the Pennes bioheat transfer equation with an outside energy source (Eq. (3.6)) and conductive media DC application (Eq. (3.7)) to implement a transient analysis. This single RFA treatment session is simulated in COMSOL software for 20 minutes (1200 seconds).

Table 3.2. Thermal and electrical properties of the materials in the case study.

Model element	Material	$\rho(\text{kg m}^{-3})$	$c(\text{J kg}^{-1}\text{ K}^{-1})$	$k(\text{W m}^{-1}\text{ K}^{-1})$	$\sigma(\text{S m}^{-1})$
Insulated shaft	Polyurethane	70	1045	0.026	1×10^{-5}
RF electrode	Ni-Ti	6450	840	18	1×10^{8}
Tissue	Liver	1060	3600	0.512	0.333
Blood perfusion	Blood	1000	4180	0.543	0.667

3.5.3 Initial and boundary conditions in the model

For the cluster-internally cooled electrode model, the initial and boundary conditions are distributed as follows:
The initial temperature equals 37 ℃ in all domains. The boundary conditions at the liver tissue outer boundaries and the RF electrode surfaces are 0 V potential (ground) and 50 V potential, respectively. And we assume they are continuous in other boundaries. There is a chilled fluid circulating inside of each needle of cluster-internally cooled electrodes to cool the needles during the RFA treatment. Therefore, a temperature boundary condition, 0 ℃, is added to the RF electrode surfaces to represent the real situation.

3.5.4 Simulation results and discussion

Figure 3.8 shows the temperature distribution after a single RFA treatment session, which lasts for 20 minutes. By adding the internally cooled system in System 4, the maximum temperature during this RFA treatment is 99.451℃ less than 100℃, which means that the roll-off has been avoided in this single RFA treatment. Otherwise, the roll-off will occur at a relative early time such that only small size TTN generated.

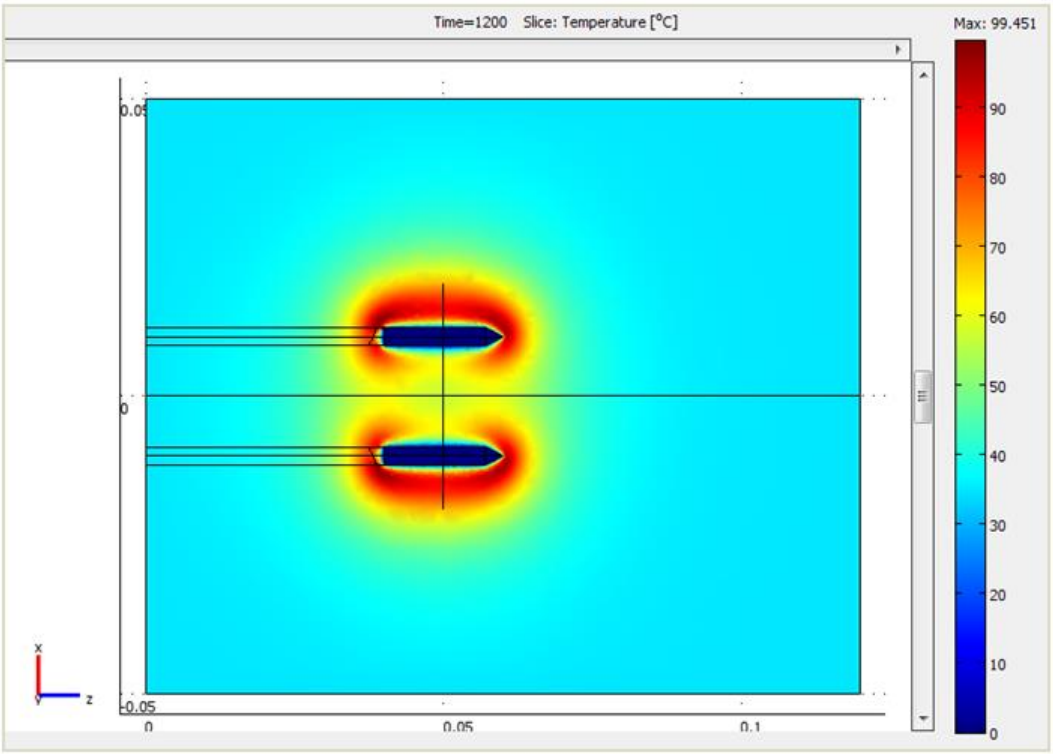

Figure 3.8. Temperature gradient after a single RFA treatment session. (the third needle is not shown in the plot)

The 50℃ isothermal contour is used to represent the profile of TTN in this case study, even if there are some debates on its effectiveness [36]. Figure 3.9 depicts the profile of TTN that the RFA System 4 could generate after a single RFA treatment session. The green shade and the solid dark lines represent the cubic of TTN and the profile of the target tissue, respectively. One could find that the target tissue is covered completely by the cubic of TTN from all directions. In other words, the large target tissue could be killed completely by RFA System 4 under the preceding protocol.

The result of this case study shows that the conclusion of the above evaluation is meaningful and that the protocol proposed in this paper is also acceptable. Although just regular ellipsoid-shape target tissue is used in this case study, the uncoupled RFA system and the protocol could be developed to other large target tissues with different shapes.

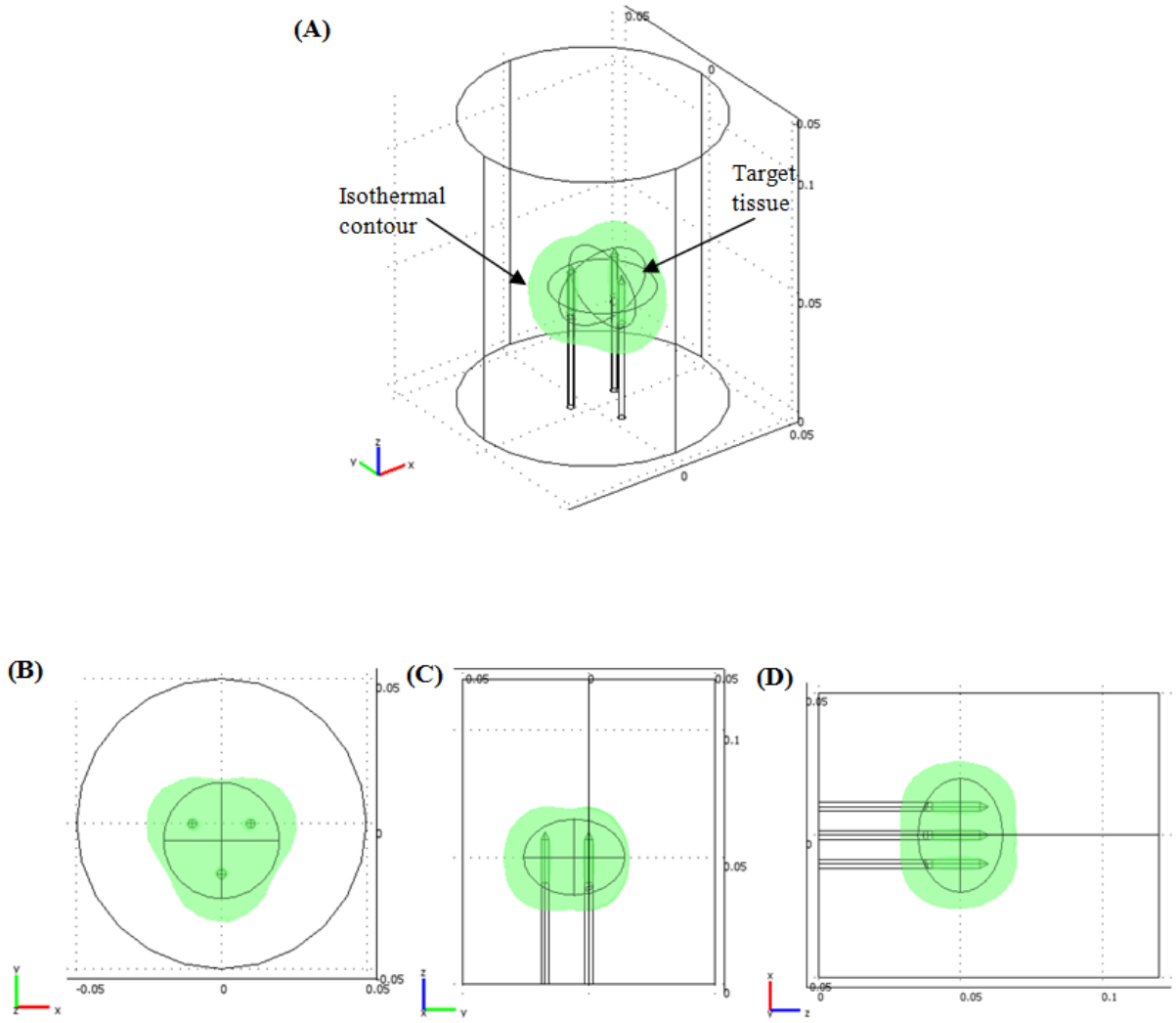

Figure 3.9. The 50℃ isothermal contour. (views of the (A) 3D model, from the (B) X-Y, (C) Y-Z, and (D) Z-X planes)

3.6 Conclusions

As a minimally invasive technique for tumour treatment, the RFA system has been popular for several decades. However, there are several limitations preventing this technique from being developed further. One of these limitations is incomplete TTN. This problem has garnered much interest from biomedical engineers and physicians. The contribution of this paper is that the current RFA systems are evaluated in terms of their design concepts by ADT in generating complete TTN. The cause of why these systems cannot generate complete TTN is analyzed, and

an uncoupled design to increase the possibility of complete TTN is determined. The results of this paper have been further verified by the numerical simulation case study and are consistent with the results of other animal experiments and clinical practices as well.

However, it is noted that some factors are ignored by this paper to simplify the question. These factors may have a large influence on the creation of complete TTN under certain circumstances. Despite this assumption, the results of this paper still could provide useful hints to physicians for managing these different RFA systems and facilitate designers in developing new RFA systems or improving the existing ones.

Declaration of conflicting interests

The authors declare that there is no conflict of interest.

Funding

This article was supported by Saskatchewan Health Research Foundation (SHRF) through the grant "BioNEMS phase I". The first author (B.Z.) also received financial support from the China Scholarship Council.

REFERENCES

1. McGahan JP, Dodd GD. Radiofrequency ablation of the liver current status. Am J Roentgenol 2001;176:3-16.
2. Tungjitkusolmun S, Woo E, Cao H, Tsai J, Vorperian V, Webster J. Thermal—electrical finite element modelling for radio frequency cardiac ablation: effects of changes in myocardial properties. Med Biol Eng Comput 2000;38:562-8.
3. Miller SF, Geiger JD, Shih AJ. Thermal-electric finite element analysis and experimental validation of bipolar electrosurgical cautery. J Manuf Sci Eng 2008;130:021015.
4. Lencioni R, Goletti O, Armillotta N, Paolicchi A, Moretti M, Cioni D, et al. Radio-frequency thermal ablation of liver metastases with a cooled-tip electrode needle: Results of a pilot clinical trial. Eur Radiol 1998;8:1205-11.
5. Pennes HH. Analysis of tissue and arterial blood temperatures in the resting human forearm. J Appl Physiol 1948;1:93-122.
6. Plonsey R, Heppner DB. Considerations of quasi-stationarity in electrophysiological systems. Bull Math Biophys 1967;29:657-64.
7. McGahan JP, Brock JM, Tesluk H, Gu WZ, Schneider P, Browning, PD. Hepatic ablation with use of radio-frequency electrocautery in the animal model. J Vasc Interv Radiol 1992;3:291-7.
8. Zhang B, Moser M, Zhang E, Zhang W. Radiofrequency ablation technique in the treatment of liver tumours: Review and future issues. J Med Eng Technol 2013; 37:150-9.
9. Rossi S, Buscarini E, Garbagnati F, Di Stasi M, Quaretti P, et al. Percutaneous treatment of small hepatic tumors by an expandable RF needle electrode. Am J Roentgenol 1998;170:1015-22.
10. Ayav A, Germain A, Marchal F, Tierris I, Laurent V., Bazin C, et al. Radiofrequency ablation of unresectable liver tumors: Factors associated with incomplete ablation or local recurrence. Am J Surg 2010;200:435-9.
11. Shiina S, Tateishi R, Arano T, Uchino K, Enooku K, Nakagawa H, et al. Radiofrequency ablation for hepatocellular carcinoma: 10-year outcome and prognostic factors. Am J Gastroenterol 2011;107:569-77.
12. Baldwin K, Katz SC, Rubin A, Somasundar P. Bipolar radiofrequency ablation of liver tumors: Technical experience and interval follow-up in 22 patients with 33 ablations. J Surg Oncol 2012;106:905-10.

13. O'Rourke AP, Haemmerich D, Prakash P, Converse MC, Mahvi DM, Webster JG Current status of liver tumor ablation devices. Expert Rev Med Devic 2007;4:523-37.

14. Gazelle GS, Goldberg SN, Solbiati L, Livraghi T. Tumor Ablation with Radio-frequency Energy. Radiology 2000;217:633-46.

15. Mulier S, Ni Y, Jamart J, Ruers T, Marchal G, Michel L. Local recurrence after hepatic radiofrequency coagulation: multivariate meta-analysis and review of contributing factors. Ann Surg 2005;242:158-71.

16. Lam VW, Ng KK, Chok KS, Cheung TT, Yuen J, Tung H, et al. Incomplete ablation after radiofrequency ablation of hepatocellular carcinoma: analysis of risk factors and prognostic factors. Ann Surg Oncol 2008;15:782-90.

17. Suh NP Axiomatic design: advances and applications. New York: Oxford University Press 2001.

18. Song K-Y, Zhang W, Gupta MM. Incorporation of axiomatic design theory into design of a microchannel system for uniform and size-controllable microspheres. Int J Adv Manuf Technol 2011;57:491-9.

19. Suh NP Fundamentals of design and deployment of large complex systems: OLEV, MH, and mixalloy. J Integrated Des Process Sci 2012;16:7-28.

20. Guenov M, Barker S. Application of axiomatic design and design structure matrix to the decomposition of engineering systems. Sys Eng 2005;8:29-40.

21. Song KY, Zhang WJ, Gupta MM. Application of axiomatic design theory to a microfluidic device for the production of uniform water-in-oil microspheres adapting an integration method. J Manuf Sci Eng 2012;134:044504.

22. Thielman J, Ge P. Applying axiomatic design theory to the evaluation and optimization of large-scale engineering systems. J Eng Design 2006;17:1-16.

23. Fan L, Fu L, Liu L, Han B, Cai M, Zhang C. Critique on the literature of axiomatic design theory and its application. Int J Adv Manuf Technol accepted.

24. Suh NP. Designing-in of quality through axiomatic design. IEEE T Reliab 1995;44:256-64.

25. Suh NP. Design of systems. CIRP Ann: Manuf Tech 1997;46:75-80.

26. Goldberg SN, Stein MC, Gazelle GS, Sheiman RG, Kruskal JB and Clouse ME. Percutaneous radiofrequency tissue ablation: Optimization of pulsed-radiofrequency technique to increase coagulation necrosis. J Vasc Interv Radiol 1999;10:907-16.

27. Mulier S, Miao Y, Mulier P, Dupas B, Pereira P, de Baere T, et al. Electrodes and multiple electrode systems for radiofrequency ablation: a proposal for updated terminology. Eur Radiol 2005;15:798-808.

28. Meijerink MR, van den Tol P, van Tilborg AA, van Waesberghe JH, Meijer S, van Kuijk C. Radiofrequency ablation of large size liver tumours using novel plan-parallel expandable bipolar electrodes: Initial clinical experience. Eur J Radiol 2011;77:167-171.

29. Haemmerich D, Staelin T, Tungjitkusolmun S, Lee Jr FT, Mahvi DM, Webster JG. Hepatic bipolar radio-frequency ablation between separated multiprong electrodes. IEEE Trans Biomed Eng 2001;48:1145-52.

30. De Baere T, Bessoud B, Dromain C, Ducreux M, Boige V, Lassau N, et al. Percutaneous radiofrequency ablation of hepatic tumors during temporary venous occlusion. Am J Roentgenol 2002;178:53-9.

31. Chinn SB, Lee FT, Kennedy GD, Chinn C, Johnson CD, Winter TC, et al. Effect of vascular occlusion on radiofrequency ablation of the liver results in a porcine model. Am J Roentgenol 2001;176:789-95.

32. Hendy MP, Recht MH, Welling RE. Radiofrequency ablation of the porcine liver with complete hepatic vascular occlusion. Ann Surg Oncol 2002;9:594-8.

33. Rossi S, Garbagnati F, Lencioni R, Allgaier HP, Marchianò A, Fornari F, et al. Percutaneous radio-frequency thermal ablation of nonresectable hepatocellular carcinoma after occlusion of tumor blood Supply. Radiology 2000;217:119-26.

34. Tungjitkusolmun S, Staelin ST, Haemmerich D, Tsai JZ, Cao H, Webster JG, et al. Three-dimensional finite-element analyses for radio-frequency hepatic tumor ablation. IEEE Trans Biomed Eng 2002;49:3-9.

35. Ebbini E, Umemura S, Ibbini M, Cain C. A cylindrical-section ultrasound phased-array applicator for hyperthermia cancer therapy. IEEE Trans Ultrason Ferroelectr Freq Control 1988;35:561-72.

36. Berjano EJ. Theoretical modeling for radiofrequency ablation: State-of-the-art and challenges for the future. Biomed Eng. Online 2006;5:24.

APPENDIX 3.1

The governing equation of RFA treatment for target biological tissue can be given as follows:

$$\rho c \frac{\partial T}{\partial t} = \nabla \cdot k\nabla T + \rho_b c_b \omega_b (T_b - T) + Q_{hs} + Q_m \tag{3.6}$$

where ρ (kg m^{-3}) is the density, c (J kg^{-1} K^{-1}) is the specific heat, T (°C) is the temperature, k (W m^{-1} K^{-1}) is the thermal conductivity, ρ_b (kg m^{-3}) is the blood density, c_b (J kg^{-1} K^{-1}) is the specific heat of the blood, and ω_b is the blood perfusion (s^{-1}), T_b is the temperature of the blood entering the tissue, Q_m (W m^{-3}) is the energy generated due to metabolic processes, which can be ignored because it is small compared to the other terms in Eq. (3.7). Q_{hs} is the distributed heat source generated by an outside energy source (i.e. RF energy in the case of RFA). At such a high frequency employed in the RFA technique and in such a small area of RF electrode, the tissue can be considered as a pure resistive lump of material. Thus, a quasi-static approach to represent the behaviour of heat and electricity is usually employed to resolve the electrical problem in conductive media; in particular $\dot{q}_{hs}$ is calculated as follows:

$$Q_{hs} = \boldsymbol{J} \cdot \boldsymbol{E} \tag{3.7}$$

where $\boldsymbol{J}$ (A m^{-2}) is the current density and $\boldsymbol{E}$ (V m^{-1}) is the electric field intensity. The two values in Eq. (3.7) are further calculated by Eq. (3.8):

$$\begin{cases} \boldsymbol{E} = -\nabla V \\ \boldsymbol{J} = \sigma \mathrm{E} \end{cases} \tag{3.8}$$

Furthermore, $\boldsymbol{J}$ and $\boldsymbol{E}$ could also be evaluated using Laplace's equation:

$$\nabla \cdot \sigma \nabla V = 0 \tag{3.9}$$

where V (V) is the voltage and σ (S m^{-1}) is the electrical conductivity.

4 STUDY OF THE RELATIONSHIP BETWEEN THE TARGET TISSUE NECROSIS VOLUME AND THE TARGET TISSUE SIZE IN LIVER TUMOURS USING TWO-COMPARTMENT FINITE ELEMENT RFA MODELLING

This chapter is derived from an article published by Taylor & Francis in ***International Journal of Hyperthermia*** *on November 27, 2014. Available online: http://www.tandfonline.com/ doi:10.3109/02656736.2014.984000.*

Abstract

Purpose: The aim of this study was to investigate the relationship between the target tissue necrosis volume and the target tissue size during the radiofrequency ablation (RFA) procedure.

Materials and methods: The target tissues with four different sizes (d_{xy} = 20, 25, 30, and 35 mm) were modelled using a two-compartment radiofrequency ablation model. Different voltages were applied to seek the maximum target tissue necrosis volume for each target tissue size. The first roll-off occurrence or the standard ablation time (12 min) was taken as the sign for the termination of the radiofrequency ablation procedure.

Results: Four different maximum voltages without the roll-off occurrence were found for the four different sizes of target tissues (d_{xy} = 20, 25, 30, and 35mm), and they were 36.6, 35.4, 33.9, and 32.5 V, respectively. The target tissues with diameters of 20, 25 mm can be completely ablated at their own maximum voltages applied (MVA) but the same finding was not found for the 35-mm target tissue. For the target tissue with diameter of 30 mm, the 50 ℃ isothermal contour (IT50) result showed that the target tissue can be completely ablated, but the same result did not show in the Arrhenius damage model result. Furthermore, two optimal RFA protocols with a minimal thermal damage to the healthy tissues were found for the target tissues with diameters of 20 and 25 mm, respectively.

Conclusions: The study suggests that target tissues of different sizes should be treated with different radiofrequency ablation protocols. The maximum target tissue volume was achieved with the MVA without the roll-off occurrence for each target tissue size when a constant RF power supply was used.

4.1 Introduction

RFA has been used as an important treatment modality for various tumours and dysfunctional tissues, such as liver [1], lung [2], breast [3], kidney [4], and cardiac arrhythmias [5], because of its minimally invasive nature. As a sub-ablative thermal therapy, RFA is also used to treat hyperopia [6], hyperopic astigmatism [7], and presbyopia [6,8]. In recent years, RFA for immune therapy has also attracted some attention [9-11]. However, RFA has a low success rate in tumour ablation for the tumours with their sizes larger than 3 cm in diameter, which seems to be likely related to the limit in target tissue necrosis (TTN) volume. Xu et al. [12] reported that the complete ablation rate in tumours $\leq$ 3 cm was 95.4% after an initial RFA treatment for hepatocellular carcinoma (HCC). However, the same rates in tumour between 3.1 to 5.0 cm and $>$ 5 cm were only 82.5% and 50%, respectively. Shiina et al. [13] also found that the 5-year survival rate of HCC after the RFA treatment was only 46.5% for the large liver tumour (> 3 cm in diameter). The same result also can be found in literature [14,15]. It is widely suggested that this limitation is due to the charring of the target tissue.

The engineering pathway of the tissue charring is as follows: The RFA procedure establishes a circuit with a power source (RF power generator) and a resistor contributed by the RF electrode, target tissue and ground pads [16]. The electrical conductivity of the target tissue, which depends on the water content and cellular makeup, is not a constant value. When the temperature of the tissue is higher than 100 ℃, the water essentially boils and begins to evaporate [17], the tissue becomes desiccated, and thus the target tissue becomes charred. The charred tissue further leads to a notable decrease in its electrical conductivity. This situation is observed in the clinical setting and termed roll-off, which is characterized by a marked growth in the impedance between the RF electrode and ground pads, and furthermore the actual output of the RF power drops.

The roll-off is a crucial situation in the RFA procedure. In the clinical setting, one of the most popular RF power supply algorithms is based on the roll-off occurrence. In particular, the RF power generator is usually turned off for a while after a roll-off occurs and during the power off period, there is a cooling process around the probe. Arata et al. [18] attempted to build the relationship between the roll-off and the tumour ablation response. These researchers used the roll-off as the end-point for the RFA procedure for ablation of the hepatic tumours and found that the local

recurrence rate at 6 months without the roll-off (45%) was higher than that with the roll-off (15%). They tended to consider the roll-off as a significant sign of local control in RFA procedure. It is well known that the lower local recurrence is mainly attributed to the incomplete ablation of target tissue [19]. Thus, the relationship between the roll-off and the TTN is crucial in the RFA procedure. Trujillo et al. [20] investigated the relationship between the roll-off occurrence and the target tissue dehydration (charring) and concluded that the roll-off usually occurs at the moment at which the RF electrode is completely encircled by the charred tissue. Controlling the roll-off is obviously an important means to enlarge the TTN volume. Some RF electrodes do have designs to provide chilled fluid inside the RF electrode to delay the roll-off occurrence. According to [21], this approach cannot eliminate the tissue charring but just shift the charred tissue 1-2 mm away from the RF electrode surface, which may further increases the TTN volume by 1-3 times compared to no chilled fluid situation [22]. Other methods to delay the roll-off occurrence can be the infusion of hypertonic saline solution into the target tissue [23] and the pulsed RF power delivery technique [24].

To date, many studies have attempted to overcome the deficiency of the RFA technique, such as the design of the RF electrode (internal-cooling electrode, cluster electrode, perfusion electrode or extendable electrode), the design of the RF power supply method (pulsed, consecutive, or switching), and the combination with other therapeutic methods (irreversible electroporation, radiotherapy or chemotherapy) [19]. However, the results achieved so far are still not good enough because the target tissue that can be killed is still relatively small in size, especially when a monopolar electrode is used.

Pursuing a large TTN volume with a monopolar electrode in a short ablation period is the ultimate objective in RFA procedure today. To reach this objective, many questions should be answered in advance. Among them is the impact of the target tissue size on the TTN volume. Understanding their relationship may give us a clue to overcome the deficiency of RFA in the treating of target tissues with large sizes. However, to the best of our knowledge, few studies have investigated in discussing this relationship. Therefore, it is our belief that any additional information about the RFA treatment for target tissues of different sizes would be very useful to control TTN volume.

In this study, we attempted to investigate the relationship between the TTN volume and the target tissue size based on a two-compartment numerical model using the roll-off as the endpoint of the RFA procedure. In the following section, the two-compartment RFA model used, the termination of computer simulation and the data collection are discussed in detail. The results with discussion are presented in Section 4.3 and several conclusions that can be drawn from this study are detailed in the last section.

4.2 Materials and methods

4.2.1 Electric-thermal model of two-compartment RFA

RFA uses the so-called frictional heating (also known as 'resistive' heating) generated by a high-frequency alternating current (f_{RF} = 350-500 kHz) to kill tumour cells [25,26]. Thus, two processes need to be considered in the mathematical modelling of RFA, namely (1) heat transfer in target tissue (biological tissue) and (2) spatial heat generation by the electrical current with high frequency.

For heat transfer in biological tissue, Pennes bioheat transfer equation [27] was used in the present study because it has computational efficiency and reasonable accuracy as well. In Pennes model, the perfusion term was considered as an isotropic heat sink without considering temperature variations in the arterial and venous blood and the structure of the local vasculature, as shown in Eq. (4.1):

$$\rho c \frac{\partial T(\mathbf{x},t)}{\partial t} = \nabla \cdot \left(k \nabla T(\mathbf{x},t)\right) + \rho_b c_b \omega_b \left(T_b - T(\mathbf{x},t)\right) + Q_m(\mathbf{x},t) + Q_{hs}(\mathbf{x},t) \qquad \mathbf{x} \in \mathbf{\Lambda} \tag{4.1}$$

where $\rho(\mathrm{kg\ m^{-3}})$ is the density, $c(\mathrm{J\ kg^{-1}K^{-1}})$ is the specific heat, $T(\mathbf{x},t)(℃)$ is the temperature, $\mathbf{x} = \{x, y, z\}$ in the Cartesian coordinate system, $\mathbf{\Lambda}$ denotes the analysed spatial domains, $k(\mathrm{W\ m^{-1}K^{-1}})$ is the thermal conductivity, $\rho_b(\mathrm{kg\ m^{-3}})$ is the blood density, $c_b(\mathrm{J\ kg^{-1}K^{-1}})$ is the blood specific heat, $\omega_b(1\ \mathrm{s^{-1}})$ is the blood perfusion rate, T_b is the temperature of the blood entering the tissue, $Q_m(\mathbf{x},t)(\mathrm{W\ m^{-3}})$ is the volumetric heat generated by metabolism, which is negligible due to its small magnitude compared with the other terms in Eq. (4.1) and $Q_{hs}(\mathbf{x},t)(\mathrm{W\ m^{-3}})$ is the spatial heat generated by the RF electrical current.

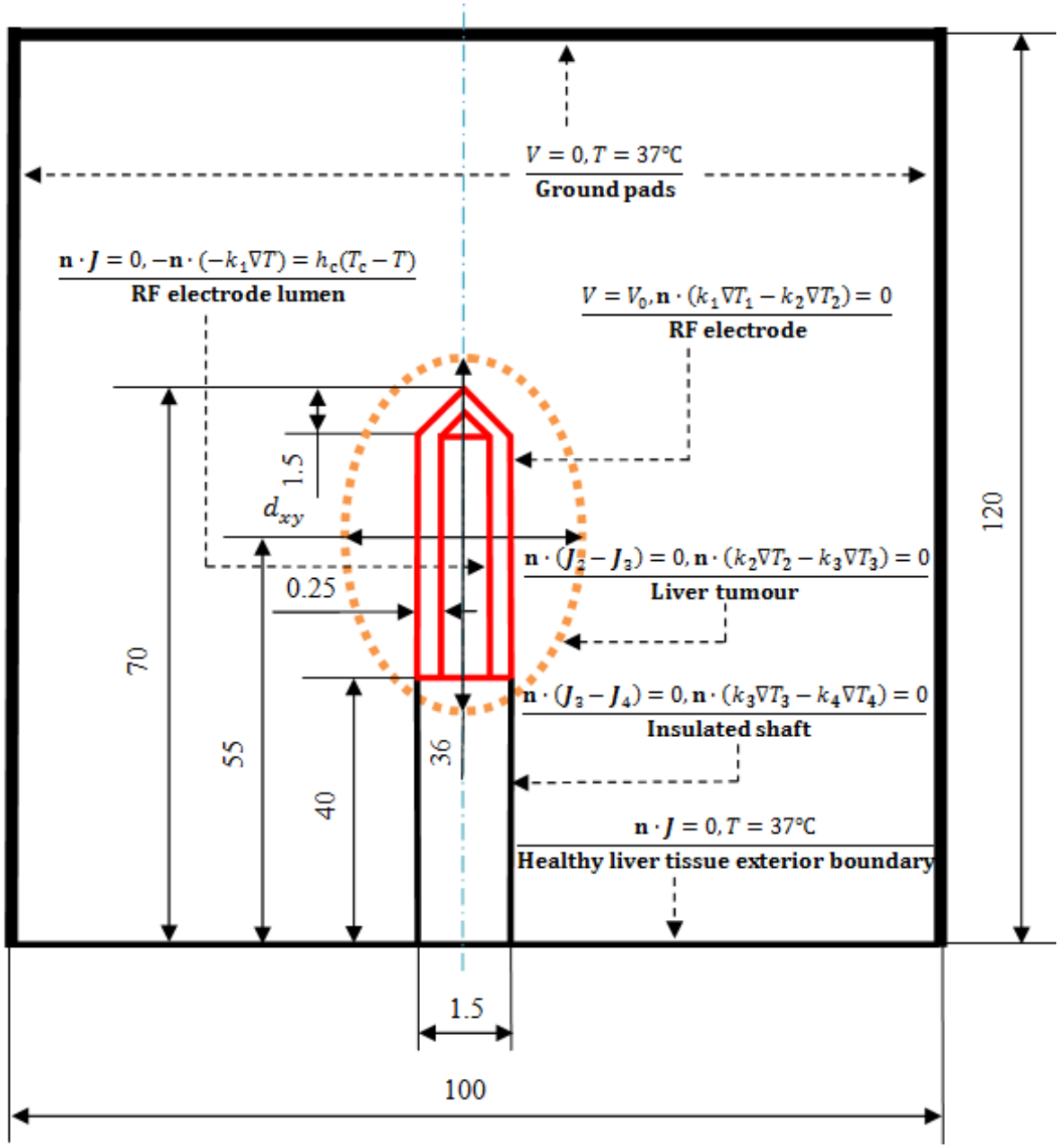

Figure 4.1. Dimensions (out of scale and in mm) and boundary conditions of the two-compartment RFA model used in the present study.

Due to the high frequency employed in the RFA and the relative small size of the work domain (RF electrode in this case), the biological tissue can be considered as a resistor only because the displacement of charges in the alternating current can be negligible. Thus, the spatial heat power generated by the electrical current can be calculated using a quasi-static approach, as shown in Eq. (4.2):

$$Q_{hs}(\mathbf{x}, t) = \boldsymbol{J} \cdot \boldsymbol{E} = \sigma |\nabla V|^2 \tag{4.2}$$

where $\boldsymbol{J}(\mathrm{A\,m^{-2}})$ is the current density, $\boldsymbol{E}(\mathrm{V\,m^{-1}})$ is the electric field intensity, $\sigma(\mathrm{S\,m^{-1}})$ is the electrical conductivity and $V(\mathrm{V})$ is the applied voltage. The voltage can be evaluated using Laplace's equation [28]:

$$\nabla \cdot \sigma \nabla V = 0 \tag{4.3}$$

Using the quasi-static approach, the value of the 'direct-current' (DC) voltage can be calculated from the model corresponding with the root mean squared (RMS) value of the RF voltage [29].

As shown in Figure 4.1, a healthy liver tissue was modelled as a cylinder with a diameter of 100 mm and a height of 120 mm. To consider the realistic clinical scenario, an elliptical liver tumour, 36 mm along the long axis, d_{xy} along the short axis (diameter of tumour tissue) was built in the centre of the healthy liver tissue. In the present study, liver tumours of four sizes, namely d_{xy} = 20, 25, 30, and 35 mm, were considered as the target tissues. A 17-gauge (1.5 mm) internal-cooling RF electrode with a 30-mm exposure length (Covidien AG, Zurich, Switzerland) was modelled and inserted into the centre of the liver tumour.

4.2.2 Finite element analysis of the two-compartment RFA model

The thermal conductivity, electrical conductivity and blood perfusion rate of the biological tissue were modelled as temperature dependent. The thermal conductivity was approximated with Eq. (4.4) [30]. For the electrical conductivity, an increase of 2 %/℃ was used in this study when the temperature was less than 100 ℃. Between 100 ℃ and 105 ℃, the electrical conductivity exhibited a rapid decrease of two orders of magnitude due to water vaporization and desiccation [30], as shown in Eq. (4.5). Because the frequency of the alternating current was not the research objective in this study, the dependence of electrical conductivity on frequency was ignored. The computation was fixed at a frequency of 460 kHz. There were some debates on how to model the blood perfusion of the biological tissue in the computational work. Most of the studies considered blood perfusion as a constant [31,32] or a piecewise function [33-35]. Some researchers [36] obtained a good agreement with the *in vivo* animal experiments when using the foregoing constant method. It is worth to mention that Schutt and Haemmerich [37] had concluded that there were significant effects on TTN volume using different blood perfusion models. They used the piecewise model, a linear decreasing model and a nonlinear decreasing model. In the nonlinear decreasing model,

they considered an increase of blood perfusion with an increase of degree of vascular stasis at the ablation zone boundary due to the hyperaemia. In the present study, a piecewise function model of vascular coagulation was used. Particularly, the perfusion rate was considered as a constant before the biological tissue reached a temperature of 60 ℃; at temperatures higher than 60 ℃, the blood perfusion rate was set to 0 because the coagulation eliminated microvascular perfusion [33]. Eq. (4.6) shows that piecewise model of blood perfusion in the present study.

$$k(T) = \begin{cases} k_{\text{ref}} + 0.0013(T(\mathbf{x},t) - T_{\text{ref}}) & T(\mathbf{x},t) \leq 100℃ \\ k_{\text{ref}} + 0.1027 & T(\mathbf{x},t) > 100℃ \end{cases} \tag{4.4}$$

$$\sigma(T) = \begin{cases} \sigma_{\text{ref}}[1 + 0.02(T(\mathbf{x},t) - T_{\text{ref}})] & T(\mathbf{x},t) \leq 100℃ \\ (-0.51084T(\mathbf{x},t) + 53.664)\sigma_{\text{ref}} & 100℃ < T(\mathbf{x},t) \leq 105℃ \\ 0.0258\sigma_{\text{ref}} & T(\mathbf{x},t) > 105℃ \end{cases} \tag{4.5}$$

$$\omega_b(T) = \begin{cases} \omega_0 & T(\mathbf{x},t) < 60℃ \\ 0 & T(\mathbf{x},t) \geq 60℃ \end{cases} \tag{4.6}$$

where T_{ref} = 21 ℃, for the healthy liver tissue, k_{ref} = 0.52 (W m^{-1}K^{-1}) and σ_{ref} = 0.20 (S m^{-1}) [38], whereas for the liver tumour, k_{ref} = 0.60 (W m^{-1}K^{-1}) and σ_{ref} = 0.50 (S m^{-1}) [38,39]. The material properties used for each element are tabulated in Table 4.1. These values were adopted from the literature [38,40-44].

Table 4.1. Thermal and electrical properties of the modelling elements used in the present study.

Modelling element	Material	ρ (kg m^{-3})	c (J kg^{-1}K^{-1})	k (W m^{-1}K^{-1})	σ (S m^{-1})	ω_0 (s^{-1})
Biological tissue	Healthy liver tissue	1080	3455	Eq. (4.4)	Eq. (4.5)	0.016
	Liver tumour	1045	3760			0.002
RF electrode	Ni-Ti	6450	840	18	1.0×10^{8}	-
Insulated shaft	Polyurethane	70	1045	0.026	1.0×10^{-5}	-
Blood vessel	Blood	1000	4180	0.49	0.667	-

The initial temperature was set to 37 ℃. The electrical boundary was set as follows (Figure 4.1): (1) the RF electrode was set to a constant voltage (V_0) boundary condition (Dirichlet boundary), (2) a zero-electric-flux (Neumann) boundary condition was applied at the liver tissue exterior boundary, and (3) the other boundaries were considered as the ground pads. The voltage at the ground pads was set to 0 V. Electrical continuity conditions were applied to the other inner boundaries of the whole two-compartment RFA model. The thermal boundary conditions

were as follows: the liver tissue outer boundary temperature was 37 ℃. The 'heat-sink' effect of the cooling effect of the chilled solution circulating inside the RF electrode was approximated by convective boundary conditions at the chilled fluid-electrode interface. Thus, the convective boundary condition of the chilled solution was realised by the heat transfer coefficient h_c = 4416.3 (W m^{-2}K^{-1}) and T_c = 10 ℃. The heat transfer coefficient was calculated using Eq. (4.7) [45].

$$\begin{cases} \mathrm{Re} = \frac{\rho u D}{\mu} \\ N_D = 4 + 0.48624 \ln^2[\frac{\mathrm{Re}\times\mathrm{Pr}\times D}{18\times L}] \\ h = \frac{N_D k}{D} \end{cases} \tag{4.7}$$

where Re is the Reynolds number, Pr = 10.859 is the Prandtl number, D is the diameter and L is the length. For the chilled fluid circulating inside the RF electrode, which has a flow rate of 45 (mL min^{-1}), ρ = 999.7(kg m^{-3}), μ = 0.0013 (kg m^{-1}s^{-1}), k = 0.588 (W m^{-1}K^{-1}) and u = 0.9549 (m s^{-1}) are the density, dynamic viscosity, thermal conductivity and average velocity of the fluid, respectively. The electrical and thermal boundary conditions on the four interfaces between liver tumour and healthy liver tissue, RF electrode and liver tumour, insulated shaft and liver tumour and insulated shaft and healthy liver tissue were considered as continuity, as shown in Figure 4.1.

The two-compartment RFA model was solved using the finite element (FE) software - COMSOL Multiphysics (COMSOL Inc., Burlington, MA, USA). FE method was used to solve Eqs. (4.1)-(4.3) on the whole research domain as shown in Figure 4.1. The research domain was discretized into tetrahedral elements in this study. At every node of the tetrahedral element, Eqs. (4.1)-(4.3) was transferred to algebraic equations and these equations were solved by computer program. The FE mesh was generated by the free meshing generator within COMSOL. The mesh was progressively refined until the maximum temperature of RFA differed by less than 0.2 ℃ compared with the previous mesh. The previous mesh was considered as the final mesh. The meshing results of the models of different target tissues with d_{xy} = 20, 25, 30, and 35 mm consisted of were 282867, 278951, 280787, and 285765 tetrahedral elements, respectively.

The IT50 and the first-order kinetics model (Arrhenius damage model) were used to measure tissue death in this study. In the first-order kinetics model, the tissue death is related to the temperature and the ablation time using a first-order kinetics relation, as shown in Eq. (4.8):

$$\Omega(t) = A\int_0^t e^{\frac{-\Delta E}{RT(\tau)}}d\tau \tag{4.8}$$

where $\Omega(t)$ is the degree of tissue death, $A(1\ s^{-1})$ is the frequency factor, $\Delta E(J\ mol^{-1})$ is the activation energy for the irreversible damage reaction, $R(J\ mol^{-1}K^{-1})$ is the universal gas constant and $T(\tau)(K)$ is the absolute temperature, which is a function of the ablation time. The kinetic parameters A and ΔE account for the morphological changes in tissue related to the thermal degradation of proteins [46] and are dependent on the tissue type [47]. The two values (A = 7.390×10^{39} $(1\ s^{-1})$ and ΔE = 2.577×10^{5} $(J\ mol^{-1})$) for the healthy liver tissue were taken from the literature [48]. For the liver tumour tissue, A = 3.247×10^{43} $(1\ s^{-1})$ and ΔE = 2.814×10^{5} $(J\ mol^{-1})$ were taken from the literature [49]. The value of $\Omega(t)$ = 1 (D63) was employed as the critical threshold to represent tissue death, which corresponds to a 63% probability of cell death [47]. At $\Omega(t) < 1$, the tissue was considered as live.

4.2.3 Computer simulation termination criteria and data collection

To simulate real clinical scenarios as closely as possible, the standard RFA ablation time (12 min) was chosen, or the computer simulation terminates when the first roll-off occurs during the 12-min RFA. In this study, we applied the finding reported by Trujillo et al [20] as the roll-off occurrence criterion, which considered that the roll-off occurs at the moment at which the RF electrode is completely encircled by the charred tissue (at 100 ℃).

In this study, five particular points were selected for the collection of the temperature data, as shown in Figure 4.2. Note that T2, T3, T4, and T5 were deliberately set on the boundaries of the four target tissues of different sizes (d_{xy} = 20, 25, 30, and 35mm, respectively). Thus, the complete TTN of each target tissue size can be investigated through an assessment of the temperatures at these particular points. The TTN volume in this study was the total volume of thermal damage (IT50 or D63) to the liver tissue, which was found by summation of the volumes of all tetrahedral elements in the liver tumour domain and the healthy liver tissue domain. The temperature on every node of such tetrahedral elements must be higher and equal to 50 ℃ or $\Omega(t)$ = 1 on every node of such tetrahedral elements. The thermal damage volume to healthy liver tissue was found in the same way but just in the healthy liver tissue domain using $\Omega(t)$ = 1.

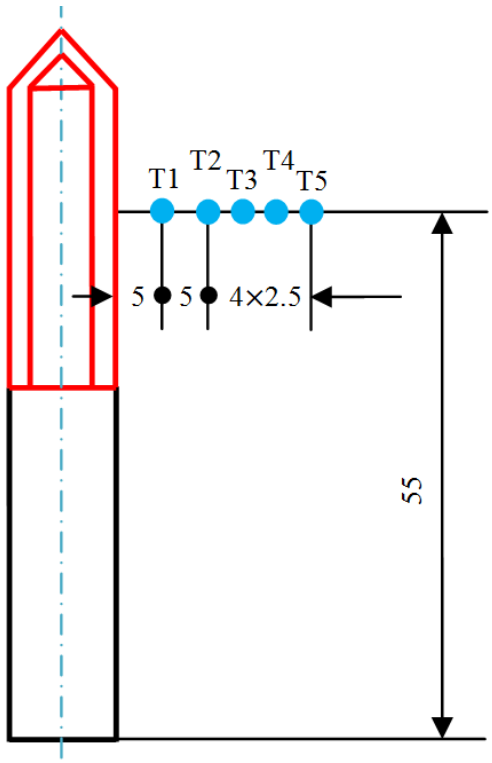

Figure 4.2. Placements of the five measured points (out of scale, dimension in mm).

4.3 Results and discussion

Table 4.2 shows the computer simulation results for the TTN area of each size of target tissue size at different voltages applied. The TTN area was found using the IT50 and the D63. D_{xy} and D_{yz} represent the longest length of the short (perpendicular to the RF electrode axis) and long (parallel to the RF electrode axis) axes of the TTN, respectively. All of the TTN were measured at the moment of the first roll-off occurrence or at 720 s, which was close to the clinical situation. For instance, 35 V-720 s means that the voltage applied was 35 and the TTN area was found at 720 s (note that no the roll-off occurred at this voltage); 37 V-490 s indicates that the voltage applied was 37 V and the TTN area was found at 490 s, which is the time when the first roll-off occurred. We found that the maximum value of D_{xy} can be achieved at a critical voltage. We also found that the critical voltage was the MVA at which the roll-off did not occur during a standard 12-min ablation time. It is necessary to note that all the MVAs were found using trial and error method and the accuracy of the MVAs was considered to be about 0.1 V.

Table 4.2. Computational results for four target tissue sizes during different RFA protocols.

Target tissue (mm)	Ablation protocol	Maximum temperature (℃)	IT50 (mm)	D63 (mm)	Complete ablation
d_{xy}= 20	35 V-720 s	105	D_{xy}= 23.445, D_{yz}= 44.303	D_{xy}= 22.103, D_{yz}= 42.491	Y
	36.6 V-720 s	105	D_{xy}= 26.270, D_{yz}= 44.023	D_{xy}= 23.499, D_{yz}= 42.792	Y
	37 V-490 s	106	D_{xy}= 25.257, D_{yz}= 43.814	D_{xy}= 22.562, D_{yz}= 42.476	Y
	40 V-170 s	108	D_{xy}= 22.990, D_{yz}= 43.165	D_{xy}= 18.312, D_{yz}= 40.780	Y
d_{xy}= 25	34 V-720 s	104	D_{xy}= 26.729, D_{yz}= 43.597	D_{xy}= 25.744, D_{yz}= 42.050	Y
	35.4 V-720 s	105	D_{xy}= 27.736, D_{yz}= 43.997	D_{xy}= 26.785, D_{yz}= 42.593	Y
	36 V-410 s	107	D_{xy}= 27.057, D_{yz}= 43.337	D_{xy}= 25.652, D_{yz}= 41.611	Y
	38 V-200 s	108	D_{xy}= 25.419, D_{yz}= 42.946	D_{xy}= 20.171, D_{yz}= 40.771	N
d_{xy}= 30	32 V-720 s	104	D_{xy}= 29.196, D_{yz}= 42.230	D_{xy}= 27.447, D_{yz}= 41.772	N
	33.9 V-720 s	105	D_{xy}= 30.641, D_{yz}= 43.400	D_{xy}= 29.806, D_{yz}= 42.576	Y-N
	34 V-620 s	105	D_{xy}= 30.431, D_{yz}= 43.208	D_{xy}= 28.340, D_{yz}= 42.438	Y-N
	37 V-185 s	106	D_{xy}= 26.322, D_{yz}= 42.407	D_{xy}= 19.802, D_{yz}= 39.345	N
d_{xy}= 35	31 V-720 s	103	D_{xy}= 31.679, D_{yz}= 41.846	D_{xy}= 29.527, D_{yz}= 40.831	N
	32.5 V-720 s	104	D_{xy}= 33.193, D_{yz}= 42.828	D_{xy}= 30.998, D_{yz}= 41.282	N
	33 V-525 s	105	D_{xy}= 32.561, D_{yz}= 42.818	D_{xy}= 20.431, D_{yz}= 39.898	N
	35 V-245 s	107	D_{xy}= 28.893, D_{yz}= 42.278	D_{xy}= 23.136, D_{yz}= 40.462	N

Y: yes, N: no

The same phenomenon can be found from the simulation results of the TTN volume. As shown in Figure 4.3, the TTN volume increases with the voltage and reaches the maximum value at the MVA and then decreases with the voltage. Due to the roll-off, a large TTN volume cannot be obtained by only increasing the voltage when a constant RF power supply is used.

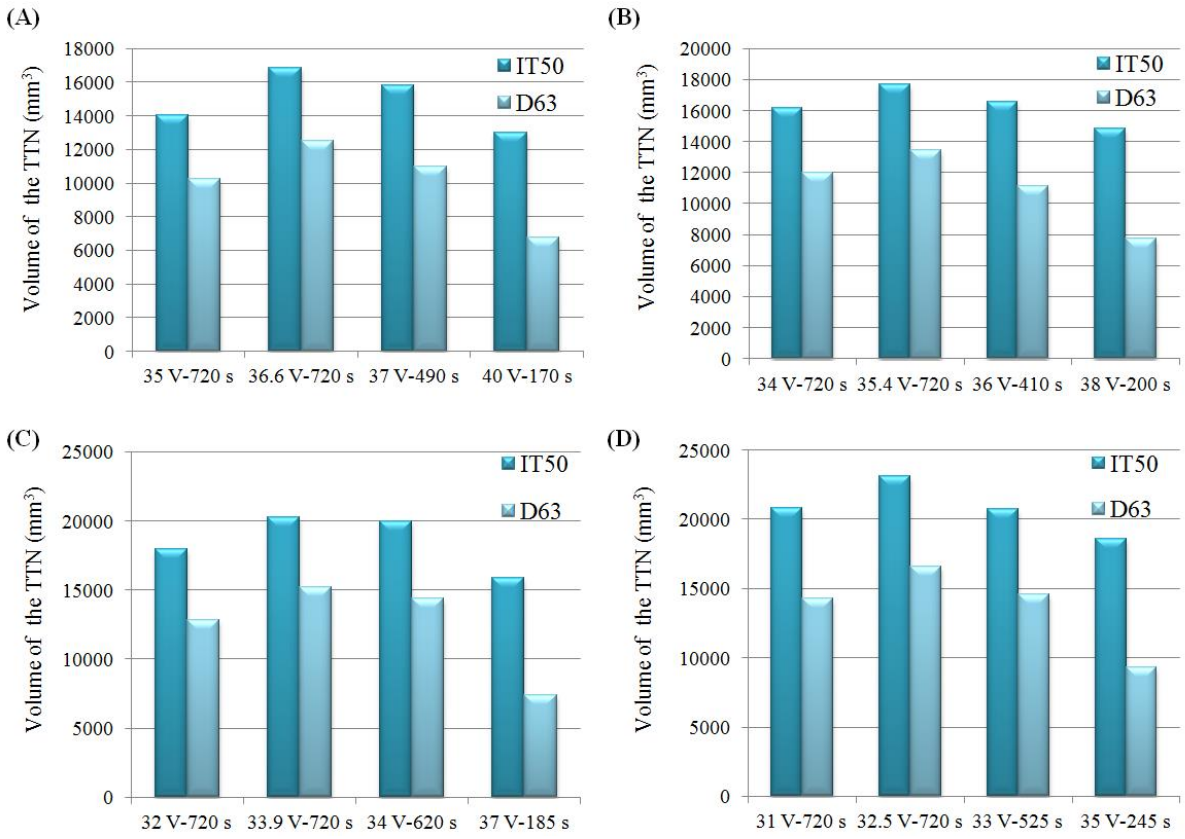

Figure 4.3. TTN volume for each target tissue size at different voltages applied: (A) d_{xy}= 20 mm, (B) d_{xy}= 25 mm, (C) d_{xy}= 30 mm, and (D) d_{xy}= 35 mm.

Another useful piece of information that can be observed from the results of this study is the change of MVAs for different target tissue sizes, as shown in Figure 4.4. We observed that the MVA decreases with an increase in the diameter of the target tissue because the target tissue that has a higher thermal and electrical conductivities and a lower blood perfusion is more sensitive to the thermal therapy [43]. For the diameters d_{xy} = 20, 25, 30, and 35 mm, the MVAs were 36.6, 35.4, 33.9, and 32.5 V, respectively. According to the results obtained in this study, it is worth to mention that different RFA protocols should be adopted for different tumour sizes in clinical setting. Thus, the same protocol is not the best choice for all clinical scenarios.

As shown in Figure 4.5, for small target tissues (d_{xy} = 20 and 25 mm), complete TTN can be achieved at the MVA. However, for relatively large target tissue, such as d_{xy} = 35 mm, complete TTN cannot be achieved at its MVA.

This phenomenon indicates that this large target tissue is unable to be ablated completely using the constant RF power supply method alone. Some auxiliary methods, such as the pulsed RF power supply method [24] or the infusion of hypertonic saline solution into the target tissue [23,50], must be considered. For the critical size of target tissue, namely d_{xy} = 30 mm, the IT50 result showed that the complete TTN can be obtained at the MVA, but the same finding was not demonstrated with the D63 result. It is noteworthy that the 30-mm diameter is a critical target tissue size for the prediction of whether the constant RF power supply method is suitable for the RFA protocol. The results are also consistent with consensus in the field regarding the RFA, which indicates that the RFA alone is not effective for target tissues with diameters larger than 30 mm.

Table 4.3. Volumetric percentage of thermal damage to the healthy liver tissue during different RFA protocols.

Target tissue (mm)	Ablation protocol	V_h (mm^3)	V_d (mm^3)	VP (%)
d_{xy}= 20	35 V-720 s	934872.2	3093.9	0.33
	36.6 V-720 s		5416.9	0.58
	37 V-490 s		3854.1	0.41
	40 V-170 s		851.5	0.09
d_{xy}= 25	34 V-720 s	930631.0	1326.3	0.14
	35.4 V-720 s		2143.3	0.23
	36 V-410 s		1078.2	0.12
	38 V-200 s		397	0.04
d_{xy}= 30	32 V-720 s	925447.1	492	0.05
	33.9 V-720 s		1031.1	0.11
	34 V-620 s		861.4	0.09
	37 V-185 s		168.3	0.02
d_{xy}= 35	31 V-720 s	919321.0	347.2	0.03
	32.5 V-720 s		636.1	0.07
	33 V-525 s		466.5	0.05
	35 V-245 s		188.6	0.02

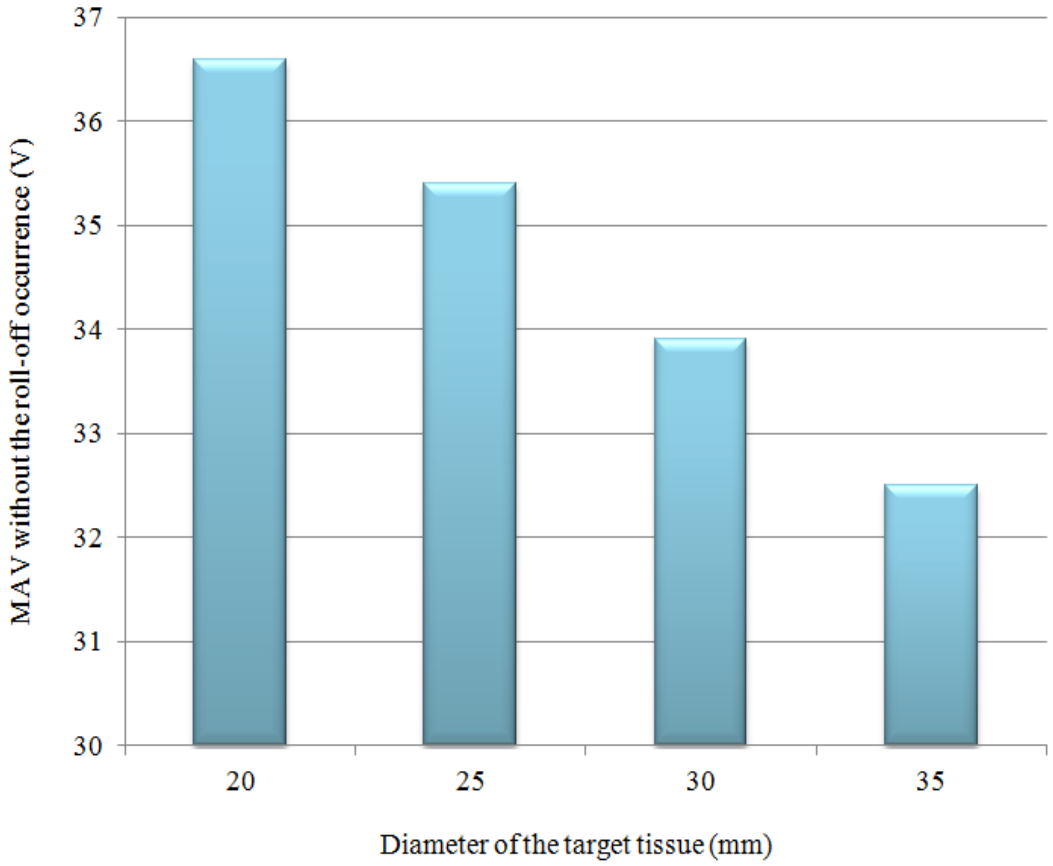

Figure 4.4. MVA without the roll-off occurrence for each target tissue size.

A minimal damage to the surrounding healthy tissue is also a critical requirement for RFA. In an ideal situation, the target issue should be completely ablated (100%) but no surrounding healthy tissue should be ablated (0%). In order to evaluate the thermal damage to the healthy liver tissue, we proposed a volumetric percentage (VP) of the damaged healthy liver tissue, which is expressed by:

$$\mathrm{VP} = \frac{\mathrm{V}_d}{\mathrm{V}_l - \mathrm{V}_{lt}} \times 100\% = \frac{\mathrm{V}_d}{\mathrm{V}_h} \times 100\% \tag{2.9}$$

where V_d is the volume of thermally damaged healthy liver tissue, V_l is the volume of the liver tissue, V_{lt} is the volume of the liver tumour and V_h is the volume of the healthy liver tissue. The VP of thermal damage to the healthy liver tissue for each RFA protocol is shown in Table 4.3. Although all the VPs were quite small (< 1%), two optimal RFA protocols could be found for the 20-mm and 25-mm target tissues and they were 40 V-170 s with 0.09% volumetric damage and 38V-200s with 0.04% volumetric damage, respectively.

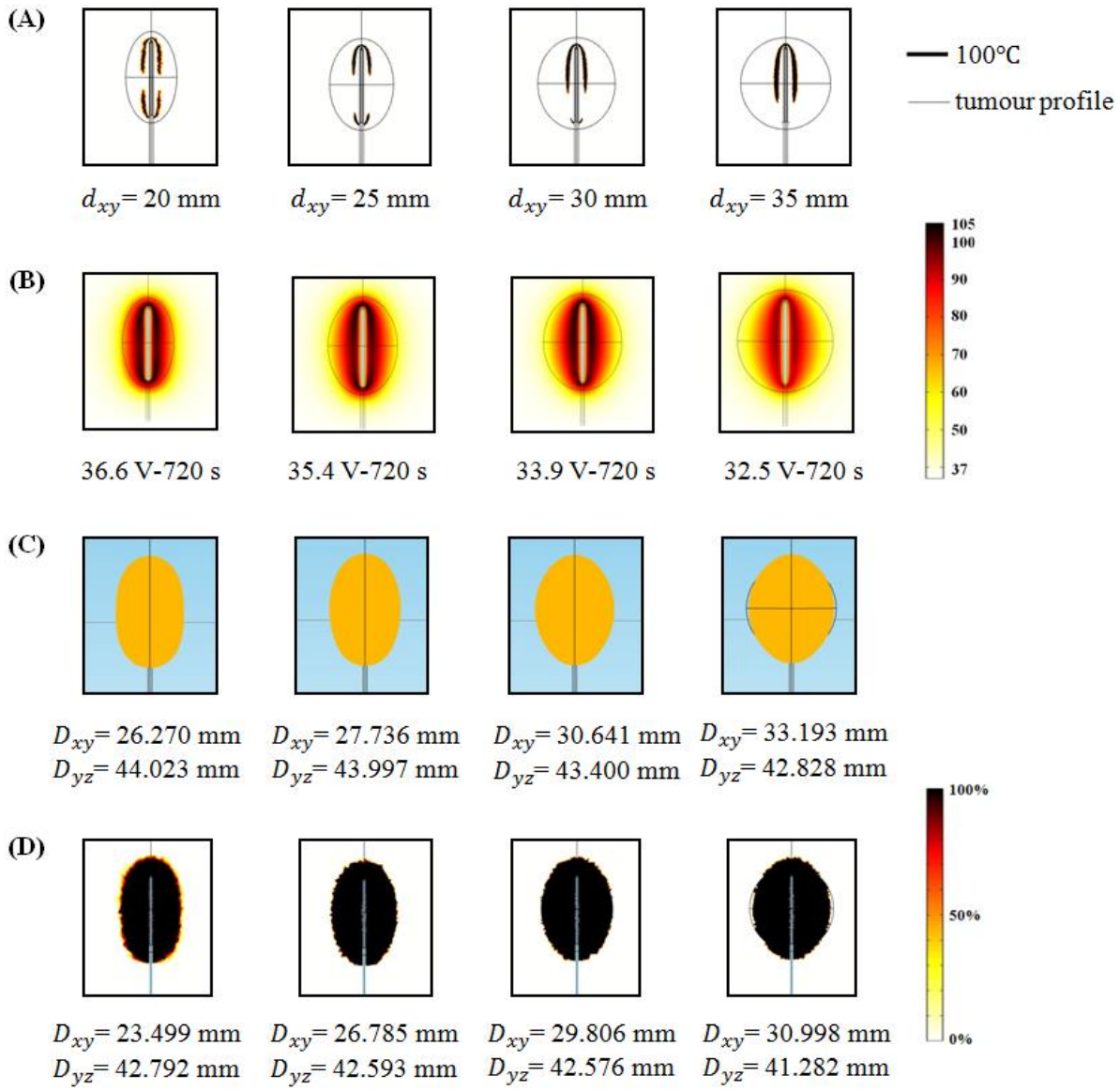

Figure 4.5. Computer simulation results for the TTN of target tissues of different sizes at the MVA (A) 100 ℃ isotherm, (B) temperature distribution (in ℃), (C) Tissue death (IT50), and (D) Tissue death rate (%) (D63).

Figure 4.6 shows the computationally determined temperature gradients for each target tissue size at its own MVA. The temperature differences between T1 and T2 decrease with an increase in the target tissue size and the temperature differences range from 27.5 ℃ (Figure 4.6A) to 22.5 ℃ (Figure 4.6D) at 720 s. The temperature differences between T2 and T3, T3 and T4, and T4 and T5 become more uniform with an increase in the target

tissue size. It is noteworthy that T2 through T5 are deliberately set at the boundaries of each target tissue. Using 50 ℃ as the standpoint for evaluating the TTN, we can find the following interesting conclusions.

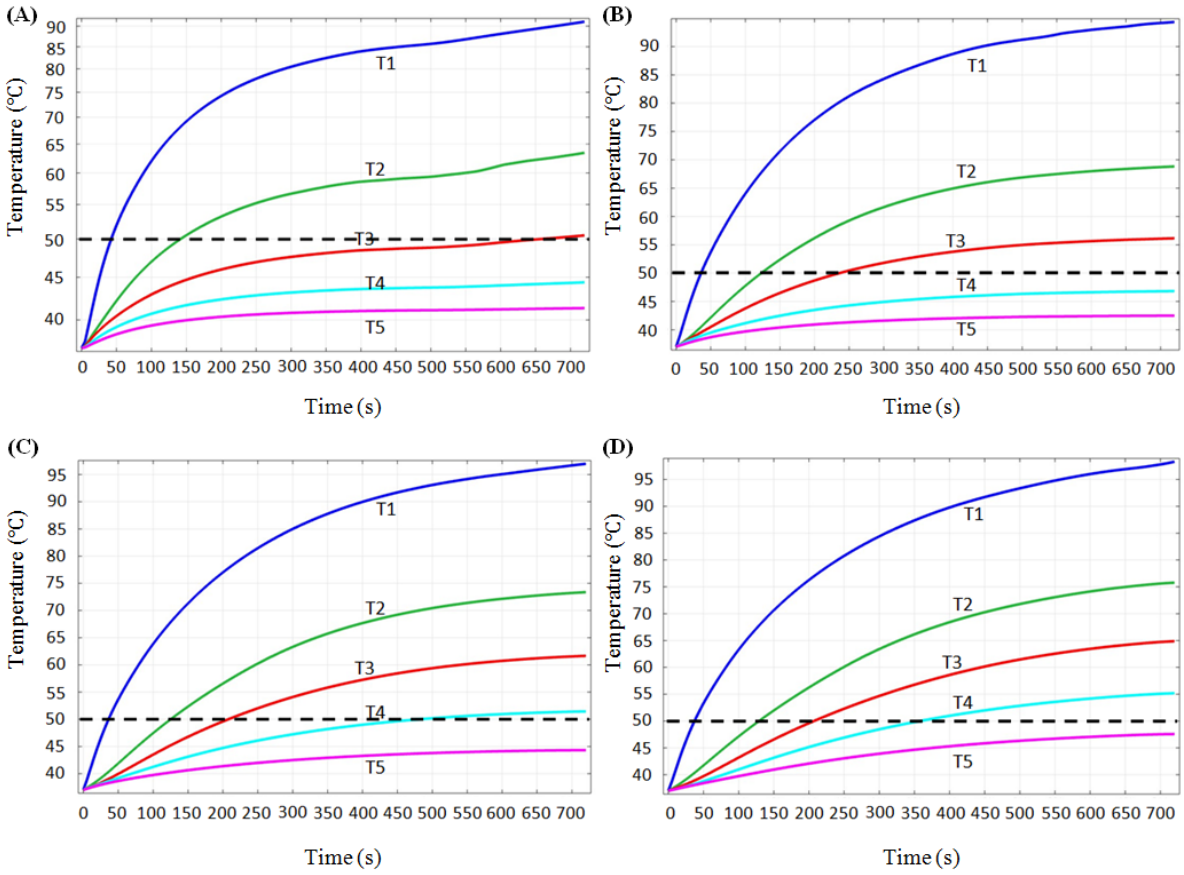

Figure 4.6. Temperature change during the 12-min ablation procedure for each target tissue at its own MVA: (A) d_{xy} = 20 mm, (B) d_{xy} = 25 mm, (C) d_{xy} = 30 mm, and (D) d_{xy} = 35 mm.

For target tissues with d_{xy} = 20 and 25 mm, T2 and T3 were greater than 50 ℃ for 10 and 8 minutes respectively, which indicates that the specific target tissues have been ablated completely. For a target tissue with d_{xy} = 30 mm, T4 was greater than 50 ℃ for more than 4 minutes. Thus, this target tissue can also be killed completely based on the so-called 50 ℃ thermal criterion. However, for a target tissue with d_{xy} = 35 mm, T5 never reached 50 ℃ throughout the 12-min RFA ablation period. The size of target tissue that can be ablated was larger than 30 mm, as shown in Figure 4.6D.

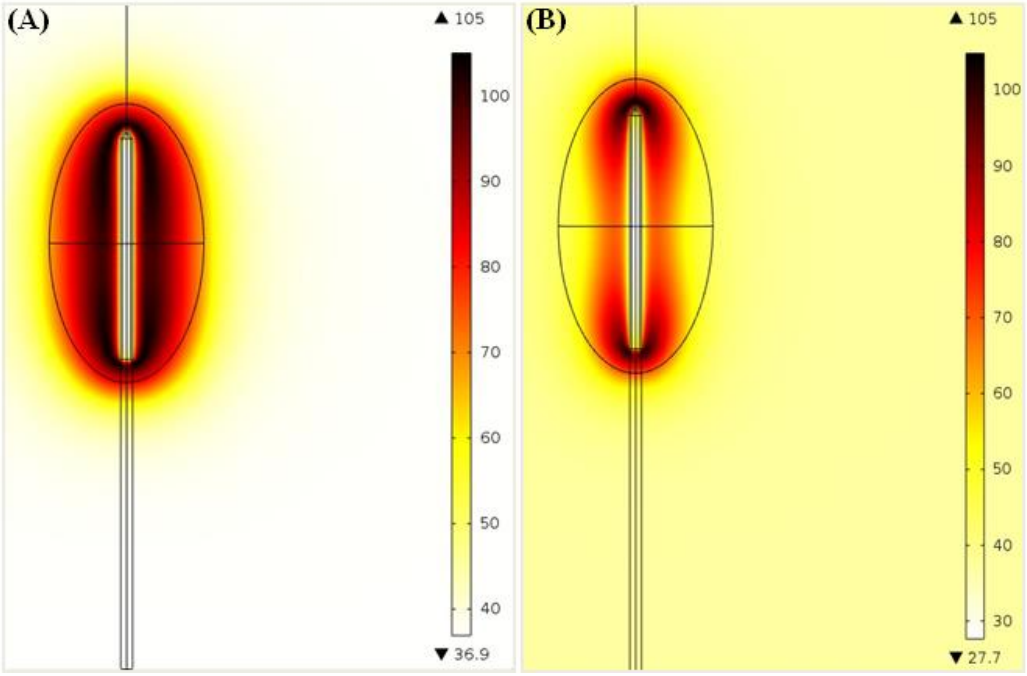

Figure 4.7. Temperature distributions (in ℃) obtained with the two-compartment RFA model (A) and the homogenous RFA model (B).

Figure 4.7 compares the temperature gradients obtained from the two-compartment RFA model and the one-compartment RFA model (homogenous RFA model). This result was simulated considering the 36.6 V-720 s scenario, whereas for the homogenous RFA model, the electrical, thermal and perfusion properties were set equal to those of the healthy liver tissue. As shown in Figure 4.7, more biological tissues around the RF electrode were heated to a temperature greater than 80 ℃ with the two-compartment RFA model compared with those obtained with the homogenous RFA model. The 100 ℃ isotherm only appeared in a small area close to the distal and the proximal parts of RF electrode in the homogenous RFA model. However, for the two-compartment model, the 100 ℃ isotherm almost encompassed the RF electrode. All of these differences prove that a more realistic RFA model should be considered when attempting to investigate the RFA technique using numerical modelling and computer simulation.

One of the limitations of the present work could be the lack of experimental validation, but the authors are confident that the information presented in this manuscript is useful for understanding the deficiency of the RFA technique for

the treatment of large tumour tissues and the effective treatment of target tissues of various sizes in clinical practice. The cooling effect of large blood vessels was also ignored in this study because the main objective focused was on target tissues of difference sizes. Another limitation is that we did not investigate the differences between the different types of liver tumours, such as malignant tumours and benign tumours, due to lack of data [51]. Our future and upcoming studies will aim to validate and improve the results presented in this manuscript using tumour tissue or tumour tissue phantom. Another interesting future work can be the investigation of the relationship between the TTN size and target tissue size in the pulsed RFA.

4.4 Conclusions

This study investigated the different results in the TTN volume on target tissues of different sizes using a two-compartment RFA model. The following three conclusions regarding the RFA procedure for the treatment of target tissues (liver tumours) can be drawn from the results of this study:

(1) While using the constant RF power supply method, the largest TTN volume can be achieved at the maximum voltage applied without the roll-off occurrence.

(2) For target tissues of different sizes, the maximum voltage applied without the roll-off occurrence is different and it decreases with an increase in the target tissue diameter.

(3) The result predicted from the two-compartment RFA model is much different from those obtained with the homogenous RFA model.

Acknowledgements

This article was supported by the Saskatchewan Health Research Foundation (SHRF) through the 'BioNEMS Phase I' grant. The first author (Bing Zhang) also received financial support from the China Scholarship Council (CSC).

Special thanks go to the anonymous reviewers' comments on this paper, which help to improve the paper considerably.

Conflict of interest

The authors report no conflicts of interest. The authors alone are responsible for the content and writing of the paper.

REFERENCES

1. Solbiati L, Livraghi T, Goldberg SN, Ierace T, Meloni F, Dellanoce M, et al. Percutaneous radio-frequency ablation of hepatic metastases from colorectal cancer: long-term results in 117 Patients. Radiology 2001;221:159-66.
2. Gillams A, Khan Z, Osborn P, Lees W. Survival after radiofrequency ablation in 122 patients with inoperable colorectal lung metastases. Cardiovasc Intervent Radiol 2013;36:724-30.
3. Kinoshita T, Iwamoto E, Tsuda H, Seki K. Radiofrequency ablation as local therapy for early breast carcinomas. Breast cancer 2011;18:10-7.
4. Zagoria RJ, Pettus JA, Rogers M, Werle DM, Childs D, Leyendecker JR. Long-term outcomes after percutaneous radiofrequency ablation for renal cell carcinoma. Urology 2011;77:1393-7.
5. Dhillon PS, Gonna H, Li A, Wong T, Ward DE. Skin burns associated with radiofrequency catheter ablation of cardiac arrhythmias. Pacing Clin Electrophysiol 2013;36:764-7.
6. McDonald MB. Conductive keratoplasty: a radiofrequency-based technique for the correction of hyperopia. Trans Am Ophthalmol Soc 2005;103:512-36.
7. Naoumidi TL, Kounis GA, Astyrakakis NI, Tsatsaronis DN, Pallikaris IG. Two-year follow-up of conductive keratoplasty for the treatment of hyperopic astigmatism. J Cataract Refract Surg 2006;32:732-41.
8. McDonald MB, Durrie D, Asbell P, Maloney R, Nichamin L. Treatment of presbyopia with conductive keratoplasty (R): six-month results of the 1-year United States FDA clinical trial. Cornea 2004;23:661-8.
9. Napoletano C, Taurino F, Biffoni M, De Majo A, Coscarella G, Bellati F, et al. RFA strongly modulates the immune system and anti-tumor immune responses in metastatic liver patients. Int J Oncol 2008;32:481-90.
10. Zerbini A, Pilli M, Laccabue D, Pelosi G, Molinari A, Negri E, et al. Radiofrequency thermal ablation for hepatocellular carcinoma stimulates autologous NK-cell response. Gastroenterology 2010;138:1931-42.
11. Widenmeyer M, Shebzukhov Y, Haen SP, Schmidt D, Clasen S, Boss A, et al. Analysis of tumor antigen-specific T cells and antibodies in cancer patients treated with radiofrequency ablation. Int J Cancer 2011;128:2653-62.
12. Xu H-X, Lu M-D, Xie X-Y, Yin X-Y, Kuang M, Chen J-W, et al. Prognostic factors for long-term outcome after percutaneous thermal ablation for hepatocellular carcinoma: a survival analysis of 137 consecutive patients. Clin Radiol 2005;60:1018-25.

13. Shiina S, Tateishi R, Arano T, Uchino K, Enooku K, Nakagawa H, et al. Radiofrequency ablation for hepatocellular carcinoma: 10-year outcome and prognostic factors. Am J Gastroenterol 2011;107:569-77.

14. Llovet JM, Bruix J. Novel advancements in the management of hepatocellular carcinoma in 2008. J Hepatol. 2008;48:S20-37.

15. Zhou Y, Zhao Y, Li B, Xu D, Yin Z, Xie F, et al. Meta-analysis of radiofrequency ablation versus hepatic resection for small hepatocellular carcinoma. BMC Gastroenterol 2010;10:78.

16. Ahmed M, Brace CL, Lee FT, Goldberg SN. Principles of and advances in percutaneous ablation. Radiology 2011;258:351-69.

17. Brace CL. Radiofrequency and microwave ablation of the liver, lung, kidney, and bone: what are the differences? Curr Probl in Diagn Radiol. 2009;38:135-43.

18. Arata MA, Nisenbaum HL, Clark TW, Soulen MC. Percutaneous radiofrequency ablation of liver tumors with the LeVeen probe: is roll-off predictive of response? J Vasc Interv Radiol 2001;12:455-8.

19. Zhang B, Moser MA, Luo Y, Zhang EM, Zhang W. Evaluation of the current radiofrequency ablation systems using axiomatic design theory. Proc Inst Mech Eng H 2014;228:397-408.

20. Trujillo M, Alba J, Berjano E. Relationship between roll-off occurrence and spatial distribution of dehydrated tissue during RF ablation with cooled electrodes. Int J Hyperthermia 2012;28:62-8.

21. Trujillo M, Berjano E. Review of the mathematical functions used to model the temperature dependence of electrical and thermal conductivities of biological tissue in radiofrequency ablation. Int J Hyperthermia 2013;29:590-7.

22. Lorentzen T. A cooled needle electrode for radiofrequency tissue ablation: thermodynamic aspects of improved performance compared with conventional needle design. Acad Radiol 1996;3:556-63.

23. Romero-Méndez R, Tobajas P, Burdío F, Gonzalez A, Navarro A, Grande L, et al. Electrical-thermal performance of a cooled RF applicator for hepatic ablation with additional distant infusion of hypertonic saline: In vivo study and preliminary computer modeling. Int J Hyperthermia 2012;28:653-62.

24. Goldberg SN, Stein MC, Gazelle GS, Sheiman RG, Kruskal JB, Clouse ME. Percutaneous radiofrequency tissue ablation: optimization of pulsed-radiofrequency technique to increase coagulation necrosis. J Vasc Interv Radiol 1999;10:907-16.

25. Andreano A, Brace CL. A comparison of direct heating during radiofrequency and microwave ablation in ex vivo liver. Cardiovasc Intervent Radiol 2013;36:505-11.

26. Zhang B, Moser M, Zhang E, Zhang W. Radiofrequency ablation technique in the treatment of liver tumours: review and future issues. J Med Eng Technol 2013;37:150-9.

27. Pennes HH. Analysis of tissue and arterial blood temperatures in the resting human forearm. J Appl Physiol 1948;1:93-122.

28. Plonsey R, Heppner DB. Considerations of quasi-stationarity in electrophysiological systems. Bull Math Biophys 1967;29:657-64.

29. Berjano EJ, Alió JL, Saiz J. Modeling for radio-frequency conductive keratoplasty: implications for the maximum temperature reached in the cornea. Physiol Meas. 2005;26:157-72.

30. Miller SF, Geiger JD, Shih AJ. Thermal-electric finite element analysis and experimental validation of bipolar electrosurgical cautery. J Manuf Sci Eng 2008;130:021015.

31. Arena CB, Mahajan RL, Rylander MN, Davalos RV. Towards the development of latent heat storage electrodes for electroporation-based therapies. Appl Phys Lett 2012;101:083902.

32. Karampatzakis A, Kühn S, Tsanidis G, Neufeld E, Samaras T, Kuster N. Antenna design and tissue parameters considerations for an improved modelling of microwave ablation in the liver. Phys Med Biol. 2013;58:3191-206.

33. Liu Z, Ahmed M, Sabir A, Humphries S, Goldberg S. Computer modeling of the effect of perfusion on heating patterns in radiofrequency tumor ablation. Int J Hyperthermia 2007;23:49-58.

34. Zhu Q, Shen Y, Zhang A, Xu LX. Numerical study of the influence of water evaporation on radiofrequency ablation. Biomed Eng OnLine. 2013;12:127.

35. Chen X, Saidel GM. Mathematical modeling of thermal ablation in tissue surrounding a large vessel. ASME J Biomech Eng 2009;131:011001.

36. González-Suárez A, Trujillo M, Burdío F, Andaluz A, Berjano E. Could the heat sink effect of blood flow inside large vessels protect the vessel wall from thermal damage during RF-assisted surgical resection? Med Phys 2014;41:083301.

37. Schutt DJ, Haemmerich D. Effects of variation in perfusion rates and of perfusion models in computational models of radio frequency tumor ablation. Med phys 2008;35:3462-70.

38. Haemmerich D, Schutt DJ. RF ablation at low frequencies for targeted tumor heating: In vitro and computational modeling results. IEEE Trans Biomed Eng 2011;58:404-10.

39. Haemmerich D, Schutt DJ, Wright AS, Webster JG, Mahvi DM. Electrical conductivity measurement of excised human metastatic liver tumours before and after thermal ablation. Physiol Meas 2009;30:459-66.

40. Tungjitkusolmun S, Staelin ST, Haemmerich D, Tsai J-Z, Cao H, Webster JG, et al. Three-dimensional finite-element analyses for radio-frequency hepatic tumor ablation. IEEE Trans Biomed Eng 2002;49:3-9.

41. González-Suárez A, Trujillo M, Burdío F, Andaluz A, Berjano E. Feasibility study of an internally cooled bipolar applicator for RF coagulation of hepatic tissue: Experimental and computational study. Int J Hyperthermia 2012;28:663-73.

42. Van Beers BE, Leconte I, Materne R, Smith AM, Jamart J, Horsmans Y. Hepatic perfusion parameters in chronic liver disease: dynamic CT measurements correlated with disease severity. Am J Roentgenol. 2001;176:667-73.

43. Zorbas G, Samaras T. Parametric study of radiofrequency ablation in the clinical practice with the use of two-compartment numerical models. Electromagn Biol Med 2013;32:236-43.

44. Sahani DV, Holalkere N-S, Mueller PR, Zhu AX. Advanced hepatocellular carcinoma: CT perfusion of liver and tumor tissue—initial experience. Radiology 2007;243:736-43.

45. Haemmerich D, Wright A, Mahvi D, Lee Jr F, Webster J. Hepatic bipolar radiofrequency ablation creates coagulation zones close to blood vessels: a finite element study. Med Biol Eng Comput 2003;41:317-23.

46. Baldwin SA, Pelman A, Bert JL. A heat transfer model of thermal balloon endometrial ablation. Ann Biomed Eng 2001;29:1009-18.

47. Chang IA, Nguyen UD. Thermal modeling of lesion growth with radiofrequency ablation devices. Biomed Eng OnLine 2004;3:27.

48. Kim B-M, Jacques SL, Rastegar S, Thomsen S, Motamedi M. Nonlinear finite-element analysis of the role of dynamic changes in blood perfusion and optical properties in laser coagulation of tissue. IEEE J Select Topics Quantum Electron 1996;2:922-33.

49. Reddy G, Dreher MR, Rossmann C, Wood BJ, Haemmerich D. Cytotoxicity of hepatocellular carcinoma cells to hyperthermic and ablative temperature exposures: In vitro studies and mathematical modelling. Int J Hyperthermia 2013;29:318-23.

50. Lee JM, Kim SH, Han JK, Sohn KL, Choi BI. Ex vivo experiment of saline-enhanced hepatic bipolar radiofrequency ablation with a perfused needle electrode: comparison with conventional monopolar and simultaneous monopolar modes. Cardiovasc Intervent Radiol 2005;28:338-45.

51. Laufer S, Ivorra A, Reuter VE, Rubinsky B, Solomon SB. Electrical impedance characterization of normal and cancerous human hepatic tissue. Physiol Meas 2010;31:995-1009.

5 NUMERICAL ANALYSIS OF THE RELATIONSHIP BETWEEN THE AREA OF TARGET TISSUE NECROSIS AND THE SIZE OF TARGET TISSUE IN LIVER TUMOURS WITH PULSED RADIOFREQUENCY ABLATION

This chapter is derived from an accepted manuscript published by Taylor & Francis in ***International Journal of Hyperthermia*** *in 2015. Available online: http://www.tandfonline.com/ doi:10.3109/02656736.2015.1058429.*

Abstract

Purpose: Radiofrequency ablation (RFA) is currently restricted to the treatment of target tissues with a small size (<3 cm in diameter). To overcome this problem with RFA, some phenomena need to be understood first. The study presented in this paper investigated the relationship between the area of target tissue necrosis (TTN) and the size of target tissue in pulsed radiofrequency ablation (PRFA).

Materials and methods: Liver tumour, one of the common targets of RFA in clinical practice, was used as the target tissue in this study. Two types of pulsed RF power supply methods (half-square and half-sine) and three target tissues with different sizes (25 mm, 30 mm, and 35 mm in diameter) were studied using finite element modelling. The finite element model (FEM) was validated by using *in vitro* experiments with porcine liver tissues. The first roll-off occurrence or 720 s, whichever occurs first, was chosen as the ablation termination criteria in this study.

Results: For each target tissue size, the largest TTN area was obtained using the maximum voltage applied (MVA) without roll-off occurrence. In this study, target tissues with a 25 mm diameter can be ablated completely but target tissues with 30-mm and 35-mm failed to be ablated.

Conclusions: The half-square PRFA could achieve a larger TTN area than the half-sine PRFA. The MVA decreases with an increase in the target tissue diameter in both the half-square PRFA and the half-sine PRFA. The findings of this study are in agreement with the clinical results that lesions (≥3 cm in diameter) have less favourable results from RFA.

5.1 Introduction

Radiofrequency ablation (RFA) is a thermal therapy technique that has been used to eradicate the tumours in the liver and other organs for many years [1,2]. However, this technique has yet to establish good clinical results in the treatment of target tissues ≥3 cm in diameter [3-5]. Zhang et al. [6] evaluated the deficiencies of current commercial RFA systems using an engineering method (axiomatic design theory) and concluded that the incomplete target tissue necrosis (TTN) of RFA for large target tissues is the main reason. Previous studies [7,8] showed that one of the determinant factors causing the incomplete TTN is the tissue charring during the procedure of RFA. The tissue charring occurs when the tissue is heated to a temperature above 100 ℃ due to water evaporation.

In the RFA technique, alternating electrical currents with high frequency (~500 kHz) are used to generate the heat to kill the target tissues. So this technique is heavily influenced by the impedance of external loads, including the target tissue and healthy surrounding tissue. When the tissues are getting charred, the impedance of external loads increases dramatically and this prevents the RF power generator from delivering further energy into the tissue. In the clinical setting, this dramatic increase of impedance, followed by a drop of RF power supply, is called 'roll-off'. The roll-off is a critical factor during the generation of TTN size in RFA. For more information about the roll-off, the readers may refer to our previous study [9].

To overcome this deficiency with the RFA technique, a better understanding of the change of TTN size prior to the roll-off occurrence is crucial. In our previous study [9], we investigated the relationship between the size of TTN (volume) and the size of target tissue in a constant radiofrequency ablation (CRFA) using a two-compartment finite element modelling approach. We concluded that the largest TTN volume can be achieved at the maximum voltage applied (MVA) without roll-off occurrence and the MVA was different for different sizes of target tissues. Our previous study also confirmed that the CRFA was unable to kill liver tumours ≥3 cm in diameter with the mathematical model. Besides, the constant RF power supply, the pulsed RF has also been used as an alternate power supply method in the current commercial RFA devices in the pursuit of getting a larger TTN size [10-12]. In the present study, we continued our work using a 2D axis symmetric FEM and tried to find the relationship between the size of TTN (area) and the size of target tissue in the PRFA. Three different sizes of liver tumours with 25, 30, and

35 mm in diameter, respectively, were taken as the target tissues. For the pulsed RF power supply method, the half-square and the half-sine methods were used in the present study.

The remainder of this paper is as follows. The FEM of PRFA and the TTN area evaluation are discussed in Section 5.2, followed by the presentation of results with discussion in Section 5.3. Some conclusions drawn from this study are given in Section 5.4.

5.2 Materials and methods

5.2.1 Finite element modelling of PRFA

The PRFA process is a coupled thermal-electric problem. The problem was represented as a 2D axis symmetric FEM. The model was created and solved numerically using COMSOL Multiphysics 4.0 software (COMSOL, Inc., Burlington, MA, USA). As shown in Figure 5.1, a healthy liver tissue was built as a cylinder measuring 50 mm in radius and 130 mm in height. An elliptical liver tumour with a 40 mm long axis and a d_x (25, 30 and 35 mm) short axis was considered in this model. An internally cooled RF applicator (Covidien AG, Zurich, Switzerland), consisting of a RF electrode and an insulated shaft, was chosen for this liver tumour and created in this 2D axis symmetric PRFA model. The RF applicator with a 1.5 mm diameter and 30 mm exposure length (length of the RF electrode) was inserted into the liver tumour. The centre of the RF electrode was put on the centre of the liver tumour in the pursuit of an optimal RF electrode placement.

The governing equation for this 2D coupled thermal-electric problem is the Pennes bioheat transfer equation [13] with the heat source generated by the RF electrical current:

$$\rho c \frac{\partial T(\mathbf{x},t)}{\partial t} = \nabla \cdot \big(k \nabla T(\mathbf{x},t)\big) + \rho_b c_b \omega_b \big(T_b - T(\mathbf{x},t)\big) + Q_m(\mathbf{x},t) + Q_{hs}(\mathbf{x},t) \qquad \mathbf{x} \in \mathbf{\Gamma} \qquad (5.1)$$

where ρ (kg m^{-3}) is the density, c (J kg^{-1}K^{-1}) is the specific heat, $T(\mathbf{x},t)$ (°C) is the temperature, $\mathbf{x} = \{\mathrm{r}, \mathrm{z}\}$ in the 2D axis symmetric coordinate system, $\mathbf{\Gamma}$ denotes the analysed 2D axis symmetric domain, k (W m^{-1}K^{-1}) is the thermal conductivity, ρ_b (kg m^{-3}) is the blood density, c_b (J kg^{-1}K^{-1}) is the blood specific heat, ω_b (s^{-1}) is the blood perfusion rate, T_b is the temperature of the blood entering the tissue, $Q_m(\mathbf{x},t)$ (W m^{-3}) is the volumetric heat

power generated by metabolism, which was neglected due to its small magnitude compared with the other terms in Eq. (5.1) in this study and $Q_{hs}(\mathbf{x},t)$ W m^{-3} is the spatial heat power generated by the RF electrical current.

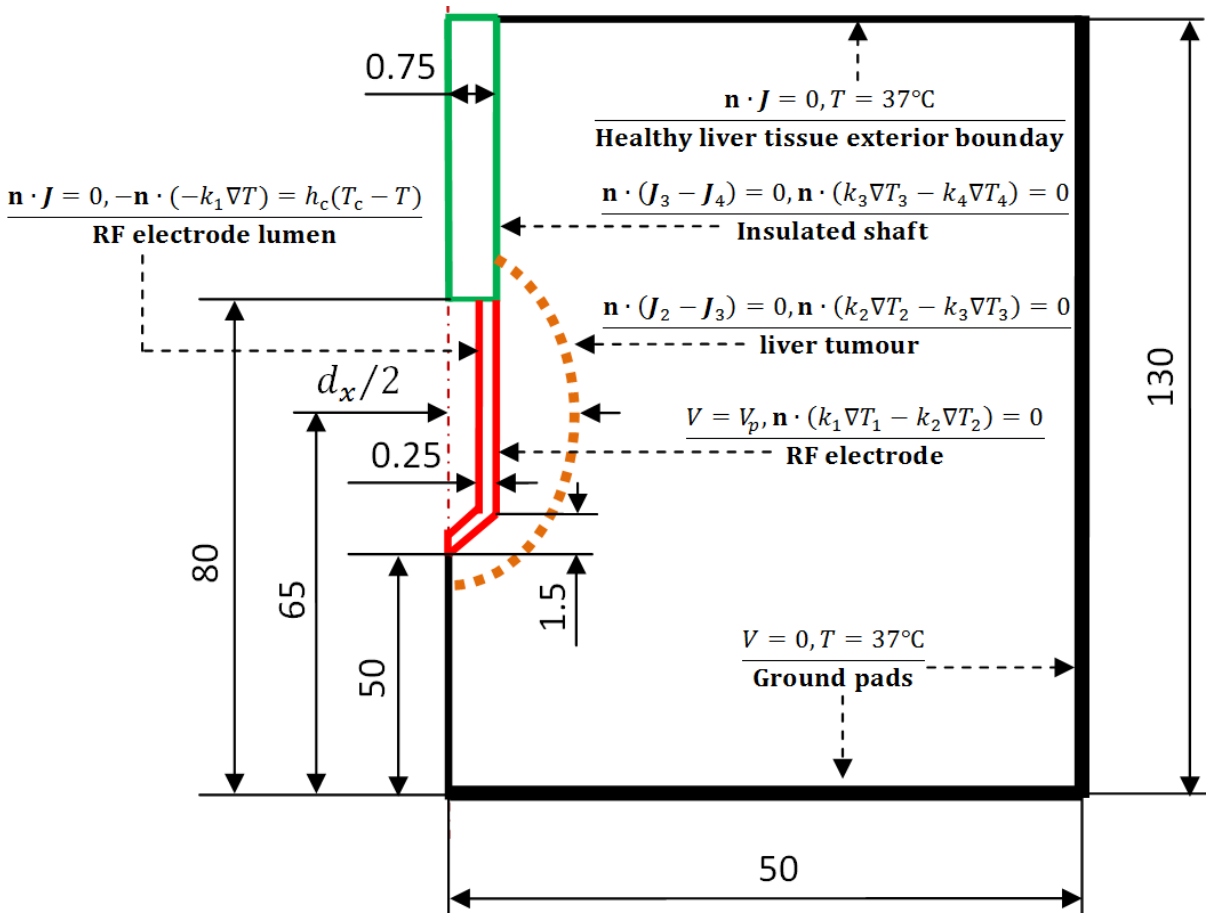

Figure 5.1. 2D axis symmetric RFA model and its boundary conditions used in the present study (out of scale, dimension in mm).

In RFA, $Q_{hs}(\mathbf{x},t)$ can be calculated by $Q_{hs}=\boldsymbol{J}\cdot\boldsymbol{E}=\sigma|\nabla V|^2$. $\boldsymbol{J}$ (A m^{-2}), $\boldsymbol{E}$ (V m^{-1}) and V (V) are the current density, the electrical field intensity and the applied voltage, respectively. By using the quasi-static approach, the value of applied voltage can be evaluated by $\nabla\cdot\sigma\nabla V=0$. The properties of all the elements in the RFA model were found from the literature [14-20] and tabulated in Table 5.1.

We considered the temperature dependence of the thermal conductivity and the electrical conductivity for both liver tumour and healthy liver tissue. Below 100 ℃, the thermal conductivity and the electrical conductivity were approximated by Eq. (5.2) and Eq. (5.3), respectively.

$$k(T) = k_{at\ 21\ ℃} + 0.0013(T(\mathbf{x}, t) - 21) \tag{5.2}$$

$$\sigma(T) = \sigma_{at\ 21\ ℃}[1 + 0.02(T(\mathbf{x}, t) - 21)] \tag{5.3}$$

Table 5.1. Thermal and electrical properties of the modelling elements used in the present study.

Modelling element	ρ (kg m^{-3})	c (J kg^{-1}K^{-1})	k (W m^{-1}K^{-1})	σ (S m^{-1})	ω_0 (s^{-1})
Healthy liver tissue	1080	3455	0.515[a]	0.203[a]	0.016
Liver tumour	1045	3760	0.60[a]	0.50[a]	0.002
RF electrode	6450	840	18	1.0×10^{8}	-
Insulated shaft	70	1045	0.026	1.0×10^{-5}	-
Blood vessel	1000	4180	0.49	0.667	-

[a] evaluated at 21 ℃.

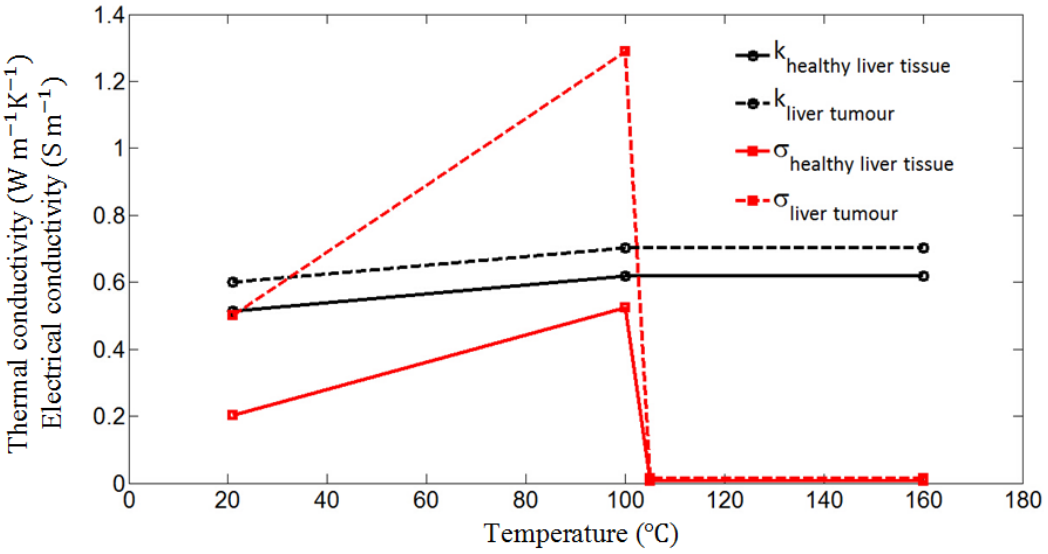

Figure 5.2. Thermal and electrical conductivities of healthy liver tissue and liver tumour used in the present study.

The thermal conductivity was considered as a constant when temperature was higher than 100 ℃. Between 100 ℃ and 105 ℃, the electrical conductivity decreased rapidly with two orders of the magnitude due to water vaporization and desiccation [21]. Over 105 ℃, it was considered as a constant, as shown in Figure 5.2. The blood perfusion rates in healthy liver tissue and liver tumour were also considered as temperature dependent. They were described by Eq. (5.4) [22].

$$\omega_b(T) = \begin{cases} \omega_0 & (T < 60℃) \\ 0 & (T \geq 60℃) \end{cases} \tag{5.4}$$

The initial temperature of the whole FEM was set to 37 ℃, which is close to the internal temperature of the human body. A pulsed voltage (V_p) and 0 V were applied on the surface of the RF electrode and ground pads, respectively. The inner side of RF electrode lumen and the healthy liver tissue exterior boundary were set as electrical insulation. All other interfaces inside the liver tissue were taken as continuity, as shown in Figure 5.1. The cooling effect of the RF electrode was approximated by using the Newton cooling law using the thermal convection coefficient (h_c) and the cooling temperature (T_c). The h_c = 3366 (W m^{-2}K^{-1}) was calculated by considering the 30-mm RF electrode and an half of the cross section area of the RF electrode lumen [23]. The flow rate of the cooling water was considered as 45 (mL min^{-1}). Note that the previous study [24] suggested that the cooling temperature have no significant effect on the TTN size. However, we still set the cooling temperature to be 10 ℃ (because it was used in many clinical settings and computational models [14,23,25]).

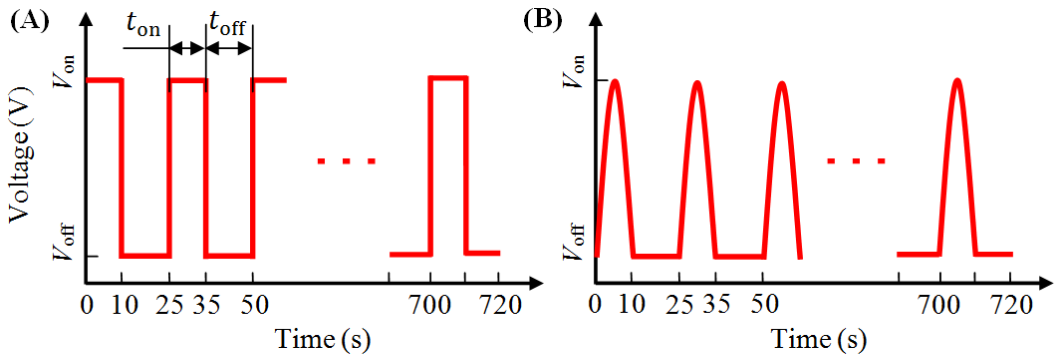

Figure 5.3. Two pulsed RF power supply methods: (A) half-square waveform and (B) half-sine waveform.

In the present study, two types of the pulsed voltages (half-square and half-sine) were taken as the RF power supply methods, as shown in Figure 5.3. Note that the half-square pulsed voltage is used in the current commercial RFA systems [11]; the half-sine pulsed voltage was investigated by some researchers [12] and they concluded that the half-sine pulsed voltage method had achieved a relatively large TTN size compared with the half-square method in the animal tissue experiments [12]. For the pulsed RF power supply method, four parameters such as V_{on}, V_{off}, t_{on} and t_{off} need to be determined. V_{on} is the applied voltage which is used to generate the heat; V_{off} is the cooling voltage, which should be small enough so that only negligible heat can be generated; t_{on} is the heating period during which the V_{on} applied; t_{off} is the cooling period. To get close to the real clinical setting in the computer simulation, 10 and 15 seconds in a pulse circle were used for t_{on} and t_{off}, respectively [10,11].

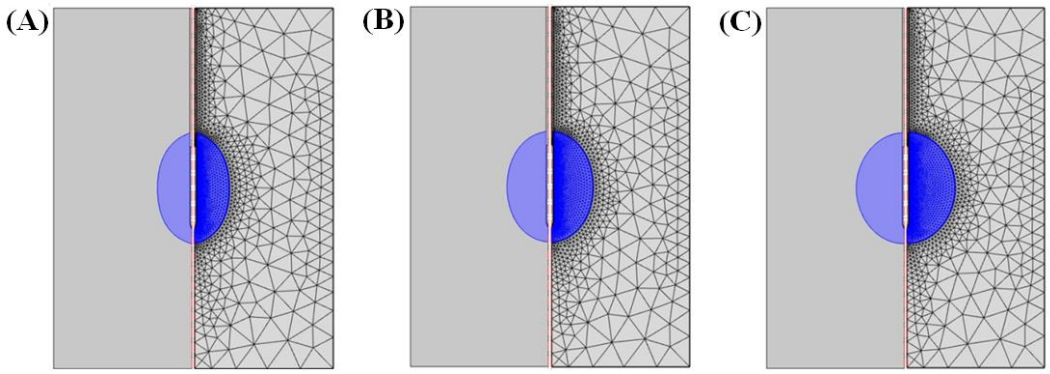

Figure 5.4. FEMs and their mesh modes used in the present study for three sizes of target tissues: (A) 25 mm, (B) 30 mm, and (C) 35 mm.

A sensitive study was performed to determine the value of V_{off}. We evaluated the maximum temperature at 720 s using a fixed V_{on} (30 V) and a decreasing V_{off}. When the difference of the maximum temperature between the two V_{off}s was less than 0.1 ℃, the previous value of V_{off} was chosen. In this study, the value of V_{off} was found as 4 V. In order to avoid the boundary effects, the same sensitive analysis was also done for the dimension of the healthy liver tissue. Three pairs of dimensions, such as (50 mm, 130 mm), (60 mm, 180 mm), and (80 mm, 200 mm), were examined. The differences of the maximum temperatures between these three dimensions were all less than 0.1 ℃. So the smallest size of healthy liver tissue was used in this study for saving the computational cost.

The convergence tests of the meshing were done using the $V_{\text{on}} = 30$ V, $V_{\text{off}} = 4$ V and 0.1 ℃ temperature difference. The whole research domain was divided into triangular elements, as shown in Figure 5.4. A fine mesh was set in the region of interest to include the RF electrode domain and the liver tumour domain, where higher temperature gradients were expected. This iterative process was continued until the convergence test was satisfied. For the target tissue with 25 mm, 30 mm and 35 mm in diameter, there were 3878, 4164, and 4477 triangular elements in the FEM, respectively.

5.2.2 TTN area evaluation

There were several methods used to evaluate the TTN in the previous literature, such as the temperature threshold, the Arrhenius model and the cumulative equivalent minutes at 43 ℃. The Arrhenius model was used to evaluate the TTN size in this study, which can be given as follows:

$$\Omega(t) = A \int_0^t e^{\frac{-\Delta E}{RT(\tau)}} d\tau \tag{5.5}$$

where $\Omega(t)$ is the degree of tissue death, A (s^{-1}) is the frequency factor, ΔE (J mol^{-1}) is the activation energy for the irreversible damage reaction, R ($\text{J mol}^{-1}\text{K}^{-1}$) is the universal gas constant and $T(\tau)$ (K) is the absolute temperature. In this study, $A = 7.390 \times 10^{39}$ (s^{-1}) and $\Delta E = 2.577 \times 10^{5}$ (J mol^{-1}) were found from the literature [26] for healthy liver tissue. For the liver tumour, $A = 3.247 \times 10^{43}$ (s^{-1}) and $\Delta E = 2.814 \times 10^{5}$ (J mol^{-1}) were found from the literature [27]. The tissue was considered as dead, if the value of $\Omega(t) = 1$, which corresponds to the 63% probability of tissue cell death [28].

As discussed before in the section of Introduction, this study focused on the change of the TTN area prior to the first roll-off occurrence or at 720 s, whichever occurred first. Trujillo et al. [23] concluded that the roll-off usually happens at the moment when the RF electrode is encircled by the charred tissue (tissue above 100 ℃). In this study, we stopped the ablation procedure using the first roll-off occurrence as a criterion. The TTN area was evaluated by summation of the areas of all triangular elements in the liver tumour domain and healthy liver tissue domain that had $\Omega(t) = 1$ on all nodes.

5.2.3 The *in vitro* experiment for validation of the FEM

To validate the accuracy of the FEM used in the present study, *in vitro* experiments with porcine liver tissue were performed. The *in vitro* experiments followed the regulation of *Biosafety Permit Protocol* of University of Saskatchewan for handling tissues. A custom-made RFA system with 50-W maximum power (450 kHz) and a no-cooling RF electrode with 1.98 mm of diameter and 30 mm of exposure length were used in the experiment. The porcine liver tissues were acquired from a local grocery store. Before the experiment, all the porcine liver tissues were heated up to an ambient temperature of 21 ℃ (room temperature). Figure 5.5 shows the experimental set up. The liver tissue was put on an aluminium foil (190×210 mm) acting as the ground pad. The electrode was inserted into the liver tissue with the insertion of about 50 mm. The distance between the ground pad and the RF electrode was set to about 20 mm to avoid the situation where the TTN grows towards the ground pad. Two ablation operations with durations of 360 s and 720 s (respectively and with 30 V (CRFA) of applied voltage were performed on the tissue. We used a total of 10 pieces of porcine liver tissues ($n = 5$ for each ablation time) and the size of each tissue was kept at least 80×60×40 mm. The initial temperature and blood perfusion rate in the FEM were set to be 21 ℃ and 0, respectively, for the consistency with the *in vitro* experiments.

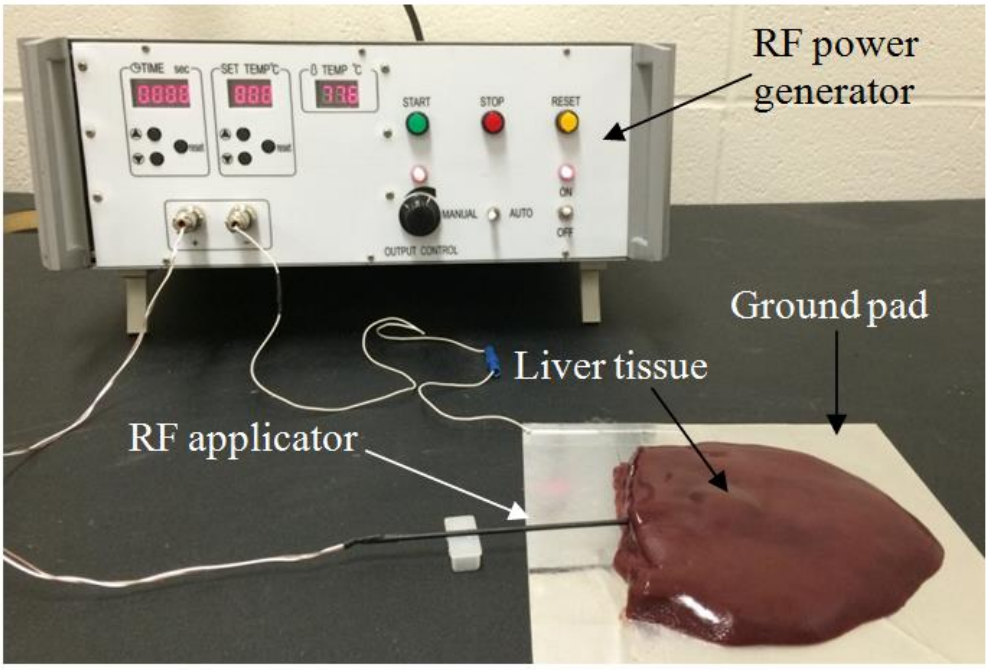

Figure 5.5. *In vitro* experimental set up for the validation of the FEM.

5.3 Results and discussion

5.3.1 Experimental results for validation of the FEM

Figure 5.6 shows the computational and experimental results at 360 s and 720 s, respectively. The two ablation times (i.e. 360 s and 720 s) were selected based on the experience of the roll-off state in the RFA procedure, learned from both the FEM simulation and in vitro experiment; particularly, when time is around 360 s, the tissue charring proceeds but prior to the roll-off, while time is around 720 s, the roll-off is certainly presented. The size of TTN in the *in vitro* experiments was determined by visual examinations. As shown in Figure 5.6, an elliptical TTN area ('pale zone') can be found. The size of TTN in the FEM was determined by the Arrhenius model ($\Omega(t) = 1$), discussed in the section of evaluation of TTN area.

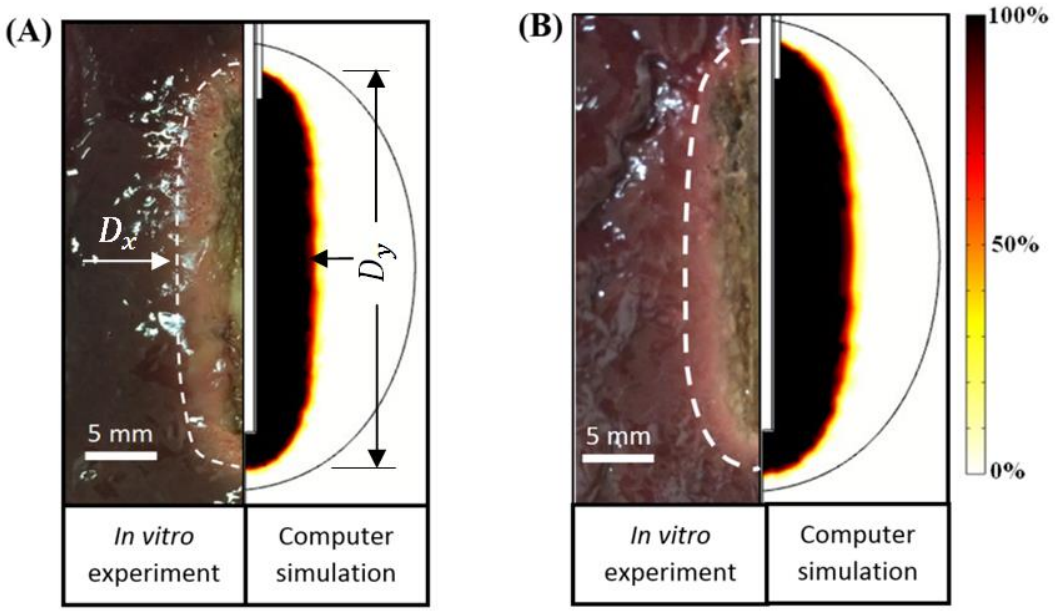

Figure 5.6. Computational and experimental results for two ablation operations: (A) 360 s, (B) 720 s.

As shown in Table 5.2, a good agreement on TTN area between the FEM and the *in vitro* experiments can be found, regardless of the ablation duration. The results of D_x and D_y, obtained from FEM, show that they are all located in the corresponding error bars of the results, obtained from the *in vitro* experiments. There are only acceptable discrepancies on TTN areas between the *in vitro* experiments and FEM at both 360 s and 720 s ablation durations

(9.3% and 8.0%, respectively). These discrepancies may come from the following two reasons: (1) not all the sliced liver tissues are in the same size and (2) underestimation of TTN size in the *in vitro* experiments using the pale zone method. A narrow zone (sub-lethal damage zone or hemorrhagic rim) around the central pale zone, where the tissue cells are dead but the proteins are not denatured completely to become whitish, can be revealed by the triphenyl tetrazolium chloride (TTC) staining technique. The comparison shows that the FEM has enough accuracy to be used as a test-bed.

Table 5.2. Comparisons of TTN areas from the FEM and *in vitro* experiments.

Ablation time (s)	TTN area	*In vitro* experiments[#]	FEM
360	D_x (mm)	10.9±0.3	11.2
	D_y (mm)	34.4±0.4	34.6
	Area (mm^2)	295.6±9.4	325.8
720	D_x (mm)	13.3±0.3	13.6
	D_y (mm)	35.9±0.3	36.1
	Area (mm^2)	374.9±10.4	407.4

[#]the results of the *in vitro* experiments were given as mean±standard deviation

5.3.2 Computational results for analysis of the pulsed RFA

Two types of pulsed RF power supply methods (half-square and half-sine) and three different sizes of target tissues (d_x= 25, 30, and 35 mm) were then examined on the FEM in this study. Twenty-four PRFA protocols were simulated with the FEM. All the TTN areas were evaluated at the time when the first roll-off occurred or at 720 s, whichever occurred first. For instance, a RFA protocol, like 47.2 V-720 s for the 25-mm target tissue meant that the applied voltage (V_{on}) was 47.2 V and the TTN area was found at 720 s, because in this PRFA protocol there was no roll-off occurring, as shown in Figure 5.7.

Figure 5.7 shows the change of the 100 ℃ isotherm and the temperature distributions. The impedance between the RF electrode and the ground pads during the whole ablation process was less than a critical value (roll-off occurred at this value), as show in Figure 5.7D. In the present study, the critical impedance value was about 45 Ω (not shown

in this paper) according to our initial work for this study. Figure 5.8 shows another PRFA protocol (48 V-145 s) in which the V_{on} was 48 V and the first roll-off occurred at 145 s. The RF electrode was encircled completely by 100 ℃ isotherm at 145 s when the impedance dramatically increased to about 85 Ω, as shown in Figure 5.8D.

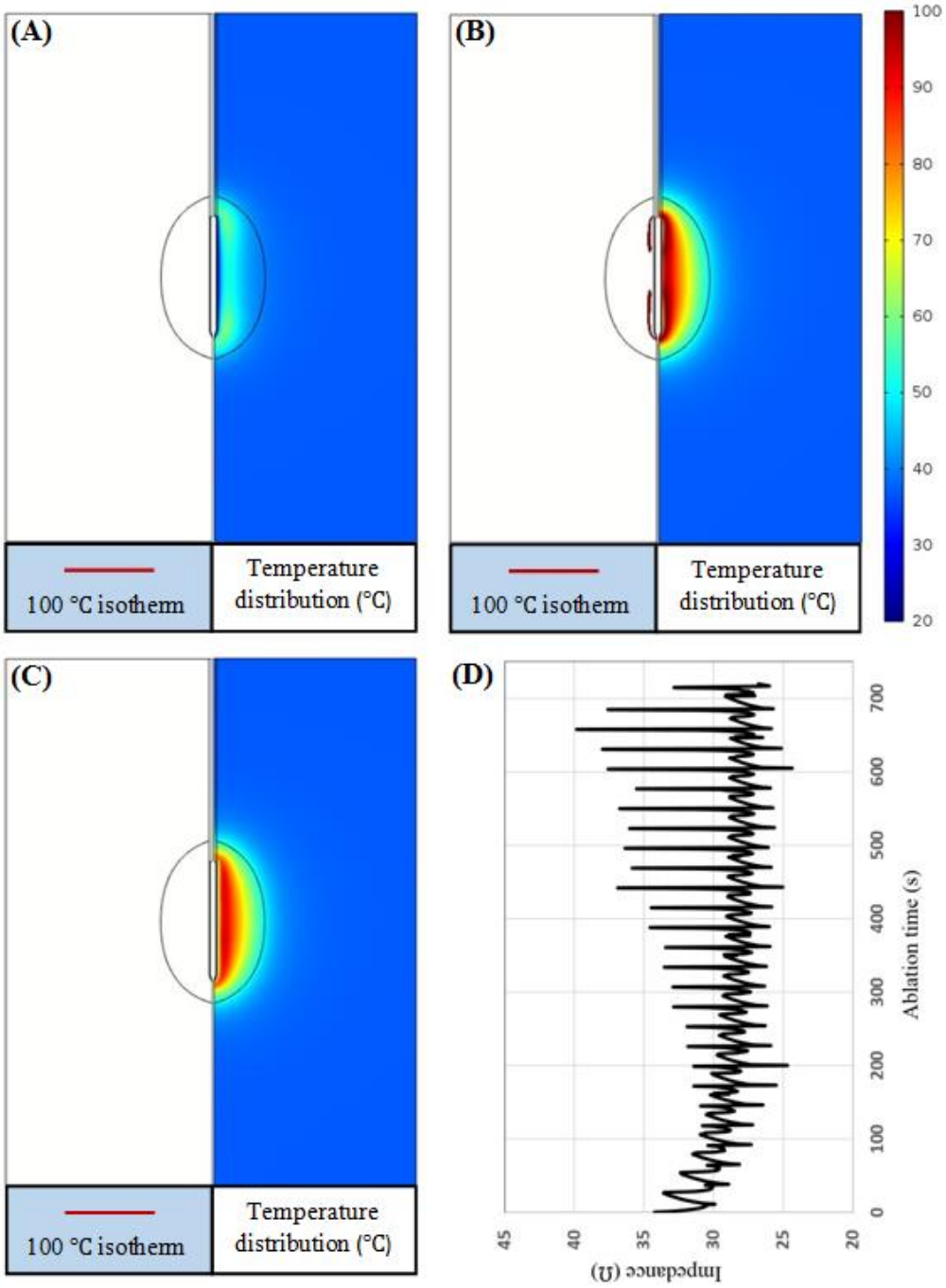

Figure 5.7. 100 ℃ isotherm and temperature distribution of the scenario of 47.2 V-720 s at 50 s (A), 442 s (B), and 720 s (C) and the change of the impedance (D).

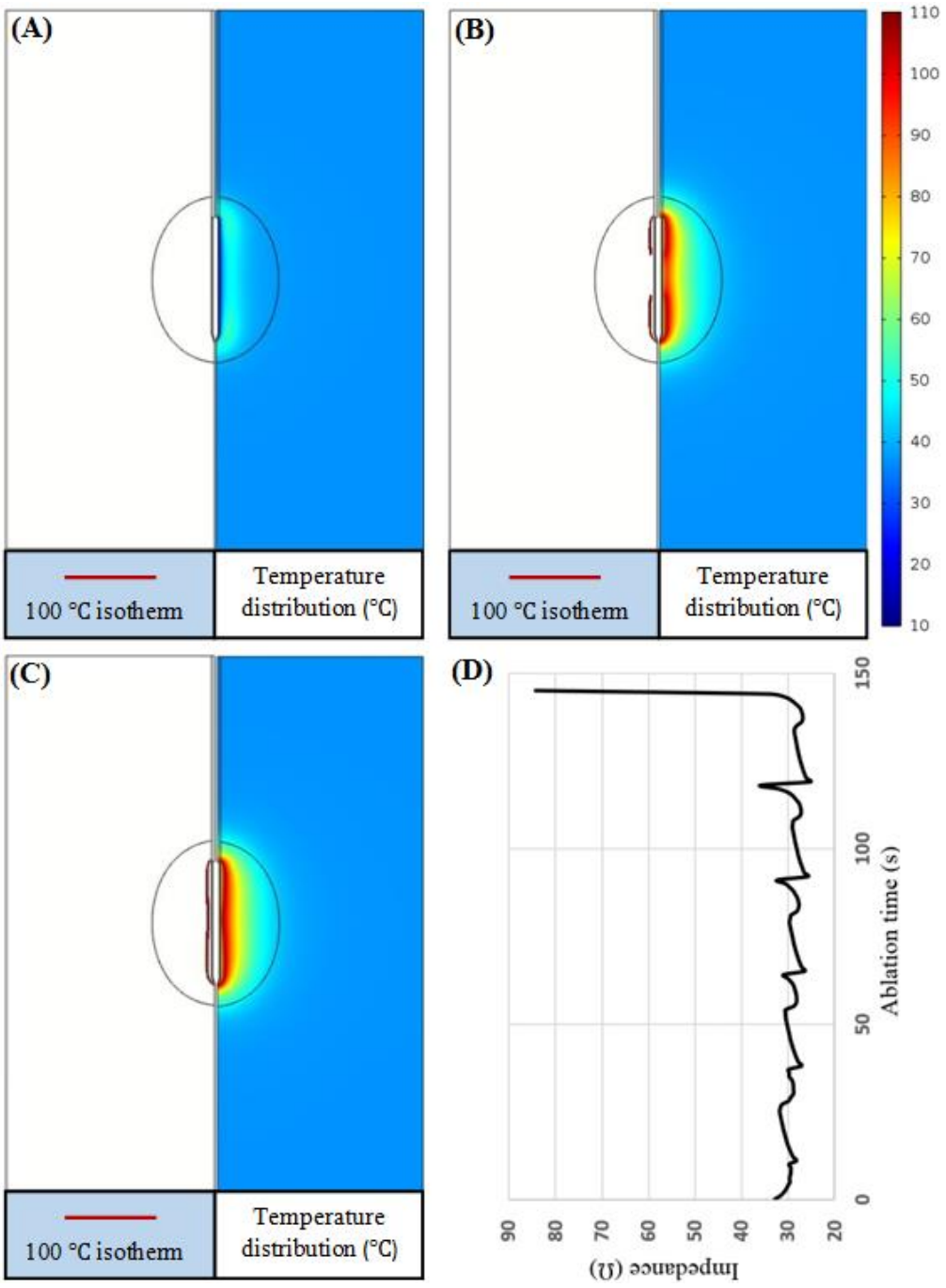

Figure 5.8. 100 ℃ isotherm and temperature distribution of the scenario of 48 V-145 s at 25 s (A), 118 s (B), and 145 s (C) and the change of the impedance (D).

Table 5.3. The computational results of TTN area for all PRFA protocols in the present study.

Target tissue (mm)	Pulsed RF waveform	Ablation protocol	D63 (mm)	Complete ablation
d_x= 25	half-square	46 V-720 s	D_x= 19.90, D_y= 40.00	N
		47.2 V-720 s	D_x= 25.00, D_y= 40.00	Y
		48 V-334 s	D_x= 15.26, D_y= 36.84	N
		51 V-118 s	D_x= 11.16, D_y= 37.36	N
	half-sine	68 V-720 s	D_x= 18.46, D_y= 36.30	N
		69.9 V-720 s	D_x= 19.18, D_y= 36.48	N
		70 V-682 s	D_x= 18.62, D_y= 35.92	N
		73 V-132 s	D_x= 9.06, D_y= 31.72	N
d_x= 30	half-square	43 V-720 s	D_x= 21.62, D_y= 39.96	N
		44.9 V-720 s	D_x= 25.38, D_y= 40.00	N
		45 V-685 s	D_x= 23.52, D_y= 39.84	N
		48 V-145 s	D_x= 12.90, D_y= 35.00	N
	half-sine	65 V-720 s	D_x= 19.70, D_y= 36.46	N
		66.5 V-720 s	D_x= 21.60, D_y= 36.50	N
		67 V-457 s	D_x= 17.82, D_y= 35.30	N
		70 V-132 s	D_x= 10.02, D_y= 32.56	N
d_x= 35	half-square	42 V-720 s	D_x= 23.96, D_y= 40.00	N
		43.3 V-720 s	D_x= 25.74, D_y= 40.00	N
		44 V-451 s	D_x= 20.96, D_y= 37.58	N
		47 V-145 s	D_x= 13.54, D_y= 34.98	N
	half-sine	63 V-720 s	D_x= 21.10, D_y= 35.52	N
		64.4 V-720 s	D_x= 22.64, D_y= 36.38	N
		65 V-432 s	D_x= 19.06, D_y= 35.42	N
		68 V-132 s	D_x= 10.70, D_y= 32.60	N

Y: Yes, N: No

Table 5.3 shows the twenty-four computational results for three different sizes of target tissues using the half-square and the half-sine PRFA. In this study, two dimensional parameters (D_x and D_y) and TTN area (Figure 5.9) were used to evaluate the PRFA protocols. D_x and D_y mean the longest length of the short and the long axis of TTN area, respectively, as shown in Figure 5.6. Similar to the results of our previous study [9], the largest TTN area was found at a particular voltage for each size of target tissue in both the half-square and the half-sine PRFA, as shown in Figure 5.9. This voltage was the MVA without the roll-off occurrence. The MVA was found using the *trial and error* method and the accuracy was about 0.1 V, which was used in our previous study [9].

We also found that the MVA for the half-square PRFA was lower than that for the half-sine PRFA for all three sizes of target tissues. The reason for this phenomenon can be explained in the following. In the situation of using the same V_{on}, the half-square PRFA has more energy than the half-sine PRFA in a pulse period ($t_{\mathrm{on}} + t_{\mathrm{off}}$) due to the different waveforms. Thus, for the half-sine PRFA, a higher V_{on} was needed to generate the same amount of TTN area with the half-square PRFA. Another salient finding in the present study is that the half-square PRFA achieved a higher TTN area than the half-sine PRFA. It is worth mentioning that this result contradicts the results found in the work of Lim et al. [12]. In their work, the half-sine PRFA had a slightly better performance on the TTN size than the half-square PRFA for D_x (8.2 vs. 8.0 mm) while for D_y, the two PRFAs had the same results. The different results between the literature [12] and the present study may be due to the following reasons: (1) they did not consider the liver tumour tissue in their model and (2) their results were achieved using the same root mean square value (25 V) of the half-square and the half-sine waveforms rather than the first roll-off occurrence. We believe that the two treatments in their work appear inadequate, and as such, our PRFA model was closer to the real clinical setting.

Figure 5.10 shows the computational results of the tissue death using D63 criteria [28] for the 25-mm, 30-mm, and 35-mm target tissues. The tissue death was evaluated using MVA, at which the largest TTN area was able to be achieved for each size of target tissue. As shown in Figure 5.10A, only a 25-mm target tissue can be killed completely using the half-square PRFA. Figure 5.10D shows the differences in the TTN area for three sizes of target tissues using the half-square PRFA and the half-sine PRFA. It is interesting to note that the differences in the TTN area were almost the same for the three sizes of target tissues before about 360 s. After that time, the larger the target tissue is, the larger the TTN area. This phenomenon was found in both the half-square PRFA and the half-sine PRFA methods. We speculated the reason for this phenomenon as follows. The target tissue is more sensitive to the thermal therapy due to its higher electrical conductivity and lower blood perfusion rate. The larger the target tissue is, the higher the sensitivity. After the critical time (about 360 s in the study), the differences in the sensitivities of the target tissues were getting larger and larger due to the high temperature. So the large TTN area can be obtained in the target tissue with the large size. Further work is necessary to study this phenomenon.

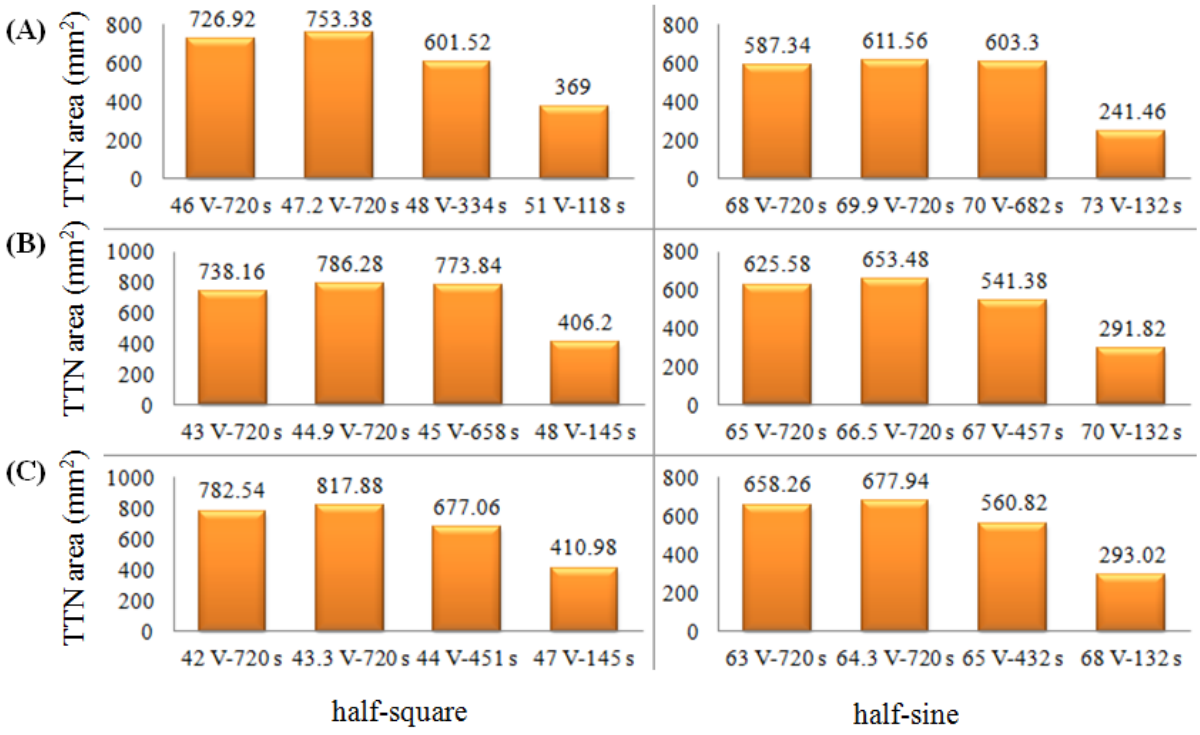

Figure 5.9. Computational results of TTN areas for target tissues with different sizes: (A) d_x= 25 mm, (B) d_x= 30 mm, and (C) d_x= 35 mm.

MVA without the roll-off occurrence decreased with an increase in the target tissue size for the half-square PRFA and the half-sine PRFA, as shown in Figure 5.11. For a whole research domain (healthy liver tissue and liver tumour), the impedance (R) was the equivalent value of the impedance of healthy liver tissue (R_{hlt}) and the impedance of liver tumour (R_{lt}) in series, namely, $R = R_{hlt} + R_{lt}$. As such, the larger the liver tumour, the smaller the impedance (R), as the liver tumour has a higher electrical conductivity than healthy liver tissue [15,29]. According to $P = U^2/R$, when the R is small, the voltage (U) we need is also small because the power (P) needed for getting TTN is a constant.

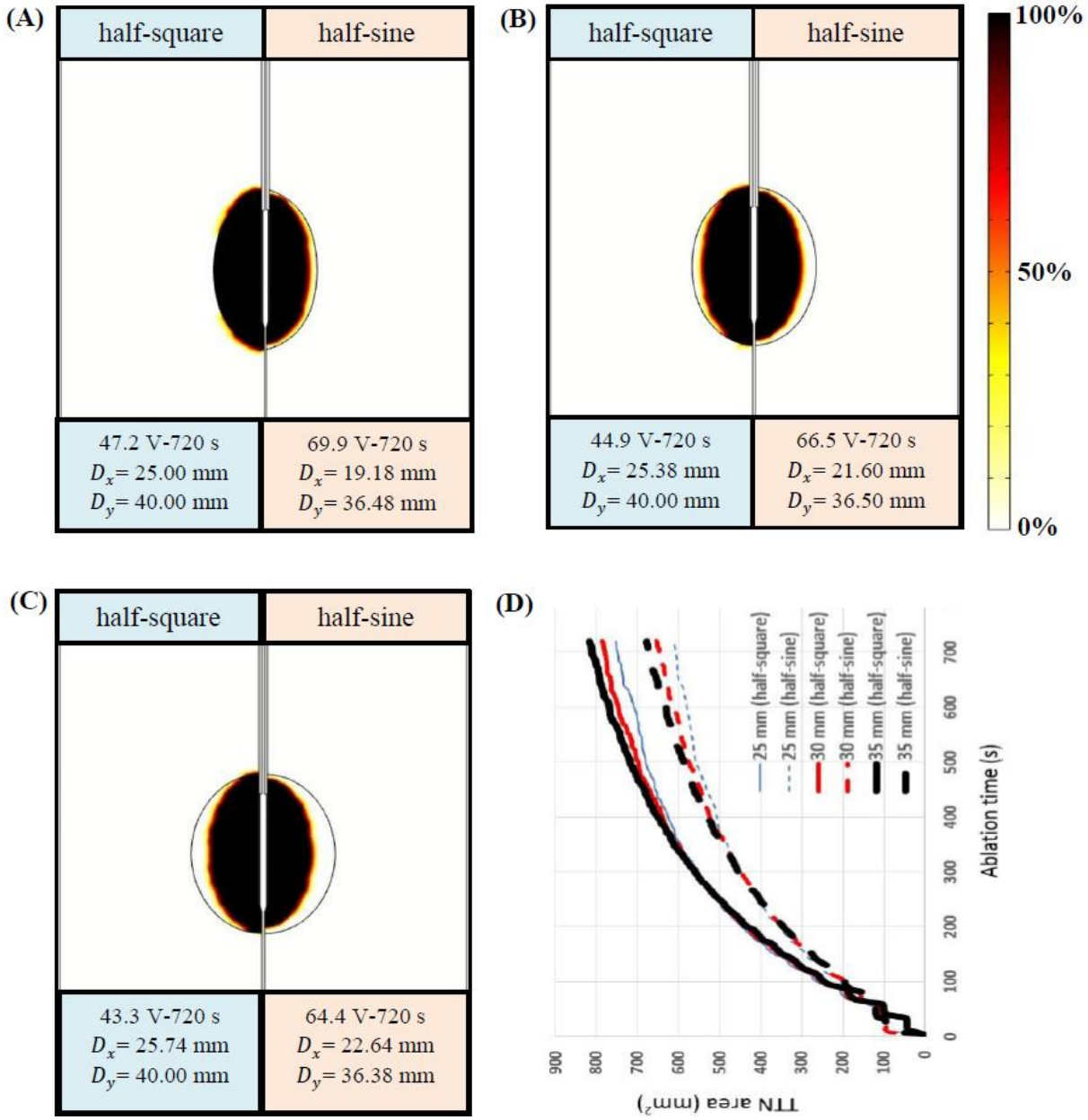

Figure 5.10. Target tissue death rate (%) (D63) at its own MVA: (A) d_x= 25 mm, (B) d_x= 30 mm, and (C) d_x= 35 mm and the changes of the TTN areas (D).

In the current commercial PRFA device, the algorithm of RF power supply is much related to the change of impedance. Another algorithm for power supply can be such that a constant RF power is usually used until the first roll-off occurs. Then, the algorithm is changed to the pulsed RF power supply because the PRFA is able to deliver more power to target tissue even after the roll-off occurrence. The reason behind this is that PRFA has the cooling

period (t_{off}) for heat dissipation from the area in the proximity of the RF electrode, which can relieve the roll-off. Although a relatively large TTN size can be obtained using PRFA compared with the CRFA, the TTN size is still a small size and PRFA is not efficient enough on the large target tissues. It is worth noting that unlike other studies [10,30], a relatively large TTN area was not achieved using the PRFA in this study because of the different ablation termination criteria. We mainly focused on the ablation duration before the first roll-off occurrence for different sizes of target tissues as we discussed above. The reason of choosing this ablation termination is that we believe that the growth of TTN before the first roll-off is worth investigating such that an optimal PRFA algorithm in a roll-off for the large TTN area can be achieved. Using the optimal algorithm within several roll-offs, a further large TTN area is expected to be achieved.

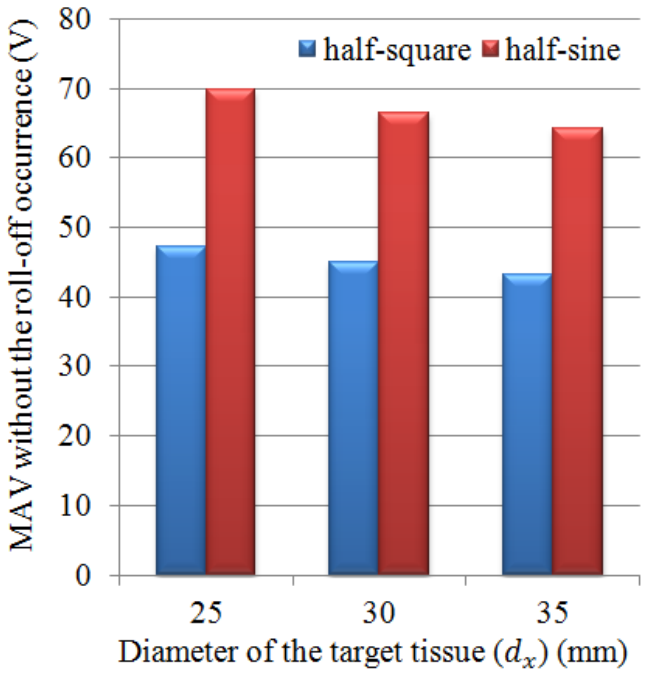

Figure 5.11. MVA without the roll-off occurrence for each size of target tissue in the present study.

5.3.3 Limitations

There are some limitations in the present study. One of them is the approximation of the blood perfusion model. There were some debates on how to model the blood perfusion of the liver tissue in the computational work. Most of the studies considered blood perfusion as a constant [6,31,32] or a piecewise function [9,22,33,34]. Some

researchers [35] obtained a good agreement with the *in vivo* animal experiments when using the foregoing constant method. However, It is worth mentioning that Schutt and Haemmerich [36] had concluded that there were significant effects on TTN size using different blood perfusion models. They used the piecewise model, a linear decreasing model and a nonlinear decreasing model. In the nonlinear decreasing model, they considered an increase of blood perfusion with an increase of degree of vascular stasis at the ablation zone boundary due to the hyperaemia. Similarly, a dynamic model of blood perfusion rate with the temperature and damaged tissue was used in a work of Bourantas et al. [37]. In their model, blood perfusion was taken as a product of constitutive perfusion rate and a dimensionless function that accounts for vessel dilation at slightly elevated temperatures [38]. In the present study, a piecewise function model of vascular coagulation was used. Particularly, the perfusion rate was considered as a constant before the biological tissue reached a temperature of 60 ℃; at temperatures higher than 60 ℃, the blood perfusion rate was set to 0, because the coagulation eliminated microvascular perfusion [22].

Although the computer model was used to achieve the data for various PRFA protocols, to make the findings of the present study more reliable, experiments with liver tumour or tumour tissue phantom are necessary in the future study. Furthermore, we also acknowledge that large adjacent blood vessels ≥3 mm in diameter around the target tissue can be another reason for the small size of TTN, namely the 'heat-sink effect'. We did not consider this heat-sink effect in our model, because we want to avoid the impacts of other factors in the present study. Certainly, a more sophisticated model considering the heat-sink effect is needed in the future study.

5.4 Conclusions

Two types of pulsed RF power supply methods and three target tissues of different sizes were studied using finite element modelling to find the relationship between the size of target tissue and the area of TTN in the PRFA. Four conclusions can be drawn from this study:

(1) The largest TTN area can be achieved using the MVA without the roll-off occurrence. For 25 mm, 30 mm and 35 mm target tissues, the largest TTN areas are 753.38 mm^2, 786.28 mm^2, and 817.88 mm^2,

respectively, using half-square PRFA, and 611.56 mm^2, 653.48 mm^2, and 677.94 mm^2, respectively, while using half-sine PRFA.

(2) Target tissues (liver tumours) with 30 mm and 35 mm in diameter cannot be ablated completely if using the first roll-off occurrence as the ablation termination criteria.

(3) The half-square PRFA achieves a greater TTN area than the half-sine PRFA.

(4) The MVA decreases with an increase in the target tissue diameter in both the half-square PRFA and the half-sine PRFA methods.

Acknowledgements

This article was supported by the Saskatchewan Health Research Foundation (SHRF) through the 'BioNEMS Phase I' grant (grant no. 2539) and the National Natural Science of China (grant no. 51175179). The first author (Bing Zhang) also received financial support from the China Scholarship Council (CSC).

Conflict of interest

The authors report no conflicts of interest. The authors alone are responsible for the content and writing of the paper.

REFERENCES

1. Zhang B, Moser M, Zhang E, Zhang W. Radiofrequency ablation technique in the treatment of liver tumours: Review and future issues. J Med Eng Technol 2013;37:150-9.
2. Nishikawa H, Kimura T, Kita R, Osaki Y. Radiofrequency ablation for hepatocellular carcinoma. Int J Hyperthermia 2013;29:558-68.
3. Xu H-X, Lu M-D, Xie X-Y et al. Prognostic factors for long-term outcome after percutaneous thermal ablation for hepatocellular carcinoma: a survival analysis of 137 consecutive patients. Clin Radiol 2005;60:1018-25.
4. Shiina S, Tateishi R, Arano T et al. Radiofrequency ablation for hepatocellular carcinoma: 10-year outcome and prognostic factors. Ame J Gastroenterol 2011;107:569-77.
5. Llovet JM, Bruix J. Novel advancements in the management of hepatocellular carcinoma in 2008. J Hepatol 2008;48:S20-37.
6. Zhang B, Moser MA, Luo Y et al. Evaluation of the current radiofrequency ablation systems using axiomatic design theory. Proc Inst Mech Eng H 2014;228:397-408.
7. Brace CL. Radiofrequency and microwave ablation of the liver, lung, kidney, and bone: what are the differences? Curr Probl Diagn Radiol 2009;38:135-43.
8. Ahmed M, Brace CL, Lee FT, Goldberg SN. Principles of and advances in percutaneous ablation. Radiology 2011;258:351-69.
9. Zhang B, Moser MA, Zhang EM et al. Study of the relationship between the target tissue necrosis volume and the target tissue size in liver tumours using two-compartment finite element RFA modelling. Int J Hyperthermia 2014;30:593-602.
10. Goldberg SN, Stein MC, Gazelle GS et al. Percutaneous radiofrequency tissue ablation: optimization of pulsed-radiofrequency technique to increase coagulation necrosis. J Vasc Interv Radiol 1999;10:907-16.
11. Solazzo SA, Ahmed M, Liu Z et al. High-Power generator for radiofrequency ablation: larger electrodes and pulsing algorithms in bovine ex vivo and porcine in vivo Settings. Radiology 2007;242:743-50.
12. Lim D, Namgung B, Woo DG et al. Effect of input waveform pattern and large blood vessel existence on destruction of liver tumor using radiofrequency ablation: Finite element analysis. J Biomech Eng 2010;132:061003.

13. Pennes HH. Analysis of tissue and arterial blood temperatures in the resting human forearm. J Appl Physiol 1948;1:93-122.

14. Haemmerich D, Schutt DJ. RF ablation at low frequencies for targeted tumor heating: In vitro and computational modeling results. IEEE Trans Biomed Eng 2011;58:404-10.

15. Haemmerich D, Schutt DJ, Wright AS et al. Electrical conductivity measurement of excised human metastatic liver tumours before and after thermal ablation. Physiol Meas 2009;30:459-66.

16. Tungjitkusolmun S, Staelin ST, Haemmerich D et al. Three-dimensional finite-element analyses for radio-frequency hepatic tumor ablation. IEEE Trans Biomed Eng 2002;49:3-9.

17. González-Suárez A, Trujillo M, Burdío F et al. Feasibility study of an internally cooled bipolar applicator for RF coagulation of hepatic tissue: Experimental and computational study. Int J Hyperthermia 2012;28:663-73.

18. Van Beers BE, Leconte I, Materne R et al. Hepatic perfusion parameters in chronic liver disease: dynamic CT measurements correlated with disease severity. Am J Roentgenol 2001;176:667-73.

19. Zorbas G, Samaras T. Parametric study of radiofrequency ablation in the clinical practice with the use of two-compartment numerical models. Electromagn Biol Med 2013;32:236-43.

20. Sahani DV, Holalkere N-S, Mueller PR, Zhu AX. Advanced hepatocellular carcinoma: CT perfusion of liver and tumor tissue—Initial experience. Radiology 2007;243:736-43.

21. Jo B, Aksan A. Prediction of the extent of thermal damage in the cornea during conductive keratoplasty. J Therm Biol 2010;35:167-74.

22. Liu Z, Ahmed M, Sabir A et al. Computer modeling of the effect of perfusion on heating patterns in radiofrequency tumor ablation. Int J Hyperthermia 2007;23:49-58.

23. Trujillo M, Alba J, Berjano E. Relationship between roll-off occurrence and spatial distribution of dehydrated tissue during RF ablation with cooled electrodes. Int J Hyperthermia 2012;28:62-8.

24. Haemmerich D, Chachati L, Wright AS et al. Hepatic radiofrequency ablation with internally cooled probes: effect of coolant temperature on lesion size. IEEE Trans Biomed Eng 2003;50:493-500.

25. Ahmed M, Liu Z, Humphries S, Nahum Goldberg S. Computer modeling of the combined effects of perfusion, electrical conductivity, and thermal conductivity on tissue heating patterns in radiofrequency tumor ablation. Int J Hyperthermia 2008;24:577-88.

26. Kim B-M, Jacques SL, Rastegar S et al. Nonlinear finite-element analysis of the role of dynamic changes in blood perfusion and optical properties in laser coagulation of tissue. IEEE J Select Topics Quantum Electron 1996;2:922-33.

27. Reddy G, Dreher MR, Rossmann C et al. Cytotoxicity of hepatocellular carcinoma cells to hyperthermic and ablative temperature exposures: In vitro studies and mathematical modelling. Int J Hyperthermia 2013;29:318-23.

28. Chang IA, Nguyen UD. Thermal modeling of lesion growth with radiofrequency ablation devices. Biomed Eng Online 2004;3:27.

29. Laufer S, Ivorra A, Reuter VE et al. Electrical impedance characterization of normal and cancerous human hepatic tissue. Physiol Meas 2010;31:995-1009.

30. Solbiati L, Livraghi T, Goldberg SN et al. Percutaneous radio-frequency ablation of hepatic metastases from colorectal cancer: long-term results in 117 patients. Radiology 2001;221:159-66.

31. Arena CB, Mahajan RL, Rylander MN, Davalos RV. Towards the development of latent heat storage electrodes for electroporation-based therapies. Appl Phys Lett 2012;101:083902.

32. Karampatzakis A, Kühn S, Tsanidis G et al. Antenna design and tissue parameters considerations for an improved modelling of microwave ablation in the liver. Phys Med Biol 2013;58:3191-206.

33. Zhu Q, Shen Y, Zhang A, Xu LX. Numerical study of the influence of water evaporation on radiofrequency ablation. Biomed Eng Online 2013;12:127.

34. Chen X, Saidel GM. Mathematical modeling of thermal ablation in tissue surrounding a large vessel. J Biomech Eng 2009;131:011001.

35. González-Suárez A, Trujillo M, Burdío F et al. Could the heat sink effect of blood flow inside large vessels protect the vessel wall from thermal damage during RF-assisted surgical resection? Med Phys 2014;41:083301.

36. Schutt DJ, Haemmerich D. Effects of variation in perfusion rates and of perfusion models in computational models of radio frequency tumor ablation. Med Phys 2008;35:3462-70.

37. Bourantas GC, Ghommem M, Kagadis GC et al. Real-time ablation simulation based on the dynamic mode decomposition method. Med Phys 2014;41:053301.

38. London RA, Glinsky ME, Zimmerman GB et al. Laser-tissue interaction modeling with LATIS. Appl Opt 1997;36:9068-74.

6 JUDICIOUS SELECTION OF TARGET CONTROL AREAS AND TARGET TEMPERATURES TO INCREASE THE SIZE OF TARGET TISSUE NECROSIS BY RADIOFREQUENCY ABLATION

*This chapter is submitted as **Bing Zhang** et al. "Judicious selection of target control areas and target temperatures to increase the size of target tissue necrosis by radiofrequency ablation" to **Medical Physics** in 2015 (**under review**).*

Abstract

Purpose: The purpose of this study was to investigate the feasibility to achieve a large target tissue necrosis (TTN) size with temperature-controlled radiofrequency ablation (RFA) by examining different control areas and set-point temperatures.

Methods: A novel approach to achieving a large (≥3 cm in diameter) TTN with RFA procedure was developed in this study. The approach was based on a feedback temperature-control strategy with the judicious selection of the best target area for feedback control and of the best set-point (target temperature) on the target tissue. A commercial internally cooled RFA electrode and the target tissue (liver tumour) were used for the study. An accurate finite element model of the RFA system (with liver tumour) was first introduced from our previous work, and the model was served as a test-bed for the study. Three control areas with 14 control points were chosen as the control positions for temperature control to increase the TTN size. Particularly, four points in Area I, six points in Area II and four points in Area III were chosen, and these areas are close to the proximal, middle, and distal part of the electrode, respectively. Temperatures (80 and 90 ℃) were taken as the set-point temperatures for every control point.

Results: Based on this test-bed, the best area was then found to be in the middle part of the electrode and the set-point to be 90 ℃. The details were given as: for Area I, the TTN areas were 775.13±39.54 mm^2 and 841.61±85.48 mm^2 at 80 and 90 ℃, respectively. For Area II, the TTN areas were 878.65±39.49 mm^2 and 954.26±26.03 mm^2 at 80 and 90 ℃, respectively. For Area III, the TTN areas were 749.16±70.18 mm^2 and 819.71±76.69 mm^2 at 80 and 90 ℃, respectively. This finding was also verified by *in vitro* experiments using porcine liver tissues. The study further demonstrated that the target tissue with the elliptic shape (3×4 cm) can be completely ablated by the proposed approach.

Conclusions: It can be concluded that the RFA procedure requires sophisticated tissue temperature control and it is possible to ablate large target tissues by the feedback temperature control strategy (selection of target control area and set-point temperature).

6.1 Introduction

Radiofrequency ablation (RFA) technique uses alternating electric current with high frequency (about 500 kHz) to generate heat on the target tissue and ablate the target tissue under the image guidance [1,2]. This method has been improved considerably since its first introduction. Its application has been expanded from the treatment of liver tumour to target tissues on other organs such as bone, lung, and kidney [3-5]. However, this technique is restricted in the treatment of small size of target tissues (i.e. <3 cm in diameter) from the clinical experience. Indeed, many clinical results have shown that the local recurrence rate for the large size of target tissues is higher than that for the small size of target tissues owing to incomplete ablation for large target tissues [6-9].

An agreed view about incomplete ablation for large target tissue is that tissue charring is one of the main cause. Unlike other thermal therapies, the configuration of RFA is such that there is a circuit like that: RF electrode → normal and target tissues → ground pad → RF power generator. By a proper setting of the RF power, heat is generated on the tissue, and subsequently the tissue is ablated due to the thermal-vaporized effect. This technique thus much depends on the electrical conductivity between the RF electrode and the ground pads. Tissue usually becomes charred when being heated up to 100 ℃. The charred tissue induces high impedance, which thus stops the further power delivery in the circuit. In clinic, tissue charring is called 'roll-off'. Details of tissue charring and roll-off may refer to our previous study [10]. Note that in our previous work, we demonstrated the similar result (only target tissue size less than 3 cm can be ablated completely) with constant RFA and pulsed RFA (respectively) as the clinic by modelling and simulation [10,11].

There are many methods developed in literature to address the foregoing problem with RFA. These methods include the designs that change the electrical and thermal conductivities of target tissues so that the tissue is less charred or the charring is under control and designs that delay the occurrence of tissue charring with the means such as the

pulsed RFA [12,13], the internally cooled electrode [14,15], and the perfusion electrode [16,17]. Note that the two improved designs may be combined. For the pulsed RFA, the accumulated heat in the areas surrounding the RF electrode can be dissipated away during the period of time that no power is delivered. For the internally cooled electrode, there is a cooling solution that circulates inside the RF electrode, which can absorb the accumulated heat surrounding the RF electrode. However, neither pulsed RFA nor internally cooled electrode is able to avoid tissue charring but just to defer tissue charring. For the perfusion electrode, the saline solution is injected into the target tissue, and this solution can then cool the tissue. The saline solution also changes the electrical and thermal conductivities of target tissue in such a way that more RF power can be delivered.

In the present study, we developed a new protocol of RFA, based on a feedback temperature-controlled strategy. A commercially available internally cooled RF electrode was employed to demonstrate the new method. The salient points with this new method include: (1) the tissue temperature rather than the electrode temperature used for the control target, (2) the judicious selection of the area in tissue, at which temperature is measured, and (3) the optimal set-up point of temperature for control.

The remainder of this paper is organized as follows. In Section 6.2.1, a finite element model (FEM) of RFA is discussed, which was used as a simulation test-bed to find the optimal area and the optimal set-up point of temperature. In Section 6.2.2, the feedback temperature-controlled RFA and selection of control areas are discussed. In Section 6.2.3, a test-bed is described to verify the findings about the control areas. The results with discussion are given in Section 6.3, followed by the conclusions with future study draw from the findings of this paper in the last section.

6.2 Materials and methods

6.2.1 Finite element model of RFA

6.2.1.1 The tissue geometrical model and governing equation

In the present study, a liver tissue was modelled as a cylinder with 50 mm in radius and 130 mm in height. An

elliptical liver tumour taken as the target tissue with 40 mm in the major axis and 30 mm in the minor axis was modelled in the centre of the liver tissue. Note that the diameter of target tissue in this study refers to the length of minor axis of the elliptical tumour. The internally cooled RF electrode (Cool-tip^{TM} RF Ablation System E Series, Covidien AG, Zurich, Switzerland) used for the present study has the electrode of 1.5 mm in diameter and 30 mm in length. The RF applicator was inserted into the target tissue in a specific position in which the centre of RF electrode coincided with the centre of the target tissue (Figure 6.1). Due to the symmetrical characteristic of the tissue and the placement of the RFA applicator, we consider half of the tissue in the sectional plane passing through the axis of the cylinder (Figure 6.1).

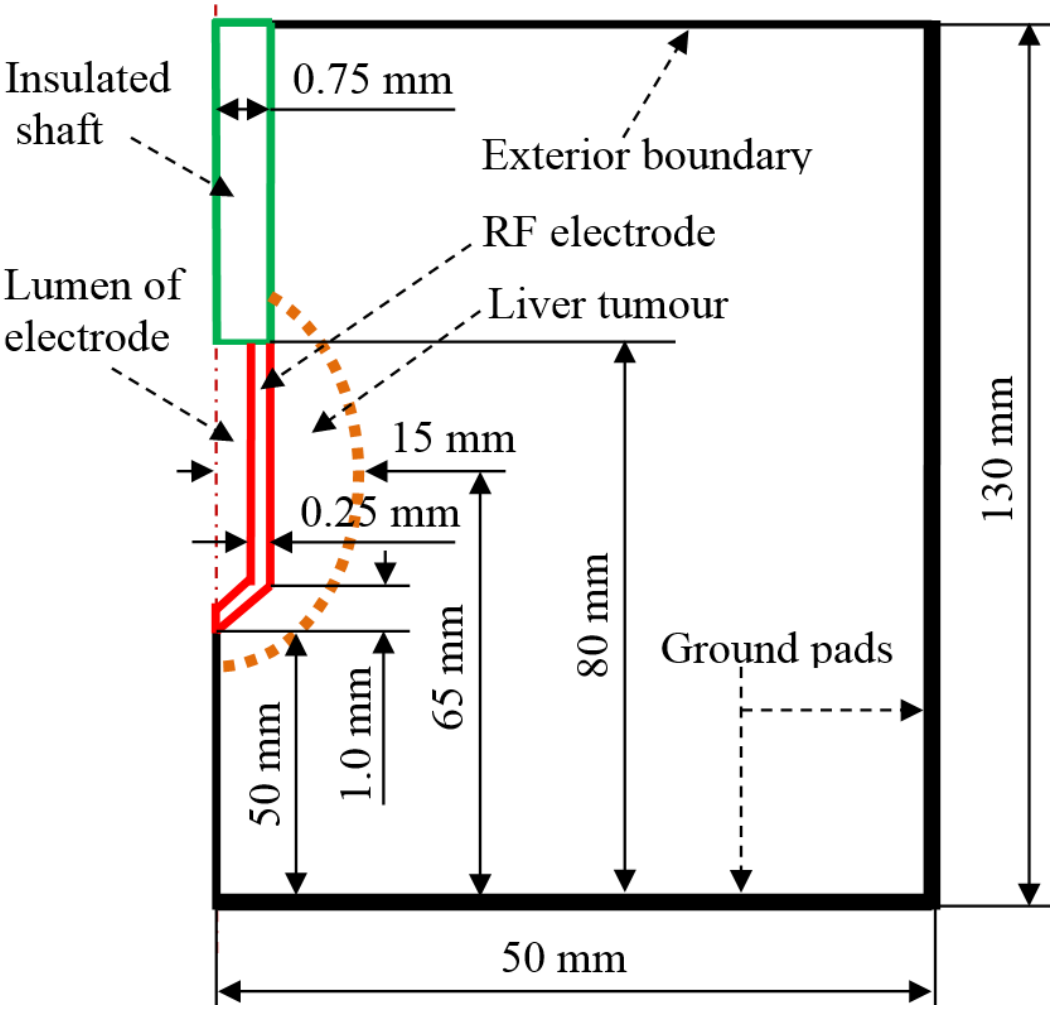

Figure 6.1. The geometric model of RFA with an elliptical liver tumor (out of scale).

The governing equation for the process of target tissue ablation with RFA follows the so-called Penne's bioheat transfer equation [18]:

$$\rho c \frac{\partial T(\mathbf{x},t)}{\partial t} = \nabla \cdot \left(k \nabla T(\mathbf{x},t)\right) + \rho_b c_b \omega_b \left(T_b - T(\mathbf{x},t)\right) + Q_m(\mathbf{x},t) + Q_{hs}(\mathbf{x},t) \qquad \mathbf{x} \in \mathbf{\Gamma} \qquad (6.1)$$

where ρ (kg m^{-3}) is the density, c (J kg $^{-1}$ K^{-1}) is the specific heat, T (℃) is the temperature, $\mathbf{x} = \{\mathrm{r}, \mathrm{z}\}$ in the 2D axis symmetric coordinate system, $\mathbf{\Gamma}$ is the analyzed domain, k (W m^{-1} K^{-1}) is the thermal conductivity, ρ_b (kg m^{-3}) is the blood density, c_b (J kg $^{-1}$ K^{-1}) is the specific heat of the blood, ω_b (s^{-1}) is the blood perfusion, T_b is the temperature of the blood entering the tissue, Q_m (W m^{-3}) is the heat power generated due to biological tissue metabolic processes, which is ignored due to its small magnitude compared with the other terms in Eq. (6.1) and Q_{hs} is the heat power generated by the RF energy and it can be calculated as follows:

$$Q_{hs} = \boldsymbol{J} \cdot \boldsymbol{E} = \sigma |\nabla V|^2 \qquad (6.2)$$

where $\boldsymbol{J}$ (A m^{-2}) is the current density, $\boldsymbol{E}$ (V m^{-1}) is the electrical field intensity, σ (S m^{-1}) is the electrical conductivity and V (V) is the applied voltage. The properties of the elements in the model in the present study were drawn from the literature [19-25] and listed in Table 6.1.

Table 6.1. Properties of the elements in the model in the present study.

Modelling element	ρ (kg m^{-3})	c (J kg $^{-1}$ K^{-1})	k (W m^{-1} K^{-1})	σ (S m^{-1})	ω_b (s^{-1})
Liver tissue	1080	3455	0.515[a]	0.203[a]	0.016[a]
Liver tumour	1045	3760	0.600[a]	0.500[a]	0.002[a]
RF electrode	6450	840	18	1.0×10^{8}	-
Insulated shaft	70	1045	0.026	1.0×10^{-5}	-
Blood	1000	4180	0.49	0.667	-

[a]evaluated at 21 ℃

The present study considered them temperature dependent the thermal, electrical conductivities and blood perfusions of liver tissue and target tissue. The thermal and electrical conductivities of both liver tissue and target tissue from 21 to 100 ℃ can be described by [26]

$$k(T) = k_{ref} + 0.0013(T(\mathbf{x},t) - T_{ref}) \qquad (6.3)$$

$$\sigma(T) = \sigma_{ref}\left[1 + 0.02(T(\mathbf{x}, t) - T_{ref})\right] \tag{6.4}$$

where k_{ref} and σ_{ref} are the reference thermal and electrical conductivity, respectively, measured at the reference temperature ($T_{ref} = 21$ ℃). At above 100 ℃, the thermal conductivity was taken as a constant. The electrical conductivity from 100 to 105 ℃ decreased on two orders of magnitude due to the water vaporization and desiccation [27]. At the above 105 ℃, thermal conductivity was set to be a constant. The blood perfusions of liver tissue and target tissue were given by [10,28]

$$\omega_b(T) = \begin{cases} \omega_b & T < 60\,℃ \\ 0 & T \geq 60\,℃ \end{cases} \tag{6.5}$$

In the present study, the Arrhenius model was taken in the RFA model to measure the damaged tissue and thus for the estimation of TTN area, and the model is given by [29]

$$\Omega(t) = A\int_0^t e^{\frac{-\Delta E}{RT(\tau)}}\,d\tau \tag{6.6}$$

where $\Omega(t)$ is the degree of tissue death, A (s^{-1}) is the frequency factor, ΔE (J mol^{-1}) is the activation energy for the irreversible damage reaction, R (J mol^{-1} K^{-1}) is the universal gas constant and $T(\tau)$ (K) is the absolute temperature. For the liver tissue and the target tissue, $A = 7.390 \times 10^{39}$ (s^{-1}) and 3.247×10^{43} (s^{-1}), respectively and $\Delta E = 2.577 \times 10^5$ (J mol^{-1}) and 2.814×10^5 (J mol^{-1}), respectively [30]. The tissue was considered as dead, if the value of $\Omega(t)$ equals 1, which corresponds to a 63% probability that the tissue is dead [29].

6.2.1.2 The initial and boundary conditions

The initial temperature of the finite element RFA model was assumed to be uniform and the same as the internal temperature of human body, namely

$$T(t = 0) = 37\,℃ \tag{6.7}$$

The electrical boundaries of RF electrode and ground pad were given by

$$V = \begin{cases} u(t) & \text{for RF electrode} \\ 0 & \text{for ground pad} \end{cases} \tag{6.8}$$

The electrical boundary conditions of exterior healthy liver tissue boundary and RF electrode lumen boundary were

taken as insulating:

$$\mathbf{n} \cdot \boldsymbol{J} = 0 \tag{6.9}$$

All other electrical boundary conditions were considered as continuity, and thus:

$$\mathbf{n} \cdot (\boldsymbol{J}_i - \boldsymbol{J}_j) = 0 \tag{6.10}$$

The thermal boundary conditions of the ground pads and exterior of liver tissue were set to be 37 ℃. The thermal boundary condition of RF electrode lumen boundary was assumed as Newton's cooling law to simulate the cooling effect of the cooling fluid circulating inside the RF electrode.

$$-\mathbf{n} \cdot (-k\nabla T) = h_c(T_c - T) \tag{6.11}$$

where h_c (W m^{-2} K^{-1}) is thermal convection coefficient, T_c (℃) is the temperature of cooling water. In this study, we used the same values with previous studies, which h_c and T_c were set to be 3366 (W m^{-2}K^{-1}) and 10 ℃, respectively [15].

All the other thermal boundary conditions were considered as continuity, and thus

$$\mathbf{n} \cdot (k_i\nabla T_i - k_j\nabla T_j) = 0 \tag{6.12}$$

6.2.1.3 Validation of the FEM of RFA

First, we wanted to make sure the mesh is a stable one. This was done by the following procedure. Let the mesh change incrementally until the maximum temperature calculated by the FEM (voltage is 30 V and length of ablation time is 200 seconds) with the particular mesh does not change (no change is defined as the temperature variation is within 0.1 ℃). As a result, the stable mesh has 3085 elements. Second, the dimensions (radius and length) of the liver tissue were also tested for a stable size. Three groups of the dimensions of liver tissue were tested, which are (50 mm, 130 mm), (60 mm, 180 mm), and (80 mm, 200 mm). Again, the variation in the maximum temperature among these three groups was defined as the change more than 0.1 ℃. As a result, the smallest size of liver tissue was found to be (50 mm, 130 mm) for the sake of reduction of computational cost. It is noted that this FEM for the RFA system was validated using *in vitro* experiments (porcine liver tissues) with an acceptable accuracy in our

previous study [11]. Thus, this FEM was used in the present study as a test-bed to simulate the feedback temperature-control RFA procedure.

6.2.2 Temperature-controlled RFA and judicious selection of the control target in the target tissue area

6.2.2.1 The feedback temperature-controlled RFA

In the present study, a proportional-integral-derivative (PID) controller was further implemented into the FEM of the RFA system, as shown in Figure 6.2. A note is given to Figure 6.2 on the FEM that plays a role as a simulated plant and will not be there in the clinical operation. The dynamic system (FEM) consisted of the RF applicator (RF electrode and insulated shaft), target tissue, liver tissue, and ground pads.

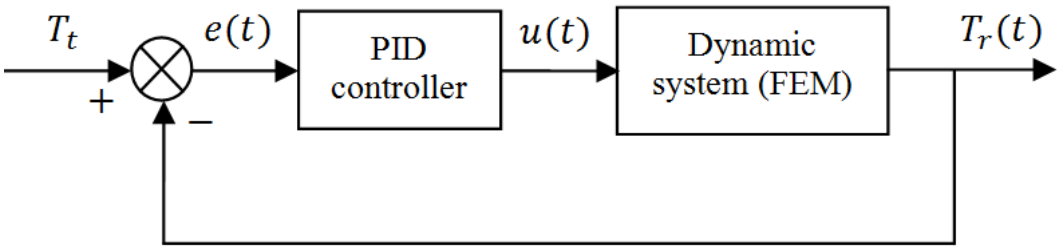

Figure 6.2. A PID closed loop control system used in the present study.

For the PID controller, the input was the difference (e) between the target temperature (T_t) and the temperature (T_r) measured at a specific position. The input of the dynamic system was the voltage $u(t)$, which was applied on the RF electrode and can be given as:

$$u(t) = K_p e(t) + K_i \int_0^t e(\tau)d\tau + K_d \frac{de(t)}{dt} \tag{6.13}$$

To implement a PID controller into the FEM, the PID controller (Eq. (13) was discretized as:

$$u(k) = K_p e(k) + K_i \sum_{m=0}^{k-1} \frac{e(m)+e(m+1)}{2} T_s + K_d \frac{e(k)-e(k-1)}{T_s} \qquad k \in \{1, 2, \cdots\} \tag{6.14}$$

where the integral and derivative part of the PID controller were realized by using the trapezoidal and forward Euler method, respectively. T_s (i.e. 1 s) is the sample time, which was set to be the same with the step size in the simulation of FEM. The thermo-electrically temperature-controlled RFA model was solved using the joint technique between COMSOL (Burlington, MA, USA) and MATLAB (Natick, MA, USA). Details of the FEM and PID can be found from the literature [31,32].

6.2.2.2 Target control points or areas for the feedback control

The target tissue is an area or volume. A feedback temperature control needs to decide the location at which the temperature is measured and used for feedback control. Another piece of information for the feedback control is the set-point (i.e. the target temperature). The previous studies in literature concluded that the small size of the TTN area of RFA was caused by the tissue charring [33,34]. The tissue charring occurs at the temperature of 100 ℃. Therefore, the set-up point must be less than 100 ℃. On the other hand, to deliver RF energy as much as possible to increase the TTN area requires that the set-point be as high as possible. In this study, we tried two set-points of 80 ℃ and 90 ℃, respectively.

It is also known from the literature that the charring occurs over the target tissue area in a non-uniform manner, and particularly the charring starts to occur from the areas surrounding the proximal and distal parts of RF electrode and then spreads to the areas surrounding the middle part of RF electrode, as shown in Figure 6.3A. As discussed before, when the RF electrode is encircled by the charred tissue ($t = t_3$, in Figure 6.3A) the impedance between the RF electrode and the ground pads reaches to the maximal value. After that point of time, the growth of the TTN area usually stops. The charred tissue in this context can be viewed as an ‘energy gate’ that can shut down the path of the RF energy delivery. One of the methods to obtain a large TTN area is to deliver the RF energy to the target tissue as much as possible in a short period of time (for the interests of patients). To achieve this goal, the proposed idea in the present study was to keep the energy gate open with a just small gap, as shown in Figure 6.3A ($t = t_2$).

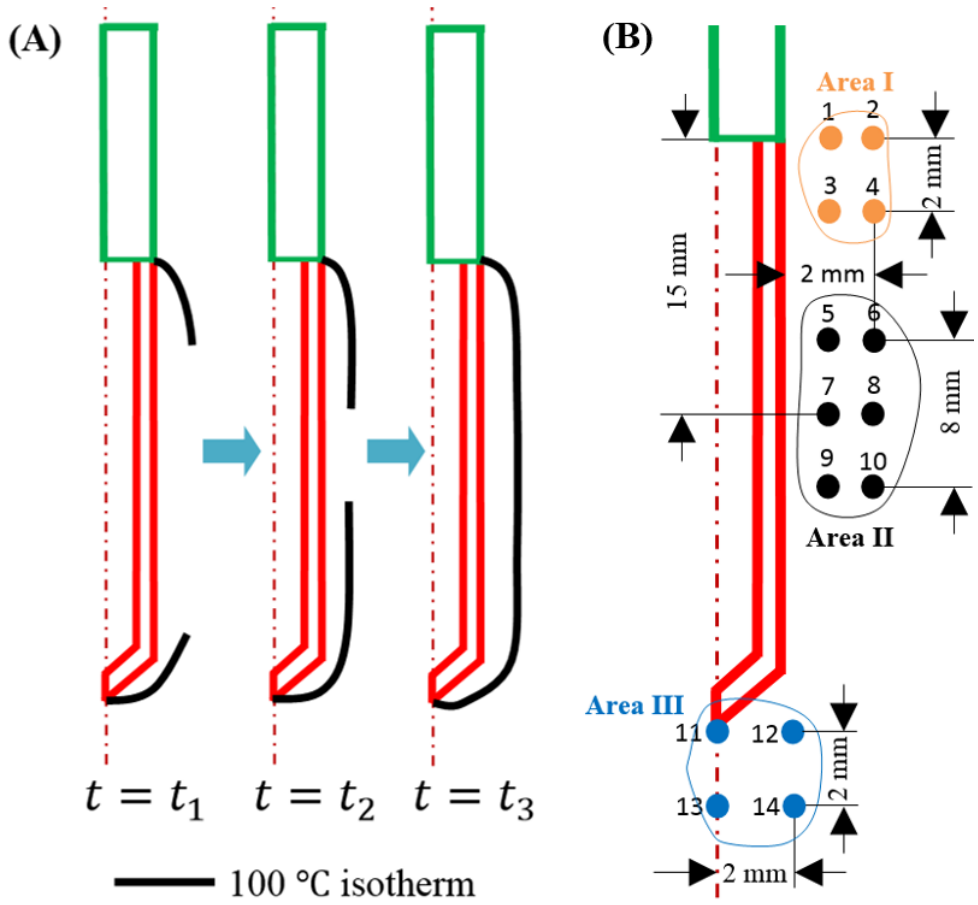

Figure 6.3. Growth of the charred tissue (A) and three control areas with 14 control points selected in the present study (B).

To verify the above idea, three areas in the target tissue with 14 points were selected as the control positions in the present study, as shown in Figure 6.3B. Four points (1-4), six points (5-10), and four points (11-14) were selected in the target tissue around the proximal, middle, and distal parts of RF electrode, respectively. For the RF electrode with the internal cooling effect, the charred tissue usually occurs at 1-2 mm away from the surface of RF electrode [35]. Thus, these control points were deliberately selected in these areas, as shown in Figure 6.3B. In the commercially temperature-controlled RFA systems, the temperature of the tip of RF electrode rather than temperature of the target tissue are measured and controlled. To compare the results of the commercially temperature-controlled RFA with that of the method in this study, point 11 was defined at the tip of RF electrode to mimic the commercially temperature-controlled RFA.

6.2.3 Validation of target control areas using *in vitro* experiments

To validate the findings in the selection of control areas, *in vitro* experiments using porcine liver tissues were designed and performed in this study. The *in vitro* experiments followed the regulation of *Biosafety Permit Protocol* of University of Saskatchewan. A custom-made RFA system designed and manufactured by our group and the porcine liver tissues were used to validate the results about the selection of control areas and set-point temperatures. The RF power generator can supply the maximum power of 50 W with 430±30 kHz. The RF electrode was made using a 316L stainless steel tubing with 1.98 mm outer diameter, 1.60 mm inner diameter and 30 mm in length, as shown in Figure 6.4. A bead wire Type K thermocouple (Omega, Stamford, CT, USA) was used to measure the temperature at required positions and send the signals of temperatures back to RF power generator for temperature control. A piece of aluminium foil (190×210 mm) was taken as the ground pad. The porcine liver tissues were bought in the local grocery store. Before the experiments, the porcine liver tissues were stored in a 5% NaCl solution and maintained at an ambient temperature of 20 ℃ (room temperature). Three control points (point *a*, *b*, and *c*) selected in the three areas (around the proximal, middle, and distal parts of RF electrode, respectively), as shown in Figure 6.4A-C, were used in this validation. As shown in Figure 6.4C, the thermocouple was inserted into the RF electrode and used to measure the temperature of the tip of RF electrode to act as the commercially available RFA system. We used a total of 30 specimen porcine liver tissues and the size of each tissue was kept at least 85×60×35 mm. For each control point, 5 pieces of porcine liver tissues were performed with the temperature-controlled RFA at each target temperature (i.e. 80 or 90 ℃) for 720 seconds, which is the commonly used ablation time in the current clinical settings [12,34]. Before the experiments, all liver tissues were examined for avoiding the influence of large blood vessel. In this initial experiment, we did not consider the cooling effect of RF electrode. In this situation, the tissue charring usually occurs in the area just around the RF electrode. So the distances between the surface of RF electrode and the point *a* and *b* were chosen as about 0.5 mm in the experiments, as shown in Figure 6.4A-B.

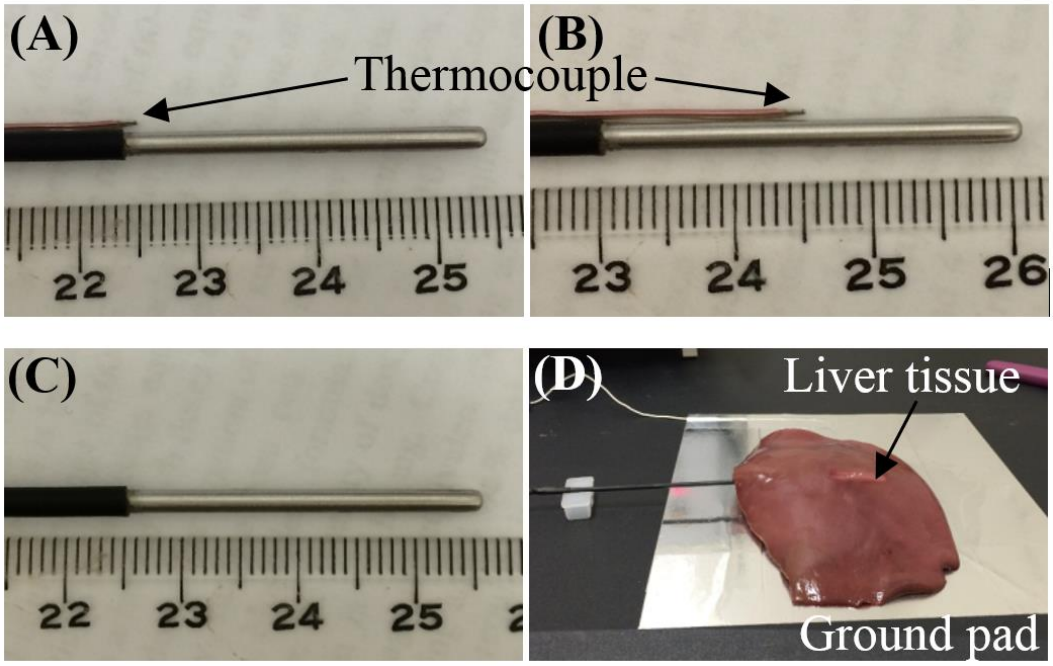

Figure 6.4. *In vitro* experimental set up for the validation.

6.3 Results and discussion

6.3.1 TTN sizes of control areas from the FEM

As said before in Section 6.2.2.2, there were 14 control target points selected for studying which points or areas would be taken as the best control target area so that the TTN can be enlarged. The difference in dynamics among these points was ignored in the present study, as the difference is intuitively very small, and this assumption is in agreement with the finding in literature [31,36]. Further, their coupling was also ignored. The 14 controls were then simplified to 14 uncoupled controls with the same control law. The control law has the following parameters: $K_p = 2, K_i = 0.5,$ and $K_d = 0.001$. The RFA procedure took the duration of 720 s according to the clinical experience.

Figures 6.5-6.7 show the simulation results of temperature (T_r) measured at points 1-4, points 5-10, and points 11-14 selected in Area I, Area II and Area III, respectively. For the points that are 0 or 1 mm away from the surface of RF electrode (i.e. points 1, 3, 5, 7, 9, and 11), the response times were about 5-20 seconds at both 80 and 90 ℃. For the points that are 2 mm away from the surface of RF electrode (i.e. points 2, 4, 6, 8, 10, 12, and 13), the response times

were about 50-100 seconds. For the point 14, which is the farthest one away from the surface of RF electrode, more power and long period of time of RF procedure were required to make it reach the target temperatures. That point is in agreement with the fact that there were a sharp peak and a valley before stabilization (as shown in Figure 6.7), and the response time was about 200 seconds.

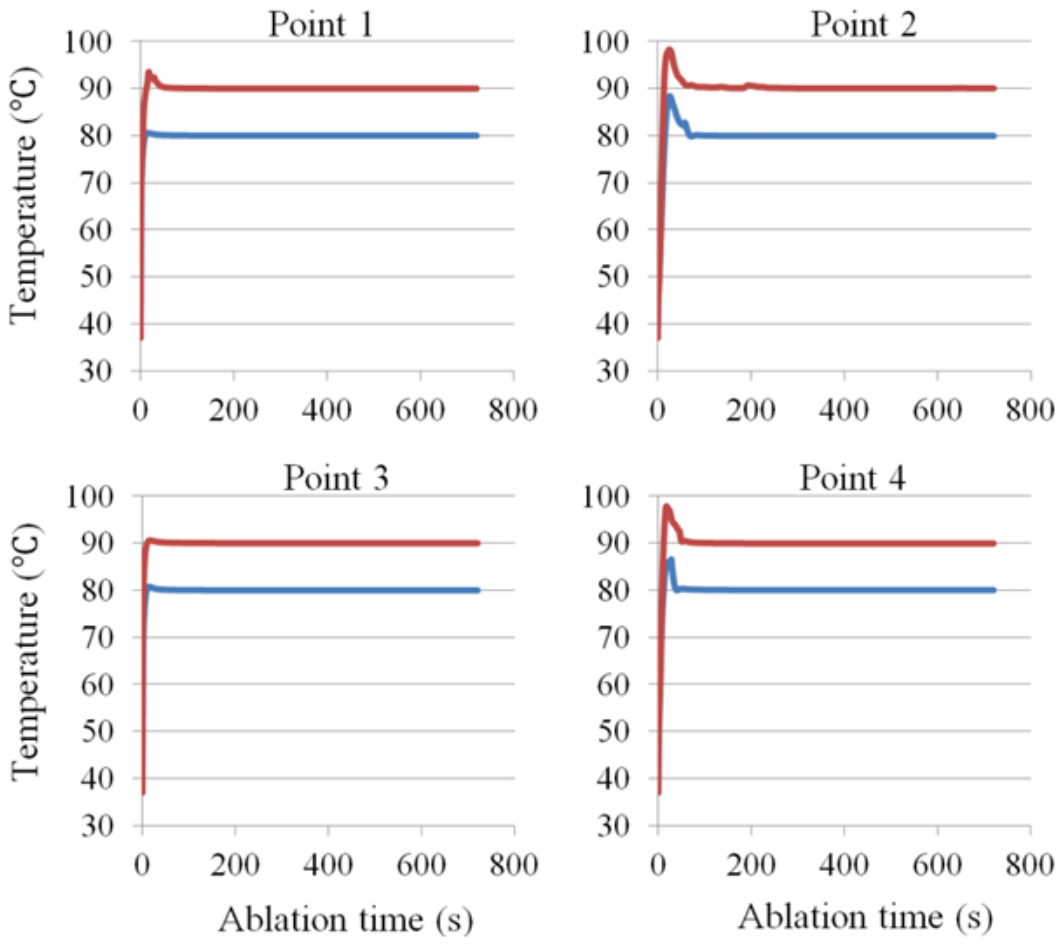

Figure 6.5. Temperatures (T_r) measured at points 1-4 selected in Area I.

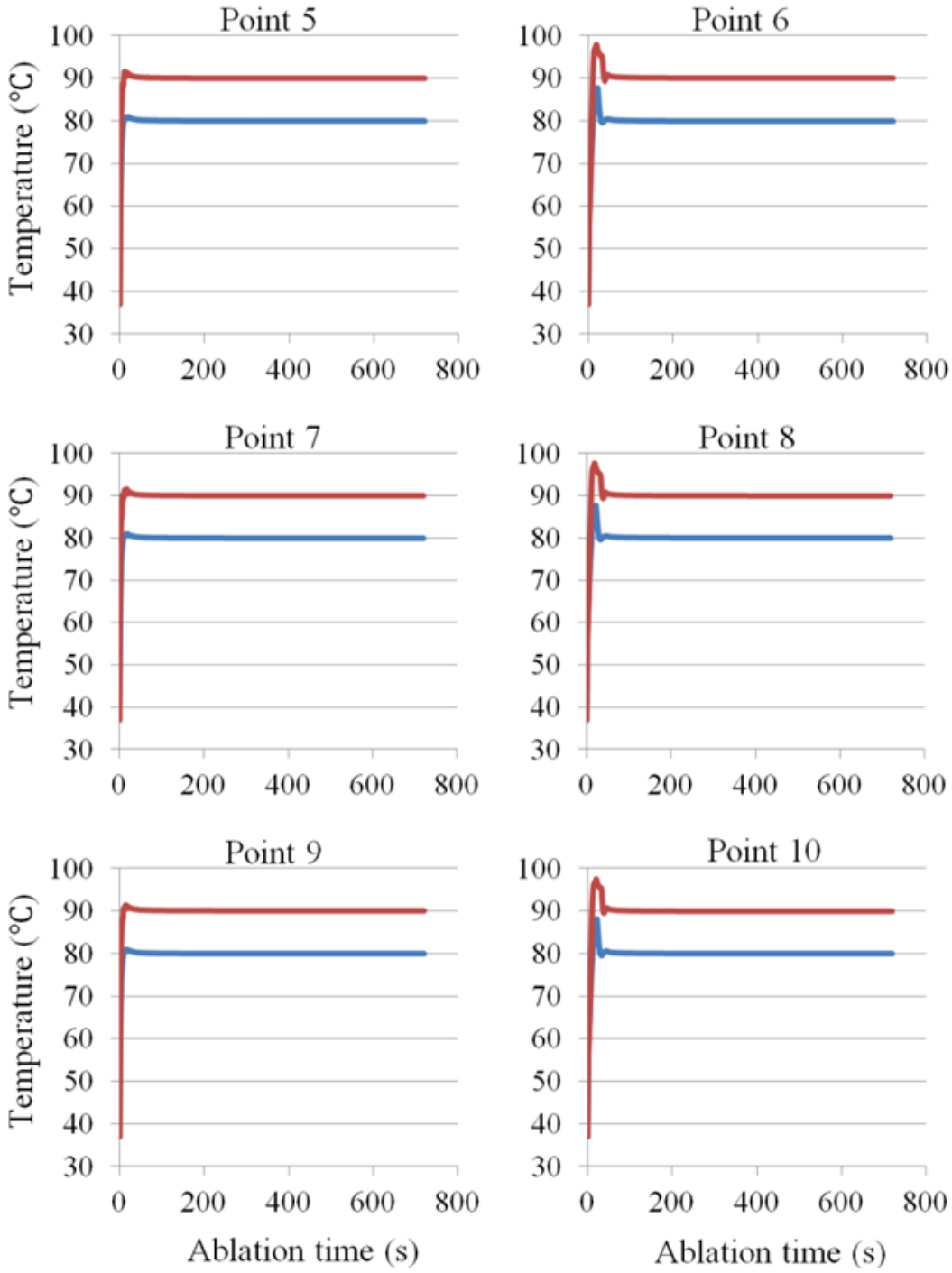

Figure 6.6. Temperatures (T_r) measured at points 5-10 selected in Area II.

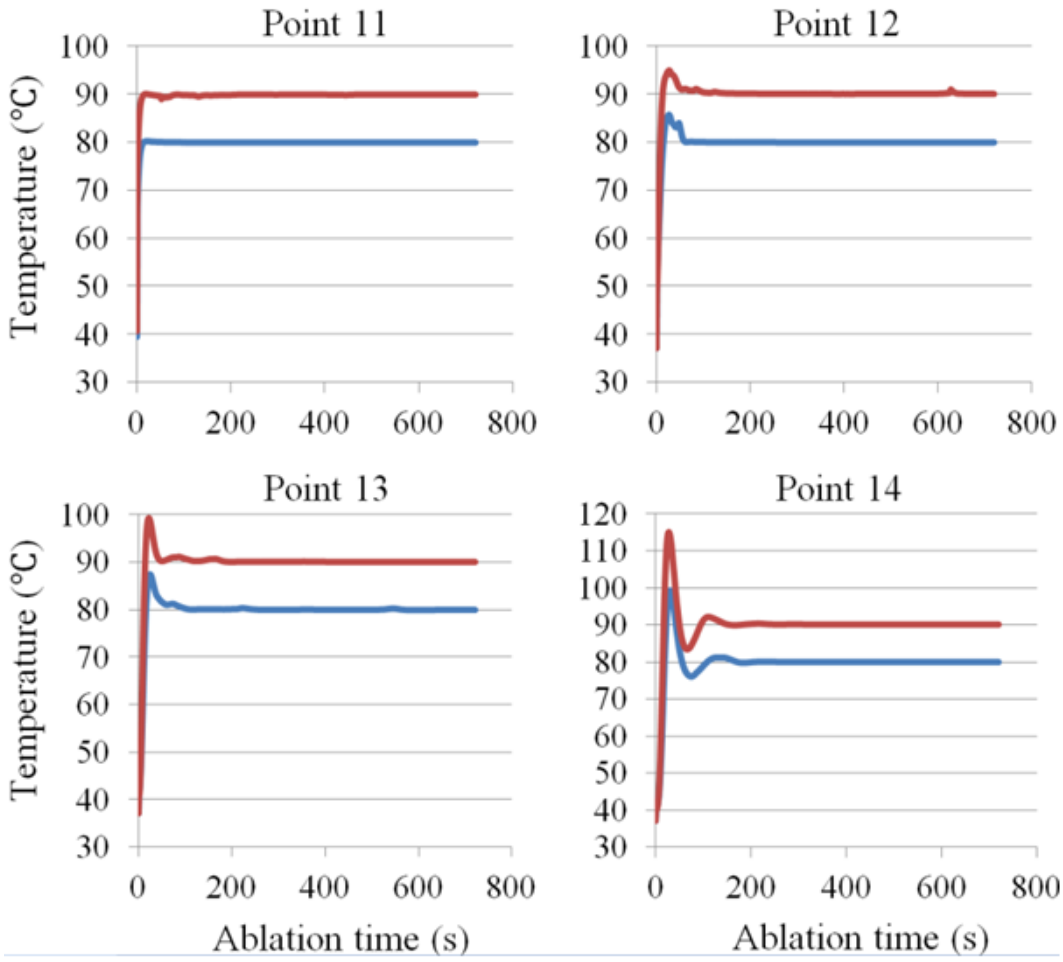

Figure 6.7. Temperatures (T_r) measured at points 10-14 selected in Area III.

Figures 6.8-6.10 show the simulation results of target tissue death for points 1-4, points 5-10, and points 11-14, respectively. The TTN area was evaluated using D63 criterion ($\Omega(t) = 1$) [29]. We added up the areas of the triangular elements in the both liver tissue domain and target tissue domain that had $\Omega(t) = 1$ on all nodes. The TTN areas obtained at 90 ℃ were larger than that obtained at 80 ℃ for all other control points with the exception on control point 2. The reason behind this phenomenon is unclear so far and it is worth studying further.

The results also show that the TTN areas from point 11 (the situation of commercially temperature-controlled RFA) were much smaller than that from the point 5 (the best result regarding TTN area) at both 80 and 90 ℃. With reference to the results of point 11, the TTN areas of point 5 increased about 31.6% (from 697.52 to 917.96 mm^2) and 24.4% (from 787.66 to 979.46 mm^2) at 80 and 90 ℃, resepectively. This result can also be noted in Figure 6.11.

For both 80 and 90 ℃, point 5 achieved the large area with the high temperature gradient. It is worth mentioning that for point 11 at 90 ℃, RF electrode was encircled by the so-called energy gate (charred tissue) at about 50 s, and no more RF energy could be delivered further after that.

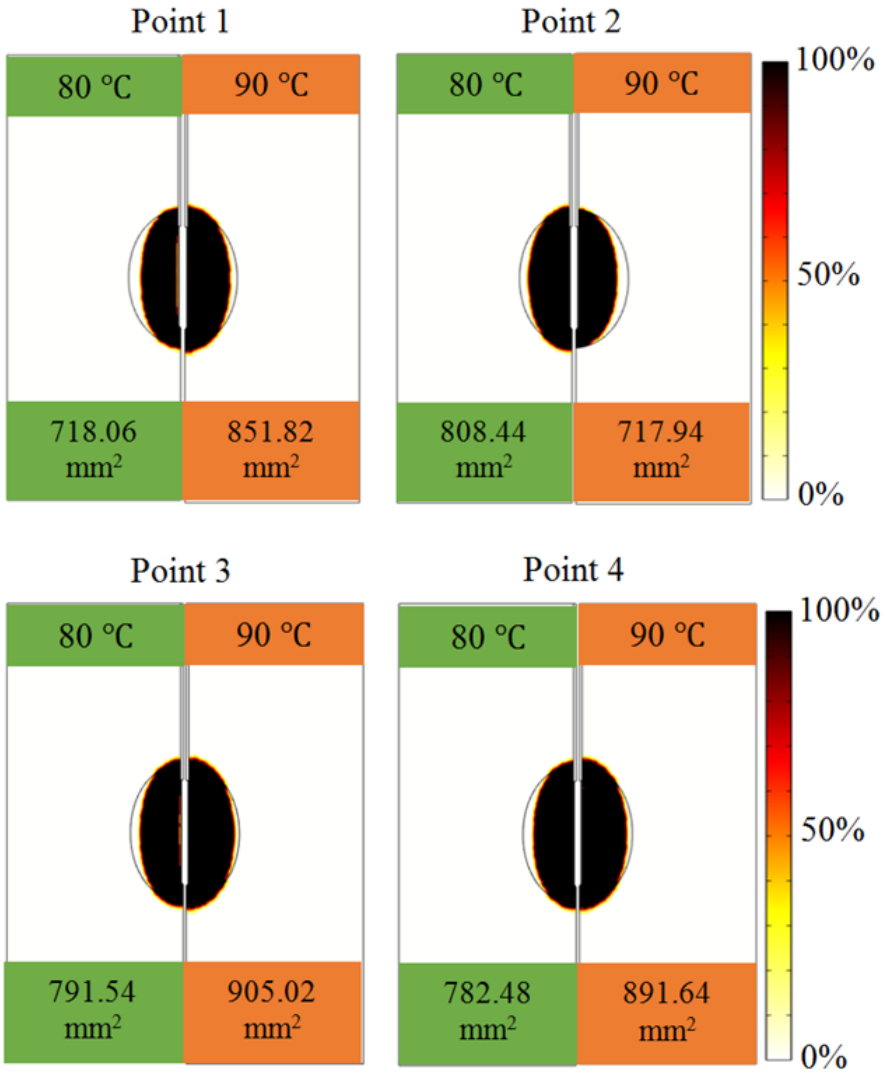

Figure 6.8. Target tissue death rate and TTN areas generated using points 1-4 selected in Area I.

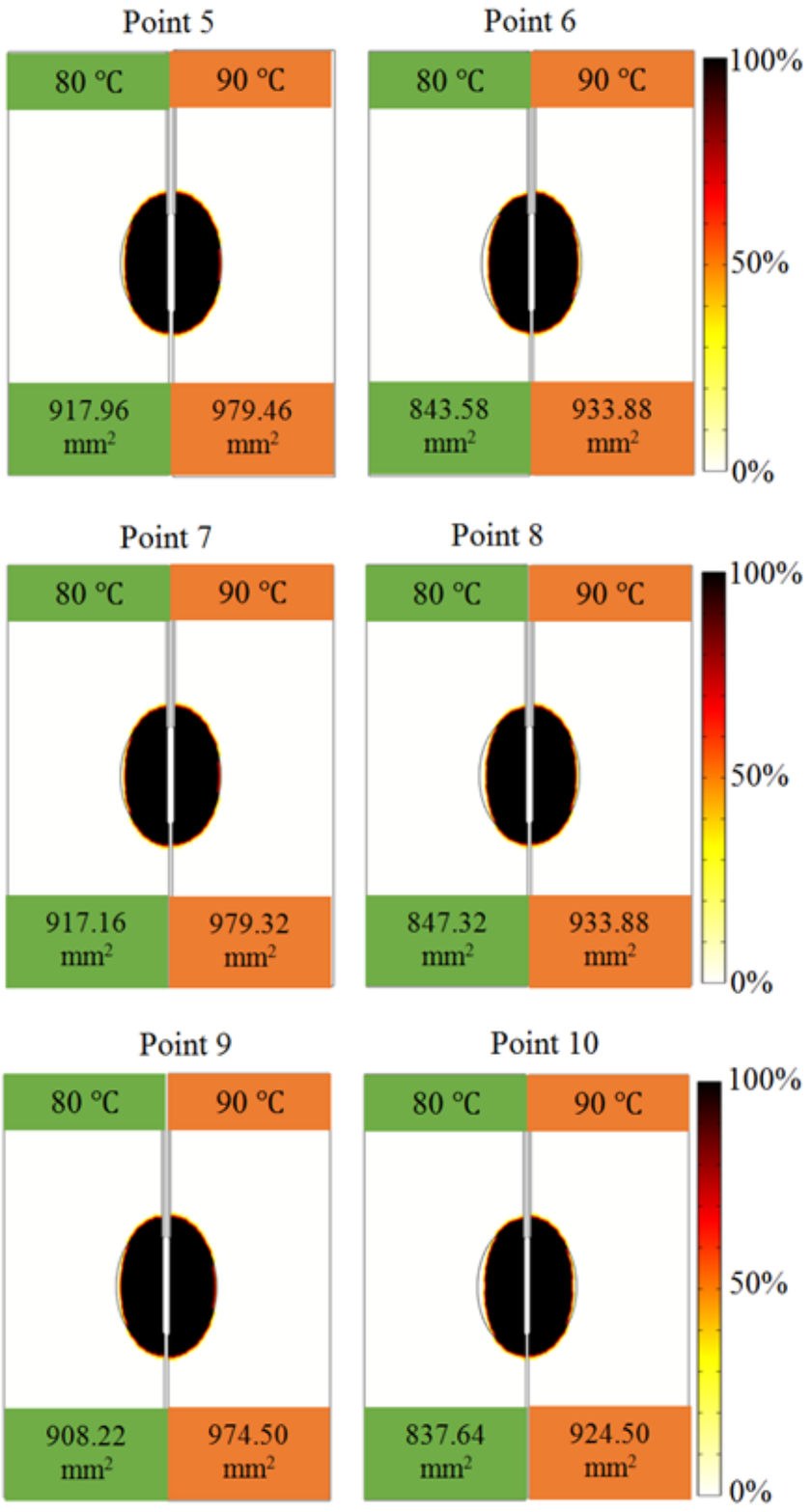

Figure 6.9. Target tissue death rate and TTN areas generated using points 5-10 selected in Area II.

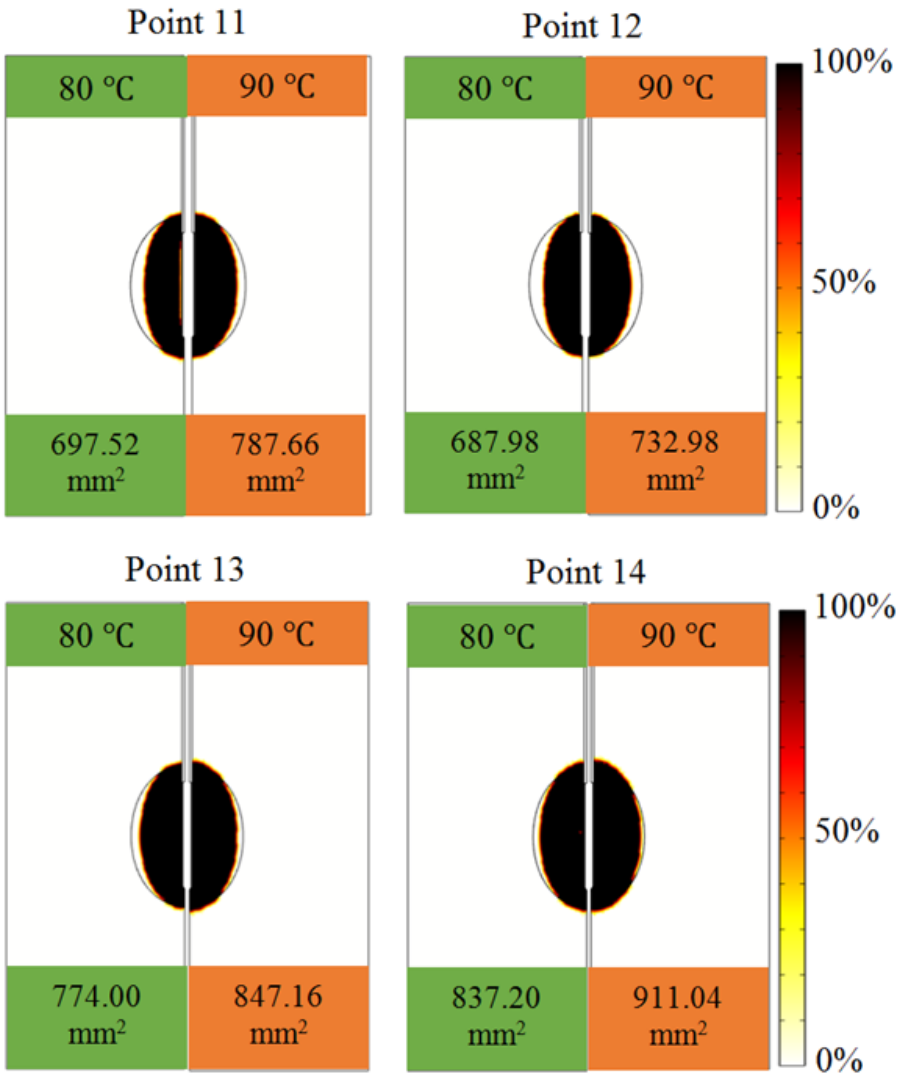

Figure 6.10. Target tissue death rate and TTN areas generated using points 11-14 selected in Area III.

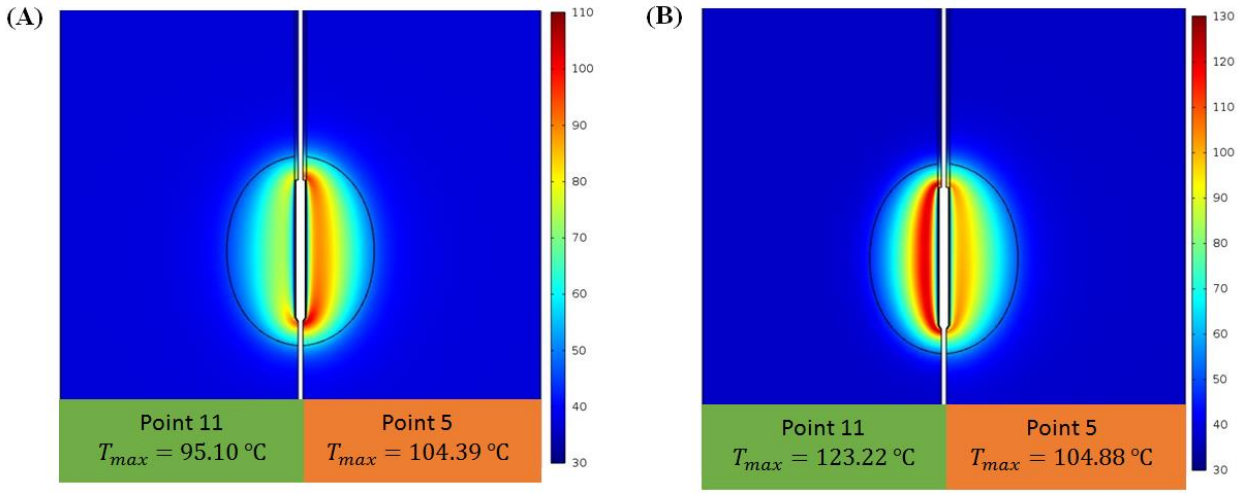

Figure 6.11. Temperature distributions (in ℃) of point 5 and point 11 at 720 s for the objective control temperatures of (A) 80 and (B) 90 ℃.

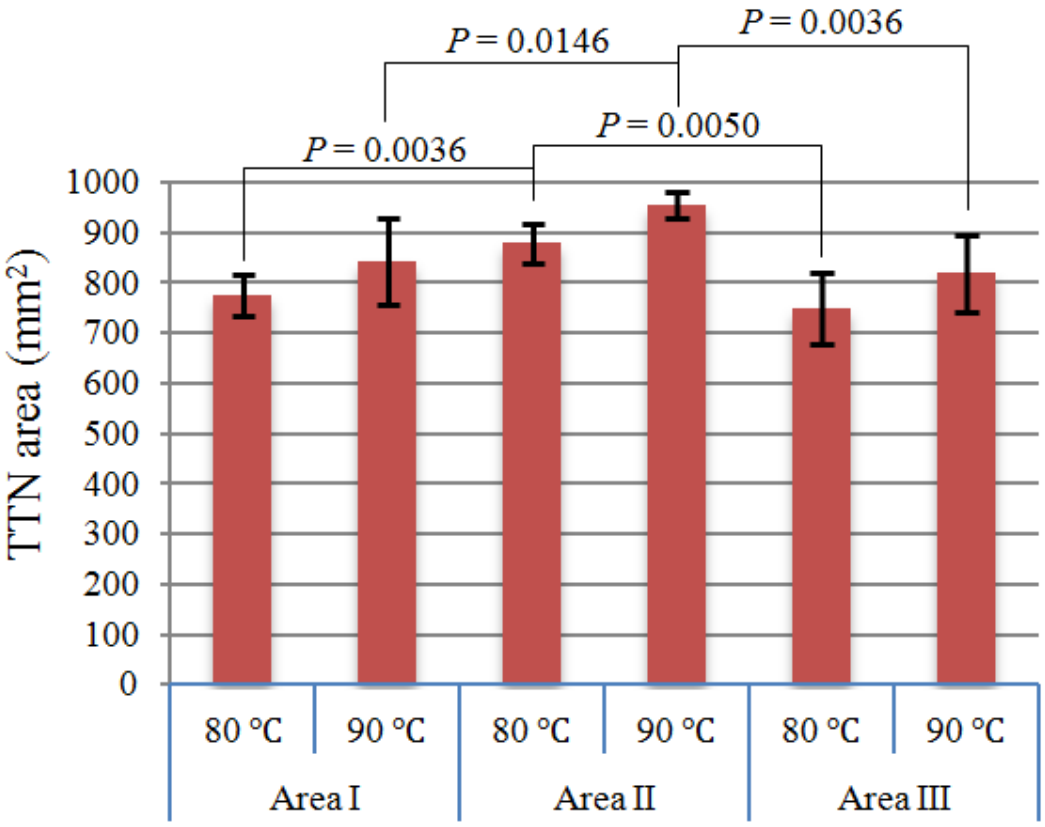

Figure 6.12. TTN areas generated using the three control areas at 80 and 90 ℃.

Figure 6.12 shows the results of TTN area generated using the three different areas at 80 and 90 ℃. For Area I, the TTN areas were 775.13 ± 39.54 mm^2 (mean $\pm$ standard deviation) and 841.61 ± 85.48 mm^2 at 80 and 90 ℃, respectively. For Area II, the TTN areas were 878.65 ± 39.49 mm^2 and 954.26 ± 26.03 mm^2 at 80 and 90 ℃, respectively. For Area III, the TTN areas were 749.16 ± 70.18 mm^2 and 819.71 ± 76.69 mm^2 at 80 and 90 ℃, respectively. At both 80 and 90 ℃, the TTN areas generated using Area II were significantly larger than the TTN areas generated using Area I ($P = 0.0036$ and 0.0146, respectively) and Area III ($P = 0.0050$ and 0.0036, respectively). However, there is no significant difference between the TTN areas generated using Area I and Area III at both 80 and 90 ℃ ($P = 0.5431$ and 0.7161, respectively). It is worth mentioning that in the present study, for both computer simulation and *in vitro* experiments, *F*-test (95% confidence level) was used to analyse the statistical significance of mean values of TTN areas between two groups of results. Further, the given elliptical target tissue (4×3 cm) can be ablated completely using the control point 5, 7 or 9 at 90 ℃, as shown in Figure 6.9.

6.3.2 *In vitro* experimental results

Figure 6.13 shows one of the results of TTN area out of the five groups from the *in vitro* experiments using porcine liver tissues. The TTN areas were measured immediately after the ablation. The tissue death board was determined by a visual examination done by the first author and second author (who is a medical doctor with more than 10 years of experience working with RFA). We considered the TTN area (pale zone as shown in Figure 6.13) as an elliptical one. The area of TTN of *in vitro* experiments was calculated as follows:

$$\text{Area} = \pi \times \frac{W}{2} \times \frac{H}{2} \tag{6.15}$$

where *W* and *H* are the minor and the major axis of the TTN area, respectively, as shown in Figure 6.13. The imprints (major axis) on the liver tissues mean the direction of RF electrode placement.

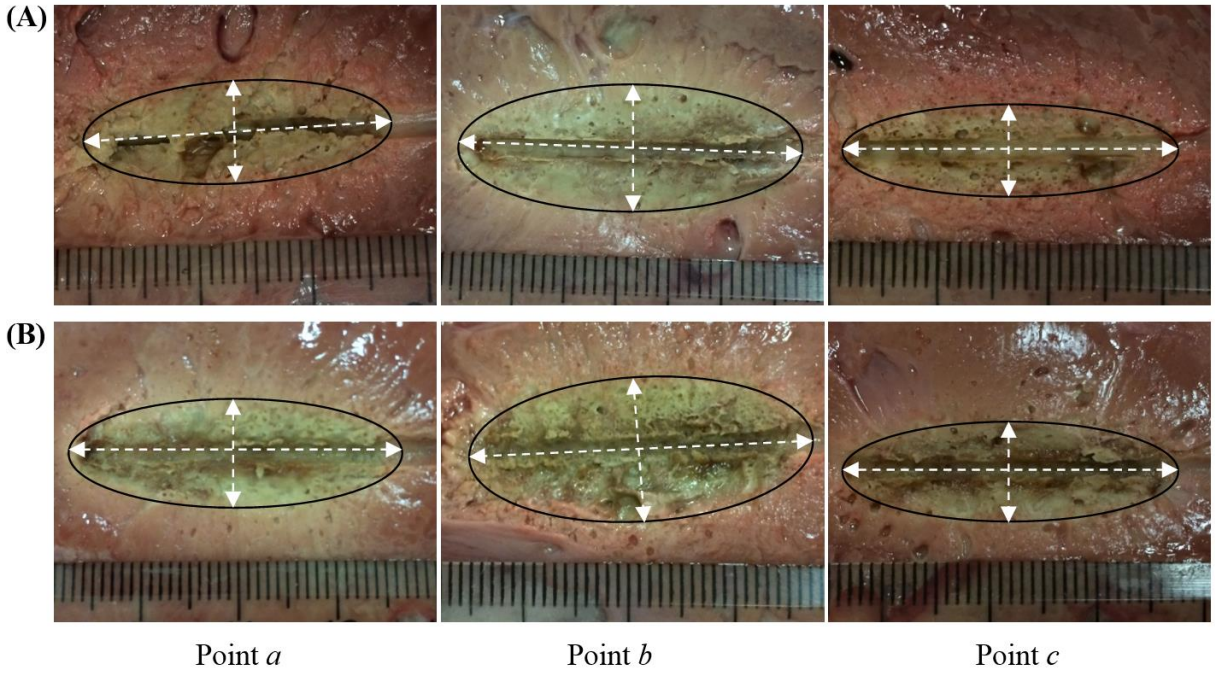

Figure 6.13. TTN areas generated using the three selected points at the control temperatures of (A) 80 ℃ and (B) 90 ℃ from the *in vitro* experiments.

Table 6.2. Results of the TTN areas from the *in vitro* experiments.

Control point	Temperature (℃)	*W* (mm)	*H* (mm)	Area (mm^2)
a	80	8.9±0.1	30.5±0.3	211.9±2.3
	90	11.1±0.2	34.0±0.5	295.9±7.3
b	80	12.1±0.3	32.8±0.8	311.6±9.6
	90	13.0±0.2	32.9±0.3	335.6±7.7
c	80	8.5±0.4	30.9±0.4	207.1±10.7
	90	10.7±0.5	32.9±1.4	276.7±19.6

As shown in Table 6.2, the same conclusions on the TTN areas of *in vitro* experiments can be achieved from the results calculated with the computer model (see the discussion in Section 6.3.1 above). At both 80 and 90 ℃, the TTN areas generated using the control point *b* were significantly larger than those generated using the control point *a* (P <0.0001 for both set-points: 80 and 90 ℃) and the control point *c* (P <0.0001 and =0.0002, respectively). Similar with the results calculated with the computer model, there was no significant difference on the TTN areas at

both 80 and 90 ℃ (P =0.3477 and 0.7176, respectively) between the control points *a* and *c*, It is noted that the *in vitro* experiments were used to validate the findings regarding these control areas (Table 6.2, Figure 6.13).

6.4 Conclusions

In the present study, we found that the large size of TTN areas can be achieved when the temperatures of the target tissue areas surrounding the middle part of RF electrode are controlled using the feedback control strategy (for example, a PID control law). This finding was validated by the *in vitro* experiments on porcine liver tissues. Further, using a commercial RF electrode (1.5 mm diameter and 30 mm in length) with the internal cooling effect, an elliptical target tissue with 4 cm in the major axis and 3 cm in the minor axis can be ablated completely by controlling the temperature of the tissue areas surrounding the middle part of RF electrode with the set-point temperature of 90 ℃ and with a standard ablation time (720 s) in clinic.

The present study can draw the following conclusions: (1) the control target should not be on the electrode, as the commercial RFA systems do, but should be on the target tissue; (2) the control target area should be carefully determined (in clinic, this can be done through a simulation model, as the one developed in the present study); (3) the control set-point (i.e. the target temperature of the control area in the case of RFA) should be carefully determined (in clinic, this can be done through a simulation model, as the one developed in the present study).

The contributions of the present work are of two folds: (1) proof of a promising perspective to the ablation of large target tissues (≥3 cm) with RFA and (2) development of an effective control strategy along with its control method for the ablation of target tissues with an indirect physical approach (e.g. thermal-based, etc.). In (2), the ultimate control target is the target tissue size, but the goal of this control is accomplished through the control of an intermediate variable, temperature in the case of RFA.

A further validation using liver tumour or tumour phantom and RF electrode with internal cooling effect for the findings of the present study is of importance for more realistically clinical settings. The future study will be focused on improving this method and optimization of the ablation protocol. On the other hand, how to measure the

temperature of the tissue in the control target area accurately with a minimally invasive way in the clinical setting is also worth studying.

Finally, in the present study, we mainly focused on the method to avoid or delay the tissue charring so as to achieve a relatively large TTN size. The ‘heat-sink’ effect of large blood vessels ≥3 mm in diameter, which is considered as another reason for the small size of TTN, was not taken into account. Future work should be directed to address this issue.

Acknowledgement

This article was supported by the Saskatchewan Health Research Foundation (SHRF) through the 'BioNEMS Phase I' grant (grant no. 2539) and the National Natural Science of China (grant no. 51175179). The first author (Bing Zhang) also received financial support from the China Scholarship Council (CSC).

Conflict of interest

The authors declare that there is no conflict of interest.

REFERENCES

1. Zhang B, Moser M, Zhang E, Zhang W. Radiofrequency ablation technique in the treatment of liver tumours: Review and future issues. J Med Eng Technol 2013;37:150-9.
2. Nishikawa H, Kimura T, Kita R, Osaki Y. Radiofrequency ablation for hepatocellular carcinoma. Int J Hyperthermia 2013;29:558-68.
3. Gillams A, Khan Z, Osborn P, Lees W. Survival after radiofrequency ablation in 122 patients with inoperable colorectal lung metastases. Cardiovasc Intervent Radiol 2013;36:24-730.
4. Kinoshita T, Iwamoto E, Tsuda H, and Seki K. Radiofrequency ablation as local therapy for early breast carcinomas. Breast Cancer 2011;18:10-17.
5. Zagoria RJ, Pettus JA, Rogers M, Werle DM, Childs D, Leyendecker JR.. Long-term outcomes after percutaneous radiofrequency ablation for renal cell carcinoma. Urology 2011;77:1393-7.
6. Xu HX, Lu MD, Xie XY, Yin XY, Kuang M, Chen JW, et al. Prognostic factors for long-term outcome after percutaneous thermal ablation for hepatocellular carcinoma: A survival analysis of 137 consecutive patients. Clin Radiol 2005;60:1018-25.
7. Shiina S, Tateishi R, Arano T, Uchino K, Enooku K, Nakagawa H, et al. Radiofrequency ablation for hepatocellular carcinoma: 10-year outcome and prognostic factors. Am J Gastroenterol 2012;107:569-77.
8. Llovet JM, Bruix J. Novel advancements in the management of hepatocellular carcinoma in 2008. J Hepatol 2008;48:S20-37.
9. Zhou Y, Zhao Y, Li B, Xu D, Yin Z, Xie F, et al. Meta-analysis of radiofrequency ablation versus hepatic resection for small hepatocellular carcinoma. BMC Gastroenterol 2010;10:78.
10. Zhang B, Moser MA, Zhang EM, Luo Y, Zhang H, Zhang W.. Study of the relationship between the target tissue necrosis volume and the target tissue size in liver tumours using two-compartment finite element RFA modelling. Int. J. Hyperthermia 2014;30:593-602.
11. Zhang B, Moser MA, Zhang EM, Luo Y, Zhang W. Numerical analysis of the relationship between the area of target tissue necrosis and the size of target tissue in liver tumours with pulsed radiofrequency ablation. Int J Hyperthermia 2015; in press.

12. Goldberg SN, Stein MC, Gazelle GS, Sheiman RG, Kruskal JB, Clouse ME. Percutaneous radiofrequency tissue ablation: Optimization of pulsed-radiofrequency technique to increase coagulation necrosis. J Vasc Interv Radiol 1999;10:907-16.

13. Lim D, Namgung B, Woo DG, Choi JS, Kim HS, Tack GR. Effect of input waveform pattern and large blood vessel existence on destruction of liver tumor using radiofrequency ablation: Finite element analysis. J Biomech Eng 2010;132:061003.

14. Goldberg S, Solbiati L, Hahn P, Cosman E, Conrad J, Fogle R, Gazelle G. Large-volume tissue ablation with radio frequency by using a clustered, internally cooled electrode technique: Laboratory and clinical experience in liver metastases. Radiology 1998;209:371-9.

15. Trujillo M, Alba J, Berjano E. Relationship between roll-off occurrence and spatial distribution of dehydrated tissue during RF ablation with cooled electrodes. Int J Hyperthermia 2012;28:62-8.

16. Lee J, Han J, Kim S, Lee J, Choi S, Choi B. Hepatic bipolar radiofrequency ablation using perfused-cooled electrodes: a comparative study in the ex vivo bovine liver. Br J Radio 2004;77:944-9.

17. Lee JM, Han JK, Kim SH, Sohn KL, Choi SH, Choi BI. Bipolar radiofrequency ablation in ex vivo bovine liver with the open-perfused system versus the cooled-wet system. Eur Radiol 2005;15:759-64.

18. Pennes HH. Analysis of tissue and arterial blood temperatures in the resting human forearm. J Appl Physiol 1948;1:93-122.

19. Haemmerich D, Schutt DJ. RF ablation at low frequencies for targeted tumor heating: In vitro and computational modeling results. IEEE Trans Biomed Eng 2011;58:404-10.

20. Haemmerich D, Schutt DJ, Wright AS, Webster JG, Mahvi DM. Electrical conductivity measurement of excised human metastatic liver tumours before and after thermal ablation. Physiol Meas 2009;30:459-66.

21. Tungjitkusolmun S, Staelin ST, Haemmerich D, Tsai JZ, Cao H, Webster JG, et al. Three-dimensional finite-element analyses for radio-frequency hepatic tumor ablation. IEEE Trans Biomed Eng 2002; 49:3-9.

22. González-Suárez A, Trujillo M, Burdío F, Andaluz A, Berjano E. Feasibility study of an internally cooled bipolar applicator for RF coagulation of hepatic tissue: Experimental and computational study. Int J Hyperthermia 2012;28:663-73.

23. van Beers BE, Leconte I. Materne R, Smith AM, Jamart J, Horsmans Y. Hepatic perfusion parameters in chronic liver disease: dynamic CT measurements correlated with disease severity. AJR Am J Roentgenol 2001;176:667-73.

24. Zorbas G, Samaras T. Parametric study of radiofrequency ablation in the clinical practice with the use of two-compartment numerical models. Electromagn Biol Med 2013;32:236-43.

25. Sahani DV, Holalkere NS, Mueller PR, Zhu AX. Advanced hepatocellular carcinoma: CT perfusion of liver and tumor tissue—Initial Experience. Radiology 2007;243:736-743.

26. Dodde RE, Miller SF, Geiger JD, Shih AJ. Thermal-electric finite element analysis and experimental validation of bipolar electrosurgical cautery. ASME J. Manuf. Sci. Eng. 2008;130:021015.

27. Jo B, Aksan A. Prediction of the extent of thermal damage in the cornea during conductive keratoplasty J Therm Biol 2010;35:167-74.

28. Liu Z, Ahmed M, Sabir A, Humphries S, Goldberg SN. Computer modeling of the effect of perfusion on heating patterns in radiofrequency tumor ablation. Int J Hyperthermia 2007;23:49-58.

29. Chang IA, Nguyen UD. Thermal modeling of lesion growth with radiofrequency ablation devices. Biomed Eng Online 2004;3:27.

30. Reddy G, Dreher MR, Rossmann C, Wood BJ, Haemmerich D. Cytotoxicity of hepatocellular carcinoma cells to hyperthermic and ablative temperature exposures: In vitro studies and mathematical modelling. Int J Hyperthermia 2013;29:318-23.

31. Haemmerich D, Webster JG. Automatic control of finite element models for temperature-controlled radiofrequency ablation. Biomed Eng Online 2005;4:42.

32. Alba-Martínez J, Trujillo M, Blasco-Giménez R, Berjano E. Could it be advantageous to tune the temperature controller during radiofrequency ablation? A feasibility study using theoretical models. Int J Hyperthermia 2011;27(6):539-48.

33. Brace C. L. Radiofrequency and microwave ablation of the liver, lung, kidney, and bone: what are the differences? Curr Probl Diagn Radiol 2009;38:135-43.

34. Ahmed M, Brace CL, Lee FT, Goldberg SN. Principles of and advances in percutaneous ablation. Radiology 2011;258:351-69.

35. Trujillo M, Berjano E. Review of the mathematical functions used to model the temperature dependence of electrical and thermal conductivities of biological tissue in radiofrequency ablation. Int J Hyperthermia 2013;29:590-7.

36. Jamil M, Ng EYK. Quantification of the effect of electrical and thermal parameters on radiofrequency ablation for concentric tumour model of different size. J Therm Biol 2015;51:23-32.

7 CONCLUSIONS AND FUTURE WORK

7.1 Conclusions

In this thesis, a critical issue related to the current RFA systems has been investigated, which is the inefficacy of RFA in the treatment of target tissues ≥3 cm in diameter. To understand comprehensively and further solve this problem, four research objectives have been proposed in Chapter 1. The work presented in this thesis has demonstrated that all the research objectives have been achieved and the conclusions related to all research objectives can be summarised as follows:

(1) *Regarding Objective 1, the current commercially available RFA systems have been evaluated using an engineering design method (i.e. ADT) in Chapter 3.* The inefficacy of RFA in the treatment of large target tissues ≥3 cm in diameter is mainly contributed to the incomplete TTN. By using ADT, the current RFA systems have been evaluated in terms of their design concepts in generating complete TTN. The cause of why the current RFA systems cannot generate complete TTN has been analysed, which is attributed to the presence of the decoupled design in their conceptual design level. Further, an uncoupled design to increase the possibility of complete TTN was proposed.

(2) *Regarding Objective 2, the size limit of target tissues in the treatment of current RFA systems is mathematically proved to be 3 cm in diameter.* This conclusion was drawn by checking the three most commonly used RFA systems (i.e. the constant, pulsed, and temperature-controlled RFA systems) in Chapters 4, 5, and 6, respectively. Using the constant RFA as well as the pulsed RFA, the largest TTN can be achieved at the maximum voltage applied (MVA) without the roll-off occurrence. The largest TTN sizes that the constant RFA and the pulsed RFA can achieve are all 2.5 cm in diameter. For the temperature-controlled RFA with the current commercially available protocol, the largest TTN is around 2.4 cm in diameter.

(3) *Regarding Objective 3, the so-called 3-cm problem of RFA can be overcome by using temperature-controlled RFA under a new protocol.* This conclusion was drawn from the results in Chapter 6 based on a feedback temperature-control strategy with the judicious selection of the best target area for feedback control and of the best set-point (target temperature). The control area should not be on the electrode, as the commercial RFA systems do, but should be on the target tissues and should be also determined carefully.

(4) *Regarding Objective 4, a radiofrequency ablation device was designed and fabricated, which is discussed in the Appendix A.* An RF power generator that can supply the maximum power of 50 W with 430 ± 30 kHz and two sizes of RF electrode (1 and 1.98 mm in diameter and 5 and 30 mm in length, respectively) were designed and fabricated. This RFA system can be taken as a test-bed for the validation of computer simulations in this thesis study and the immunotherapy of RFA in the future.

7.2 Future work

Along with the work presented in this thesis, some further studies that may be needed to improve the thesis are given as follows:

(1) *Considering the 'heat-sink' effect of large blood vessels ($\geq$3 mm in diameter)*

In this thesis, we only study the 3-cm problem of RFA based on the reason of tissue charring. But, besides the tissue charring, the 'heat-sink' effect of large blood vessels is also a reason of incomplete ablation of RFA. This effect will make the temperature of target tissues in the areas close to the large blood vessels cannot reach to a fatal level. Thus, tumour cells in these areas will survive from the treatment of RFA, which usually leads to local recurrence and poor clinical results. In recent clinical settings, the most used method in avoiding the heat-sink effect is blood inflow occlusion. However, this method is fulfilled by surgery or injection of chemo drugs, which both have serious side effects. Thus, further research on the heat-sink effect of large blood vessels is needed to improve the technique of RFA, especially using methods, which are not against the minimal invasiveness of RFA.

(2) *Validation using* in vivo *experiments with tumour tissues*

In Chapters 5 and 6, *in vitro* experiments with porcine liver tissues were used in the verification of the mathematical model of RFA used in this thesis and the findings on the selection of control areas. It is acceptable to use *in vitro* experiments with tissues having similar properties in the relevant experiments for validating the effectiveness of the new method. However, it is worth noting that more convinced conclusions maybe drawn if the *in vivo* experiments with tumour tissues can be used for the validation. A couple of reasons support this statement. First, the blood perfusion has been ignored in the *in vitro* experiments, which may create errors in the mathematical model of RFA. Second, the conclusion drawn from Chapter 6 that the target tissue (liver tumour, 3×4 cm) can be ablated completely should be validated using an *in vivo* experiment with tumour tissues and the commercial RFA system.

(3) *Immunotherapy of RFA*

In recent years, the immune therapy of the RFA has also attracted the interest of researchers. An interesting conjecture raised about RFA is that it may not just cause TTN locally but also generates systemic immunity response to tumour metastases. Unlike surgery, the treated target tissues are not ablated from the body. Instead, in cases of RFA, the necrotic target tissues are left in the body and a robust immune response is triggered to remove the debris. Many researchers expect that the induced immune responses can be used to create an immune memory that might expand the treatment beyond the local ablation site and create more of a systemic therapy. These induced immune responses, however, are mostly weak and not sufficient for the complete eradication of established target tissues or durable prevention of disease progression. There are still many unclear issues in the immune response of RFA needing to be addressed elaborately. One of them can be what the RFA temperature for inducing the largest extent systemic immune response.

APPENDIX A A RADIOFREQUENCY ABLATION DEVICE FOR SMALL ANIMALS

Due to some restrictions in the current commercially available systems, a simple but effective radiofrequency ablation system especially for small animal models has been designed and fabricated. This device was also used as a test bed to validate the accuracy of FEM in Chapters 4 and 5 and the findings about the control areas in Chapter 6. This design and fabrication mainly include two parts, namely RF power generator and RF applicator.

A.1 RF power generator

To satisfy the design objectives mentioned above, the RF power generator was designed as an alternating current source, which is not influenced by the impedance of external load. As shown in Figure A.1, two square wave signals with high frequency are generated by the UC1825 (Texas Instruments, Dallas, Texas, USA), a pulse-width modulation (PWM) circuit, which is usually for high-frequency switched mode power supply applications. These two signals are transferred to the gate ports of two MOSFETs (IRF630) (ST, Geneva, Switzerland), in the part of power amplifier, respectively. A positive DC voltage source is used to supply power to the drain ports of the two MOSFETs through a DC voltage regulator. So an alternating current with high frequency and magnitude in a square wave is generated. Then, the square wave current is converted into sinusoidal wave with required frequency by a LC low-pass filter circuit, as shown in Figure A.1. The alternating sinusoidal current is delivered out through RF electrode and ground pad. A sampling circuit was used to convert the real-time alternating output current into DC voltage signal that would be fed back to DC voltage regulator to control the alternating output current. The current sampling circuit was composed of a small ratio of transformer and a bridge rectified filter. The magnitude of the output alternating current could be controlled by changing the magnitude of the DC voltage source through DC voltage regulator in two different ways: manually and automatically.

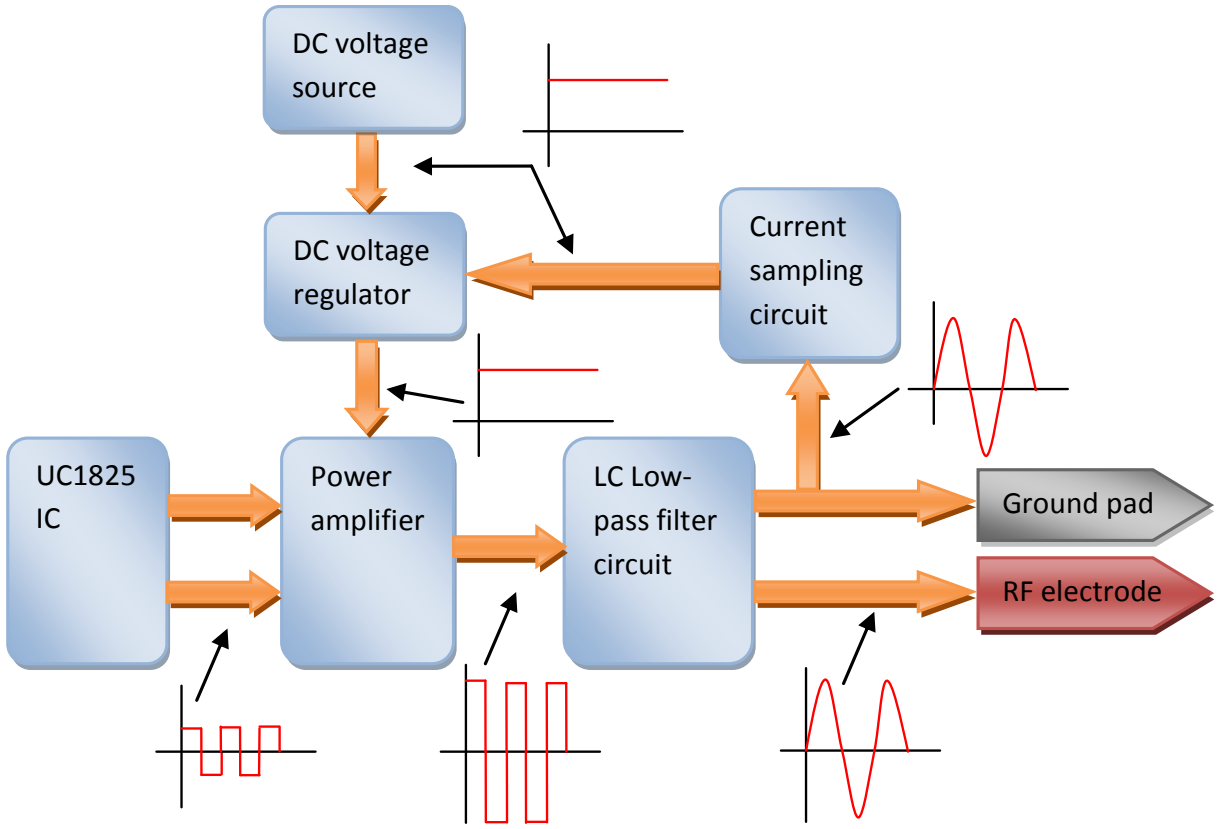

Figure A.1. Diagram of the design for the RF power generator.

A.2 RF applicator

In the design of RF applicator, a small size of 316L stainless steel tubing with 1 mm outer diameter and 0.81 mm inner diameter (McMaster-Carr, Clevelan, OH, USA) was taken as the RF electrode for small animals. A large size of RF electrode with 1.98 mm outer diameter and 1.60 mm inner diameter was also made using the same material with the small size of electrode for the validation of results of computer simulations in this thesis. The tubing was covered with modified polyamide nylon (PA66) tubing (Finlumen, Beijing, China) for insulation from the surrounding tissue, representing the insulated shaft. So the small and the large size of electrodes have about 5 mm and 30 mm in length, respectively. In addition to the RF electrode and insulated shaft, in order to measure and control the temperature of the RFA, a K type micro-thermocouple (Huanbang, Shanghai, China) with 0.5 mm

diameter was inserted into the steel tubing for each electrode. The themrmocouple can be used to feedback the real temperatures at the tip of RF electrode to RF power generator.

A.3 Testing of the RFA system

In order to test the device to see whether or not it can satisfy our design objectives, 8 small freshly excised porcine muscle tissues (around 15 g each tissue) were performed the RFA ablation. All the tissues were purchased from the local butcher and the tissue experiments followed the regulation of biosafety and ethics of University of Saskatchewan. In this experiment, five different RFA temperatures, like 50, 60, 70, and 80 ℃ were tested for 6 and 12 mins of the ablation durations. Figure A.2 shows the experimental set-up and the RFA device, which includes the RF power generator, RF applicator and ground pad (aluminum foil).

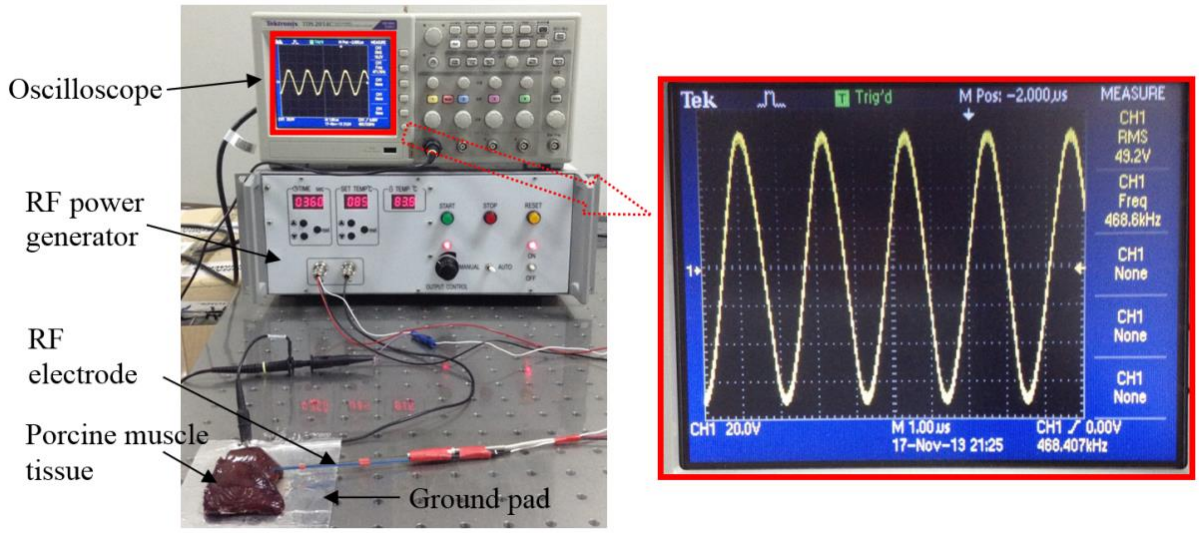

Figure A.2. Experimental set up of the RFA device.

Figure A.3 shows the results of 4 tested temperatures (50, 60, 70, and 80 ℃) at the tip of RF electrode (T_a) for 6 and 12 mins of ablation durations. The temperature of the tissue at the location of 2.5 mm away from the surface of RF electrode (T_b) was also measured. As expected, T_b was changing with the same tendency with that of T_a. The temperature gap between T_a and T_b was about 20 ℃. From the testing results, it can be concluded that the

instrument deisgned satisfies our requirements for immune research on the small animals. After the testing of this system, the specification of RF power generator can be given as follows:

Frequency:	430±30 kHz.
Maximum output voltage:	70 V
Maximum output current:	0.7 A
Maximum output power:	50 W

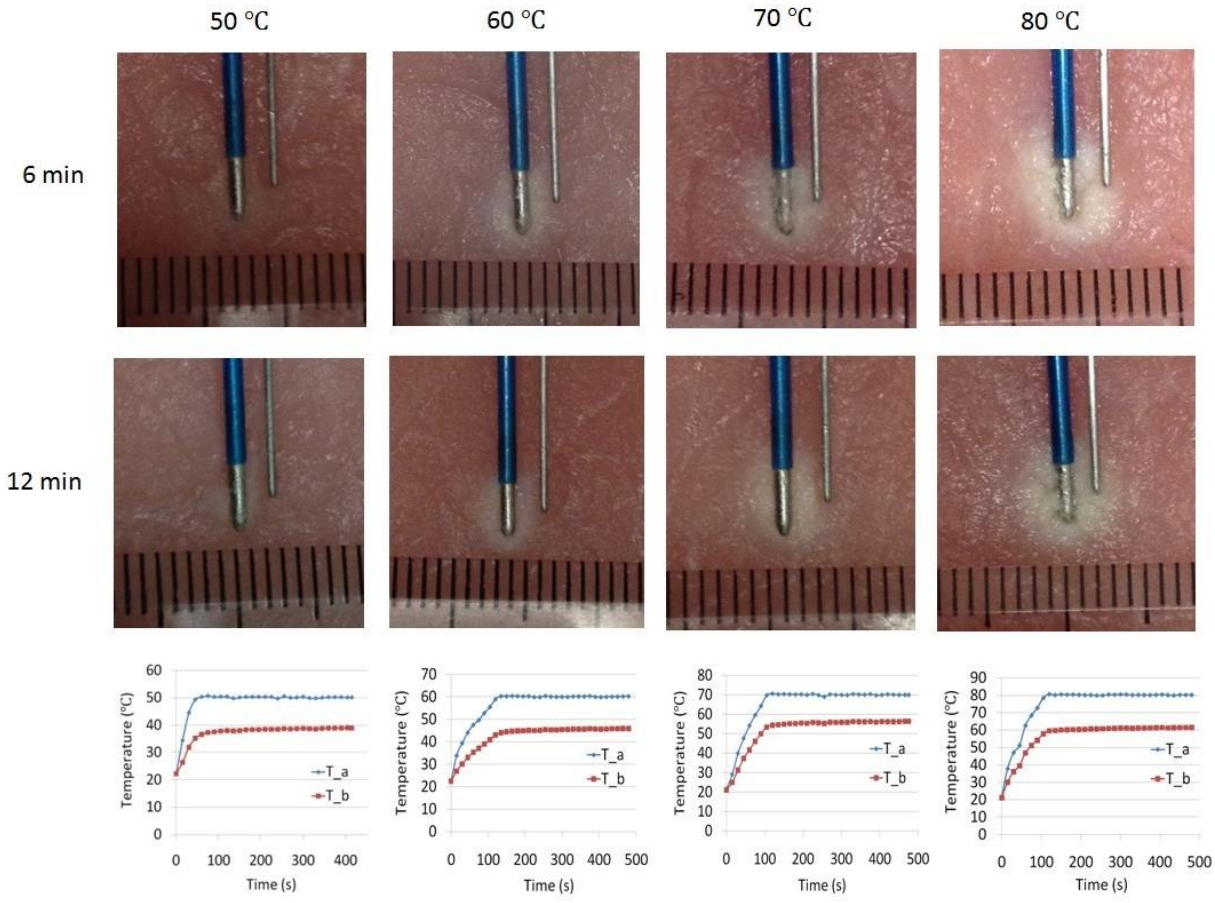

Figure A.3. Results of testing experiments using *in vitro* porcine muscle tissues.

APPENDIX B LIST OF PUBLICATIONS

1. **B Zhang** et al., Large target tissue necrosis of radiofrequency ablation: A review of clinical results and mathematical modelling. *Physica Medica* 2015, **Under Review**.
2. **B Zhang** et al., A novel feedback temperature control approach to radiofrequency ablation of large target tissue necrosis. *Medical Physics* 2015, **Under Review**.
3. **B Zhang** et al., Numerical analysis of the relationship between the area of target tissue necrosis and the size of target tissue in liver tumours with pulsed radiofrequency ablation. *International Journal of Hyperthermia* 2015, **In Press**.
4. **B Zhang** et al., Study of the relationship between the target tissue necrosis volume and the target tissue size in liver tumours using two-compartment finite element RFA modelling. *International Journal of Hyperthermia* 2014, **30**(8): 593-602.
5. **B Zhang** et al., On understanding of the limiting factors in radiofrequency ablation on target tissue necrosis volume. *2015 World Congress on Medical Physics & Biomedical Engineering* 2015, **In Press**.
6. **B Zhang** et al., Evaluation of the current radiofrequency ablation systems using axiomatic design theory. *Proceedings of the Institution of Mechanical Engineers, Part H: Journal of Engineering in Medicine* 2014, **228**(4): 397-408.
7. **B Zhang** et al., Radiofrequency ablation technique in the treatment of liver tumours: review and future issues. *Journal of Medical Engineering & Technology* 2013, **37**(2): 150-159.

APPENDIX C COPYRIGHT PERMISSIONS

The copyright permissions of the following published papers presented in the thesis:

B Zhang, MA Moser, Y Luo, EM Zhang, and W Zhang. Evaluation of the current radiofrequency ablation systems using axiomatic design theory. *Proceedings of the Institution of Mechanical Engineers, Part H: Journal of Engineering in Medicine* 2014, **228**(4): 397-408.

B Zhang, MA Moser, EM Zhang, Y Luo, H Zhang, and W Zhang. Study of the relationship between the target tissue necrosis volume and the target tissue size in liver tumours using two-compartment finite element RFA modelling. *International Journal of Hyperthermia* 2014, **30**(8): 593-602.

are given in the following pages.

Title: Evaluation of the current radiofrequency ablation systems using axiomatic design theory:
Author: Bing Zhang, Michael AJ Moser, Yigang Luo, Edwin M Zhang, Wenjun Zhang
Publication: Proceedings of the Institution of Mechanical Engineers, Part H: Journal of Engineering in Medicine
Publisher: SAGE Publications
Date: 04/01/2014

Gratis Reuse

- Without further permission, as the Author of the journal article you may:
  - post the accepted version (version 2) on your personal website, department's website or your institution's repository. You may NOT post the published version (version 3) on a website or in a repository without permission from SAGE.
  - post the accepted version (version 2) of the article in any repository other than those listed above 12 months after official publication of the article.
  - use the published version (version 3) for your own teaching needs or to supply on an individual basis to research colleagues, provided that such supply is not for commercial purposes.
  - use the accepted or published version (version 2 or 3) in a book written or edited by you. To republish the article in a book NOT written or edited by you, permissions must be cleared on the previous page under the option 'Republish in a Book/Journal' by the publisher, editor or author who is compiling the new work.
- When posting or re-using the article electronically, please link to the original article and cite the DOI.
- All other re-use of the published article should be referred to SAGE. Contact information can be found on the bottom of our 'Journal Permissions' page.

Our Ref: MD/IHYT/H108
3rd July 2015

Dear Bing Zhang,

'Study of the relationship between the target tissue necrosis volume and the target tissue size in liver tumours using two-compartment finite element RFA modelling' Bing Zhang et al International Journal of Hyperthermia Vol.30:8 (2014) pp.593-602

Thank you for your correspondence requesting permission to reproduce the following article published in our journal in your printed thesis entitled 'Large Target Tissue Necrosis of Radio Frequency Ablation Using Mathematical Modelling' and to be posted in your university's repository at the University of Saskatchewan.

We will be pleased to grant permission on the sole condition that you acknowledge the original source of publication and insert a reference to the article on the Journals website:

This is the authors accepted manuscript of an article published as the version of record in International Journal of Hyperthermia 2014 http://www.tandfonline.com/toc/ihyt20/30/8#.VZa46PlVhBd

Please note that this license does not allow you to post our content on any third party websites or repositories.

Thank you for your interest in our Journal.

Yours sincerely

Michelle Dickson– Permissions & Licensing Executive, Journals.
Routledge, Taylor & Francis Group.
4 Park Square, Milton Park, Abingdon, Oxon, OX14 4RN, UK.
Tel: +44 (0)20 7017 7413
Fax: +44 (0)20 7017 6336
Web: www.tandfonline.com
e-mail: Michelle.Dickson@tandf.co.uk
Taylor & Francis is a trading name of Informa UK Limited,
registered in England under no. 1072954